UNIVERSIDAD COMPLUTENSE DE MADRID

FACULTAD DE CIENCIAS MATEMÁTICAS

TESIS DOCTORAL

Mathematical models for brain diseases: formation of senile plaques and neurofibrillary tangles in Alzheimer's disease

Modelos matemáticos de enfermedades cerebrales : formación de placas seniles y ovillos neurofibrilares en la enfermedad de Alzheimer

MEMORIA PARA OPTAR AL GRADO DE DOCTORA

PRESENTADA POR

Verónica Tora

Directores

Bruno Franchi
Miguel Ángel Herrero

Madrid
Ed. electrónica 2019

Universidad Complutense de Madrid

Programa de doctorado:
Investigación Matemática

Mathematical models for brain diseases: formation of senile plaques and neurofibrillary tangles in Alzheimer's disease.

Modelos matemáticos de enfermedades cerebrales: formación de placas seniles y ovillos neurofibrilares en la enfermedad de Alzheimer.

Autor:
Veronica Tora

Director:
Prof. Bruno Franchi

Director:
Prof. Miguel Angel Herrero

Facultad de Matemáticas, Universidad Complutense de Madrid y Facoltà di Matematica, Università di Bologna

To my family ...

Acknowledgements

I would like to express my warmest thanks to professor Bruno Franchi and professor Miguel Angel Herrero for their deep culture, competence and curiosity in science and for their support during my phD studies and during the preparation of this thesis. I am also very grateful to them for introducing me in the field of the scientific research and for stimulating my interest towards mathematical modeling of brain diseases. The things I have learned from them are priceless.

I sincerely thank all my PhD colleagues (the Italian and the Spanish ones) for accompanying me with friendship during these years.

My special thanks go to all my family for their deep love and support. Without them, this work could not have been possible.

Abstract

Alzheimer's disease (AD) is characterized by the presence of two specific structures in brain of patients: senile plaques (SP) and neurofibrillary tangles (NTFs). Oligomers of beta amyloid protein are the main component of SP, while NFTs are constituted by oligomers of aberrantly phosphorylated tau protein. The aim of this thesis is to present two studies concerning the process of diffusion and agglomeration of tau protein first into fibrils and eventually up to neurofibrillary tangles. The aforesaid researches share the use of Smoluchowski-type equations (including diffusion and monomers production) on a finite weighted graph, which is conceived as a theoretical approximation of the human brain, where each vertex represents a cerebral area of interest, while the connections between them are described by the edges.
In the first chapter, we present a model for the aggregation and diffusion of hyperphosphorylated tau based on a finite dimensional Smoluchowski-type system on a finite graph, aimed at reproducing tau patterns in human brain obtained through suitable *in vivo* measurements. In such model, clusters whose length exceeds an *a priori* established critical threshold are defined to be tangles. Statistical analysis is performed, comparing the model-predicted tau concentrations (in monomeric, oligomeric form and in tangles) with cortical atrophy data and empirical tau measurements in AD patients provided by *in vivo* neuroimaging.
The second research considers the process of aggregation in tangles of hyperphosphorylated tau protein as a result of a coagulation process of this protein. The formation of neurofibrillary tangles is mathematically characterized in terms of a sol-gel phase transition for a polymerization problem, modelled by means of infinite dimensional Smoluchowski-type system on a finite graph.

From a biological point of view, the process of formation of gel is a suitable tool for the description of the process of formation of neurofibrillary tangles, since it allows one to formulate conjectures and to provide insights on the nature of this phenomenon in AD scenario. This could open new interesting perspectives concerning the role of NTFs in neurodegenerative disorders.

Riassunto

La malattia di Alzheimer si caratterizza per la presenza di due strutture specifiche nell'encefalo dei pazienti: le placche senili e i *neurofibrillary tangles*. Le placche senili sono formate da polimeri di proteina beta amiloide, mentre i *tangles* sono composti da polimeri di proteina tau iperfosforilata. L'obiettivo di questa tesi consiste nel presentare due studi inerenti il processo di diffusione e aggregazione della proteina tau, prima in fibrille (ovvero polimeri di lunghezza moderata) e successivamente in *tangles*. Tali studi sono accumunati dall'utilizzo di equazioni di tipo Smoluchowski (in cui sono presenti termini di diffusione e di produzione di monomeri) in un grafo finito, concepito come una approssimazione teorica dell'encefalo umano, nella quale ciascun vertice rappresenta una regione cerebrale di interesse, mentre le connessioni tra queste ultime sono rappresentate dagli spigoli del grafo.

Nel primo capitolo della tesi si presenta un modello per l'aggregazione e il trasporto della proteina tau iperfosforilata basato su un sistema di tipo Smoluchowski di dimensione finita avente l'obiettivo di riprodurre dati sperimentali consistenti in concentrazioni di proteina tau ottenute mediante neuroimmagini *in vivo*. In tale modello, i polimeri, la cui lunghezza supera una certa soglia stabilita *a priori*, vengono considerati *tangles* per definizione. In tale studio, si costruisce una rete cerebrale approssimata, individuando alcune regioni cerebrali funzionalmente omogenee che faranno le veci dei vertici e si ottengono misure di connettività tra queste regioni a partire da immagini di risonanze magnetiche (MRI) di soggetti sani.

Al fine di testare se il modello proposto è in grado di predire l'evoluzione spazio-temporale degli oligomeri di tau (ovvero, polimeri composti da poche unità monomeriche) e dei *tangles*, si postula che le regioni e le connessioni della rete empirica in questione corrispondono rispettivamente ai vertici e agli spigoli del grafo in cui le equazioni per l'aggregazione e il trasporto di proteina tau vengono considerate. In tal modo, si confrontano mediante l'analisi statistica le concentrazioni di tau predette dal mod-

ello (in forma monomerica, oligomerica e *tangles*) in ogni vertice del grafo con i dati dell'atrofia corticale e le misure empiriche di tau nella regione cerebrale rappresentata da quel vertice, ottenute mediante neuroimmagini *in vivo* nei malati di Alzheimer. I dati dell'atrofia corticale vengono ricavati dallo studio pubblico "Alzheimer's Disease Neuroimaging Initiative (ADNI)", mentre le misure empiriche di concentrazioni di proteina tau sono state ottenute mediante uno studio effettuato presso l'Università di Yonsei, Corea del Sud.
I risultati dell'analisi statistica effettuata nella tesi ci consentono di proporre che il nostro modello per la distribuzione della proteina tau iperfosforilata è in grado di riprodurre le concentrazioni misurate in malati di Alzheimer nella base di dati considerata.

Nel secondo capitolo si considera il processo di aggregazione in *tangles* da parte della proteina tau iperfosforilata come risultato di un processo di coagulazione di questa proteina, in cui un'altra proteina, la beta amiloide, possiede un ruolo induttore. La formazione dei *tangles* viene caratterizzata matematicamente in termini di una transizione di fase di tipo sol-gel per un problema di polimerizzazione, formulato mediante un sistema di equazioni di tipo Smoluchowski di dimensione infinita in un grafo finito. Il contributo principale di questo lavoro risiede nella dimostrazione, per opportune scelte dei coefficienti di coagulazione, dell'occorrenza di una transizione di fase di tipo sol-gel che, inoltre, è associata a una perdita di regolarità della soluzione. A nostro giudizio, questa transizione di fase può essere interpretata come un segnale della comparsa dei *neurofibrillary tangles*. La maniera in cui la suddetta transizione viene identificata si può riassumere come segue. In primo luogo, si dimostra l'esistenza di una soluzione debole globale per il sistema di Smoluchowski di dimensione infinita considerato. Per tempi sufficientemente piccoli, tale soluzione debole risulta essere una soluzione classica e la massa totale di tutti i polimeri di proteina tau cresce linearmente in seguito alla presenza del termine sorgente, corrispondente all'azione della proteina beta amiloide. Tuttavia, con il passare del tempo si osserva una forte decrescita della massa e si stimano i bound superiore e inferiore per l'istante in cui ciò accade (il cosiddetto tempo di gelificazione che segnala la transizione di fase). Infine, si dimostra il blow up in tempo finito del secondo momento della soluzione, un criterio abituale per individuare la formazione del gel in problemi di polimerizzazione.

Da un punto di vista biologico, riteniamo che il modello di formazione del gel in una transizione di fase rappresenti uno strumento adeguato per la descrizione del processo di formazione dei *neurofibrillary tangles*, dato che ci consente di formulare congetture,

che possono essere soggette a verifica sperimentale, inerenti tale fenomeno nel contesto della malattia di Alzheimer. Ciò potrebbe aprire delle nuove prospettive circa il ruolo dei *neurofibrillary tangles* nelle patologie neurodegenerative.

Contents

Resumen

La enfermedad de Alzheimer se caracteriza por la presencia de dos estructuras especificas en el cerebro de los pacientes: placas seniles y ovillos neurofibrilares. Las placas seniles están formadas por polímeros de la proteína beta amiloide, mientras que los ovillos neurofibrilares están compuestos por polímeros de proteína tau hiperfosforilada. El objetivo de esta tesis consiste en presentar dos estudios sobre el proceso de difusión y agregación de la proteína tau, que dan lugar a polímeros de longitud moderada (fibrillas) en primer lugar y en un estado posterior a ovillos. Estos estudios comparten el uso de ecuaciones de tipo Smoluchowski (incluyendo términos de difusión y de producción de monómeros) en un grafo finito, concebido como una aproximación teórica del cerebro humano, en la que cada vértice representa una región cerebral de interés, mientras que las conexiones entre estas están representadas por las aristas del grafo.

En el primer capítulo de esta memoria se presenta un modelo para la agregación y el transporte de proteína tau hiperfosforilada basado en un sistema de tipo Smoluchowski de dimensión finita con el objetivo de reproducir datos experimentales de concentraciones de proteína tau obtenidas por medio de neuroimágenes *in vivo*. En este modelo, aquellos polímeros cuya longitud excede un umbral critico establecido *a priori* se consideran ovillos por definición. En el curso de este estudio se construye una red cerebral aproximada, definiendo unas regiones cerebrales funcionalmente homogéneas que harán las veces de vértices y se obtienen medidas de la conectividad entre dichas regiones a partir de unas imágenes de resonancia magnética (MRI) de sujetos sanos.

Para probar si el modelo propuesto es capaz de predecir la evolución espaciotemporal de los oligómeros de tau (o sea, polímeros compuestos por pocas unidades monoméricas) y de los ovillos, se postula que las regiones y las conexiones de la red empica en cuestión corresponden respectivamente a los vértices y las aristas del grafo en el que las ecuaciones para la agregación y el transporte de proteína tau están consideradas. De esta manera, se comparan por medio de análisis estadístico las concentraciones de tau predichas por

el modelo (en forma monomérica, oligomérica y ovillos) en cada vértice del grafo con los datos de atrofia cortical y las mediciones empíricas de tau en la región cerebral representada para aquel vértice, obtenidas por medio de neuroimágenes *in vivo* en enfermos de Alzheimer. Los datos de atrofia cortical proceden del estudio publico "Alzheimer's Disease Neuroimaging Initiative (ADNI)", mientras que las medidas empíricas de concentraciones de proteína tau surgen de un estudio en la Universidad de Yonsei, Corea del Sur.

Los resultados del análisis estadístico realizado permiten proponer que nuestro modelo para la distribución de la proteína tau hiperfosforilada es capaz de reproducir las concentraciones medidas en pacientes con enfermedad de Alzheimer en la base de datos considerada.

En el segundo capítulo se considera el proceso de agregación en ovillos de proteína tau hiperfosforilada como resultado de un proceso de coagulación de esta proteína, en el que otra proteína, la beta amiloide juega un papel inductor. La formación de los ovillos neurofibrilares se caracteriza matemáticamente en términos de una transición de fase de tipo sol-gel por un problema de polimerización, formulado mediante un sistema de tipo Smoluchowski de dimensión infinita en un grafo finito. La contribución principal de este trabajo consiste en la demostración, para adecuados coeficientes de coagulación, de la aparición de una transición de fase de tipo sol-gel que está asociada a una pérdida de regularidad de la solución. A nuestro juicio, esta transición de fase puede ser interpretada como una señal de la aparición de los ovillos neurofibrilares. La manera en la que se identifica esta transición está relacionada con la regularidad de las soluciones del problema considerado y se puede resumir como sigue. En primer lugar, se demuestra la existencia para todo tiempo de una solución débil para el sistema de Smoluchowski de dimensión infinita considerado. Para tiempos suficientemente pequeños, esta solución débil es además una solución clásica y la masa total de todos los polímeros de la proteína tau considerada crece linealmente, debido a la presencia de un término fuente, correspondiente a la acción de proteína beta amiloide. Sin embargo, en el transcurso del tiempo se observa una disminución brusca de la masa y se estiman los limites superior e inferior para el momento en que esto ocurre (el llamado tiempo de gelificación, que señala la transición de fase). Por último, se demuestra la explosión en tiempo finito del segundo momento de la solución, un criterio habitual para detectar a formación de un gel en problemas de polimerización.

Desde un punto de vista biológico, consideramos que el modelo de formación de un gel en una transición de fase puede ser un instrumento adecuado por la descripción del proceso de formación de los ovillos neurofibrilares, dado que nos permite formular conjeturas susceptibles de verificación experimental sobre este fenómeno en el contexto de la enfermedad de Alzheimer. Esperamos que esto pueda abrir nuevas perspectivas sobre el papel de los ovillos neurofibrilares en las enfermedades neurodegenerativas.

Introduction

Alzheimer's Disease (AD) is the most common form of dementia. As of 2015, it was estimated to affect 29,8 million of people over 65 years of age worldwide [25]. Its main symptoms include memory loss, language and disorientation problems, psychiatric or behavioral disturbances and serious difficulties to carry on daily living activities.

AD was described for the first time in 1907 by Alois Alzheimer, a German psychiatrist and neuropathologist, who reported the results of the autopsy of a 55-year-old woman who died after a progressive behavioral and cognitive disorder. Upon post-mortem inspection, the patient's brain showed the presence of two distinct anatomical findings: neurofibrillary tangles (NFTs), that Alzheimer correctly surmised that originated from abnormal intracellular aggregates, and neuritic plaques, which were described as "minute miliary foci which are caused by the deposition of a special substance in the cortex" [3].
This "special substance" was eventually isolated in 1984 [43] and identified as the beta amyloid peptide (Aβ), while tangles were later shown to be composed of hyperphosphorylated [1] forms of tau protein.

The actual causes of Alzheimer's disease and its mechanisms of progression remain largely unknown to this day and are the subject of active scientific research. In particular, both findings reported by Alzheimer, the presence of beta amyloid plaques and that of neurofibrillary tangles have been investigated as key factors of the corresponding neurodegenerative process. It remains unclear, however, whether they are active agents of disease propagation or just the signature of ordinary waste clearance in homeostatic brain tissue. For instance, it has been suggested that a significant role in neurodegeneration is played by beta amyloid (the so-called *amyloid cascade hypothesis*, see [48], [94], [28]).

[1] The hyperphosphorylation is a biochemical process in which a molecule acquires phosphoryl groups in multiples sites up to saturation.

Beta amyloid is a 40-42 aminoacid peptide normally produced by neurons. In fact, beta amyloid monomers result from the sequential cleavage of the amyloid precursor protein (APP), a large trans-membrane protein involved in various signal transduction pathways. The physiological role of Aβ is linked to the modulation of synaptic activity, but it is still controversial [85]. By unknown reasons, some neurons start to present an imbalance between production and clearance of β-amyloid during aging. In fact, the presence of amyloid generates an inflammatory response in which the main role is played by the microglial cells, that act as a clean-up crew in charge of clearing amyloid deposits [77].
However, in pathological conditions like AD, microglia seem not to perform their functions properly. Thus, the protein starts accumulating in the cerebral tissue and to coagulate, first in longer polymers and then in the form of insoluble fibrils [48]. The latter aggregate outside neurons in spherical deposits known as senile plaques [77].
It is important to underline, however, that amyloid plaques are commonly present in the brains of cognitively intact elderly people [96], so that their role in Alzheimer's disease is not well understood as yet.

Actually, there is increasing evidence that soluble Aβ oligomers, and particularly the oligomeric isoforms [2] Aβ_{40}, Aβ_{42}, are highly toxic for cerebral tissues and can be considered a significant effector of neuronal death and eventually of dementia [114], [112]. In fact, soluble oligomers correlate much better with the presence and degree of cognitive deficits than plaques [21]. This evidence, coupled with the fact that large plaques present much less Aβ surface area to neuronal membranes compared with a multitude of small oligomers that can diffuse into synaptic clefts, hints at that such soluble assembly forms are better candidates for inducing neuronal and/or synaptic dysfunction than plaques [112].
However, large plaques of fibrillar Aβ in AD brains typically show surrounding dystrophic neurites, indicating that insoluble aggregates might also contribute to neuronal injury. The problem is that large, insoluble protein aggregates are likely to be intimately surrounded by a number of smaller, more diffusible, assemblies (for example, monomers or oligomers) [96]. Thus, it becomes difficult to establish if the large aggregates are directly inducing local neuronal injury and dysfunction.

[2] An isoform is a member of a family of highly similar proteins that have a similar but not identical aminoacid sequence.

Another major role in neurodegenerative diseases (including Alzheimer's) is played by tau protein, which is found within the neurons in homeostatic conditions, where it is instrumental in the assembly of tubulin into microtubules and the subsequent stabilization of their structure . Interestingly, the role of tau protein in AD caught on in the scientific community later with respect to the beta-amyloid [102]. It is currently assumed that, in pathological conditions, tau protein undergoes hyperphosphorylation, loses its stabilizing function, and eventually aggregates into neurofibrillary tangles (NFTs) [71], [6].Importantly, a significant link between tau protein and Aβ has been unveiled, as the latter is able to enhance the phosphorylation of monomeric τ, possibly through the action of enzyme GSK3 (see [6], [7], [8]). More precisely, there is evidence that an excess of activity of enzyme GSK3 accounts for tau hyperphosphorylation and increase β-amyloid production [54]. Further information about biological facts concerning tau protein will be provided in Chapter 1 and 2 of the thesis.

As a matter of fact, neurodegeneration is a complex process in which several molecules are involved and often interact with Aβ or tau protein in ways that are only partially understood. A particular exampIe of such interaction concerns the modification of protein topology. In general, proteins function properly when their constituent aminoacids are correctly folded. However, proteins may undergo changes in their structure, when protein folding takes place in abnormal ways (misfolding). This process is often associated with the change of a physiological function to a pathological one. In particular, such molecules may become toxic and start aggregating in longer clusters. In addition, they interact with native [3] proteins, to catalyze their transition into a toxic state. The newly formed toxic proteins can repeat this cycle to initiate a self-sustaining loop [5].
For instance, PrP is a chromosomally-encoded protein that can exist in multiple isoforms. The most common are the normal PrP^C and the pathologic PrP^{Sc}. Differences among isoforms concern protein structure which, in case of the PrP^{Sc}, is related to toxic effects. Indeed, PrP^{Sc} is linked with a variety of diseases like the bovine spongiform encephalopathy etc., and shows the so-called prion property that consists in spreading the disease-associated form by inducing other protein of the same type to adopt a similar geometrical conformation [103].
Recent findings suggest that there may be a relationship between Alzheimer's disease and PrP^C protein [60], [13]. More precisely, the latter has been reported to mediate the neurotoxic effect of Aβ oligomers. In fact, PrP^C exhibits high capacity to bind

[3]The form in which a protein folds naturally is said native state

to Aβ and modulate the inhibitory effect of Aβ oligomers on the synaptic plasticity with consequent impairment of memory and cognitive functions [75]. In addition, the binding of soluble amyloid to PrP^C can activate several biochemical processes that result in the promotion of tau phosphorylation, underlining the prion connection that links together the two hallmark pathological events in AD [73].

Interestingly, there is evidence that also aggregated Aβ or tau possesses prion-like activity [102].

Possible mechanisms underlying the assembly of tau and β-amyloid in oligomers and the subsequent spreading of the pathological isoform alike to misfolded PrP, have been proposed to follow the above described scheme [60]. In fact, it seems that the acquisition by the Aβ of a particular, non-homeostatic structure during the process of folding, is responsible of aggregation in clusters and toxicity [95]. On the other hand, as regards tau protein, hyperphosphorylation is the triggering event of a series of processes, including changes in the structure of the molecule, that lead tau to become pathological and to polymerize [6], [102]. Further details about misfolding and aggregation of tau protein will be provided in Chapter 1.

Another protein involved in neurodegeneration is Apolipoprotein E (ApoE). Its physiological function is related to the transport of cerebral cholesterol and it is present in brain tissue in different isoforms. The most common are: e2, e3 and e4; among these, ApoE e4 represents the main genetic risk factor for AD, while ApoE e2 is associated with the lower risk [68]. This can be due to structural differences among isoforms, that are responsible of the reduction of stability of e4 (compared to other isoforms) and increase its ability to interact with lipid and cell membrane. Studies suggest that Apolipoprotein E is involved in the clearance of beta amyloid [68], [69]. In fact, it seems that ApoE-containing lipoprotein particles may sequester Aβ and modulate the cellular uptake of an ApoE-Aβ complex or, alternatively ApoE may modulate Aβ removal from the brain to the systemic circulation by transport across the blood-brain-barrier [69]. Experimental evidence hints at that ApoE e4 is less efficient in clearing amyloid compared to other isoforms [117].

In addition, it seems that the amount of cholesterol in the neuronal membrane is linked to the production of the toxic isoform Aβ_{42} [122]. High quantities of cholesterol are associated with an increase of enzymatic activity that gives rise to Aβ_{42}. ApoE e4 seems to be less efficient to clear excess of cholesterol compared with other ApoE

isoforms [22] and therefore that molecule might be responsible of a rise in the production of harmful Aβ_{42} in neurons. On the other hand, it has been observed that the level of ApoE in brain increases following neuronal injuries [68]. Hence, it has been hypothesized that ApoE can contribute to neurological healing by redistributing lipids and cholesterols for membrane repair and synaptic plasticity. Furthermore, *in vivo* and *in vitro* studies reveal that ApoE e3 augments synaptic plasticity and exerts neurorepair effects more efficiently than ApoE e4 [4]. Finally, there is evidence that ApoE e4 molecule may interact with tau protein and contribute to tau phosphorylation [33].
From a macroscopic point of view, the result of the above-mentioned pathological processes is cerebral atrophy, i.e. a loss of neurons and synapsis in the cerebral cortex and in some subcortical regions with the consequent reduction of the volume and loss of function of the affected areas.

We next discuss briefly on the approach followed in this memoir. In recent years there has been a considerable interest in the mathematical modeling of biomedical problems such as tumor growth ([110], [19] [100],[62]) and cardiovascular diseases ([67], [66], [108], [107] etc). However, comparatively less effort has been devoted to modelling neurodegenerative diseases as AD (see for instance [27], [109], [20]). In fact, when dealing with medical disorders as Alzheimer´s disease, one has to face what represents a central problem in mathematical modelling in biomedicine. Specifically, one has to decide what is the purpose of the model to be eventually produced, and what is the role of experimental data in the modelling process. We will shortly elaborate on these issues in the sequel.
Concerning data, these could be retrieved from *in vitro* experiments or *in vivo* measurements, or can be extracted from the biomedical literature available. Data from *in vitro* experiments are comparatively easier to obtain although they frequently are not representative of the complex environments of proteins in living tissues. On the other hand, realistic and accurate measurement *in vivo* are difficult to obtain due to ethical, medical and technological reasons. It is precisely for these reasons that *in silico* experiments, that is the formulation, analysis and simulation of carefully chosen mathematical models, are important. Such models can be used to test preliminary new theories, quickly discerning the most relevant hypotheses or rejecting those less likely to lead to new insights. Therefore, the mere reproduction of already known facts, which is certainly a preliminary quality control test for any biomedical model, is just a starting point and not the main goal to be pursued. What we retain important indeed is that

modeling could suggest new insights on the dynamics of the biological process considered that are not easily arrived at by other means. Furthermore, models should have a predictive value, including the possibility of designing experiments that could prove (or disprove) the validity of the hypotheses made, as well as that of the conclusions obtained.

We next discuss on the models presented in this thesis. At the mathematical level, we will deal with processes involving mass transfer and aggregation taking place in undirected graphs. Specifically, we shall be concerned with polymerization processes represented by Smoluchowski–type equations ([118],[119],[80]) coupled with polymer transport along the edges of given graphs. The use of graphs as underlying space structures represents a substantial change with respect to classical results in polymerization theory as those recalled before, as well as with recent models related to Alzheimer's diseases like [1], [10], [36], [37]. In particular, in these latter works, Smoluchowski's equations with diffusion defined in the usual continuous setting were considered to describe the process of agglomeration and diffusion of beta amyloid in AD.

The aim of this thesis is to present and analyze two models concerning disease-associated processes involving tau protein based on Smoluchowski-type equations on a finite graph. More precisely, the focus is on the transport and coagulation of hyperphosphorylated tau protein in human brain, first into fibrils and eventually up to neurofibrillary tangles which, according the current biomedical literature, are relevant steps in the onset and progression of the AD (although there is still no general agreement on whether their role is detrimental or beneficial for brain cells; see, for instance, [76]).
In the first model, the formation of tangles is postulated to occur when clusters 'length exceeds an a priori established critical threshold, while in the second model the same phenomenon is associated with the onset of a gel state in a phase transition. In both situations, the finite graph is conceived as a theoretical approximation of the human brain, where each vertex represents a cerebral area of interest and the connections between them are provided by the edges.

The contents of this thesis can be summarized as follows.

In Chapter one, we present a model for the aggregation and transport of hyperphosphorylated tau protein based on a finite dimensional Smoluchowski-type system on finite weighted graph. The aim here consists in reproducing tau patterns in diseased

brain obtained through suitable in vivo measurements.

To this purpose, we follow [91], where a cerebral network is empirically built through a medical and computational study. To that end, functionally homogeneous brain regions and suitable measurements of the connectivity between them were extracted from a dataset of healthy subjects' MRI. However, differently from [91] in which the focus is on studying the progression in the brain of a generic so-called disease factor, our work is concerned with the role of phosphorylated tau oligomers in the development of AD.
In order to test whether the proposed model is able to predict the spatiotemporal evolution of tau oligomeric species and tangles, we postulate that the regions and the connections of the empirical network under consideration correspond respectively to the vertices and the edges of the graph in which the equations for diffusion and agglomeration of tau protein are considered. In this way, the model-predicted tau concentrations (in monomeric, oligomeric form and in tangles) in each vertex of the network can be compared with empirical data on the cerebral region associated with that vertex and consisting in tau measurements in AD patients provided by *in vivo* neuroimaging and in cortical atrophy data. The latter come from the public Alzheimer's Disease Neuroimaging Initiative (ADNI), while tau patterns' imaging data emerge from a study at Yonsei University, South Korea (see [37]).

Statistical analysis is performed between the two pairs of data samples (model-predicted tau against empirical tau and model-predicted tau against cortical atrophy data). On the grounds of such study, we are able to propose that our model for hyperphosphorylated tau protein is able to replicate tau patterns measured in AD brains during the course of the disease.

These results come from a collaboration with professor Ashish Raj of University of California at San Francisco and a group of Korean researchers: Hanna Cho, Jae Yong Choi, Young Hoon Ryu, Chul Hyoung Lyoo, and are currently being prepared for publication.

In chapter two, the beta amyloid hypothesis in the formation of neurofibrillary tangles (NFTs) is discussed in a particular setting. Specifically, we assume that beta amyloid acts as a source of aggregation of tau monomers, which in turn coagulate according to specific rates characteristic of classical polymerization problems. The overall process is described in terms of infinite dimensional Smoluchowski-type systems

(including mass transfer and monomers production) on a finite weighted graph. This kind of systems (without monomers injection) have been introduced in the field of Chemical Engineering with the classic work [99] and their mathematical properties have been actively studied in recent years; see, for instance, [86] and [80]. In the latter work, the problem of characterization of sol-gel phase transition in a open bounded subset of the euclidean space $\mathbb{R}^N$ is considered. In this thesis, instead, the spatial domain of our model is a finite graph, that is considered a suitable approximation of the human brain.

The main contribution of this study consists in the proof, under suitable choices of coagulation coefficients, of the occurrence of a sol-gel phase transition in finite time that is associated with a loss of regularity of the solution. We further suggest that this transition can be understood as the onset of NFTs. The way in which this phase transition is identified can be succinctly summarized as follows. We first show that, for sufficiently small times, the polymerization process occurs in a smooth way, characterized by the existence of classical solutions and the steady increase in total mass of tau polymers, the latter resulting from the beta amyloid source term. However, after some time has elapsed, a sharp decrease in the total mass is detected, and upper and lower bounds for the time at which this occurs (the so-called gelation time) are provided. Finally, we prove the blow up in finite time of the second moment of the solution of our system, a standard test in detecting the onset of gels in polymerization problems. From a biological point of view, we deem the onset of a gel to be a suitable tool for the description of the formation of neurofibrillary tangles. We retain that this approach could open new interesting perspectives concerning the role of NTFs in neurodegenerative disorders.

We conclude this work with an Appendix, where we provide an overview of about graph Laplacian and its main property, focusing on the known results that we use in the proofs of this thesis.

Chapter 1

A combined model for the aggregation and diffusion of τ protein in Alzheimer's Disease

In this chapter we present a mathematical model for the aggregation and transport of *tau*-protein in Alzheimer's disease. The model is object of the paper *A combined model for aggregation and network diffusion in Alzheimer's disease recapitulates regional human tau-PET patterns*, whose authors are Ashish Raj, *Department of Radiology and Biomedical Imaging, University of California at San Francisco*, Veronica Tora *University of Bologna*, Hanna Cho, *Department of Neurology, Gangnam Severance Hospital, Yonsei University College of Medicine*, Jae Yong Choi, *Department of Nuclear Medicine, Gangnam Severance Hospital, Yonsei University College of Medicine*, Young Hoon Ryu, *Department of Nuclear Medicine, Gangnam Severance Hospital, Yonsei University College of Medicine*, Chul Hyoung Lyoo, *Department of Neurology, Gangnam Severance Hospital, Yonsei University College of Medicine*, Bruno Franchi *University of Bologna*.

In that work we investigate the process of aggregation of tau protein in human brain, that takes place at microscopic level, as it occurs inside the neuron, and subsequent spreading of aggregated tau from one cerebral region to another. The latter is a macroscopic process, as it regards the entire brain network.

Thus, we unify the macroscopic and microscopic scale in a single model capable of predicting the spatio-temporal evolution of tau oligomers and tangles in human brain affected by AD, due to the fact that it is comparable with τ patterns in diseased brain and MRI-derived atrophy, obtained from *in vivo* human neuroimaging data. That work will give further support to the central role of τ protein in AD and can be used to

understand the etiology and the mechanism of progression of neurodegeneration.
The contribution of the authors can be summarized as follows:
Raj, Franchi and Tora conceived the study, developed the model and wrote the paper; Raj implemented the model, validated on human imaging data, generated results, performed statistical analysis; Cho, Choi, Ryu, Lyoo performed human imaging, study enrollment, consenting, image processing, quality checks, helped improve the manuscript.

1.1 Biological setting and related litterature

Alzheimer's disease (AD) is characterized by widespread and progressive deposition of amyloid beta protein in cortical plaques and of protein tau in tangles [11, 104]. Several alterations of such proteins from their native form and their aggregation (first in soluble oligomers, then in insoluble fibrils) have been proposed as prime initiator and cause of several neurodegenerative conditions [12].
Studies assert that the process of plaques formation starts with increased concentrations of Aβ that gradually lead to oligomerization and ultimately to creation of amyloid deposits [113], [48]. Modifications in structure of Aβ, rather than its sequence of aminoacids, play the principal role in Aβ-induced toxicity [16].
According to a general setting, the typical driving force in protein aggregation is believed to be destabilization of the native protein to yield a population of partially folded intermediates with increased aggregation propensity [42]. One of the first biophysical models of this process was the "heteromer" model of Pruisiner and colleagues [89], followed by nucleated polymerization (NPM)[81].
Protein structural change is typically described as "monomer activation" [83]. Subsequent fibrillation follows a nucleation-elongation process [94, 42].
Such model for protein aggregation has been proposed for several diseases involving protein misfolding, included, for istance, the β-amyloid in AD [94]. Two phases have been identified in protein aggregation: a lag (nucleation) phase followed by an elongation phase. In the initial lag-phase misfolded monomers start to form small olygomers when a critical concentration is exceeded within the local environment to provide an ordered nucleus to catalyze the further growth of the polymers by providing a template for fibril growth during the more rapid elongation phase. Once the nucleus has developed, it provides a seed for the growth of larger, fibrillar aggregates which in turn associate into mature fibril-like structures [94, 42].
Studies in cells culture and on transgenic AD mice support the view that amyloid

aggeregation and deposition take place according to the above described seeding process similar to molecular templating of prion proteins [64].
The protein aggregation literature is extensive. As regards the $A\beta$ protein, numerous recent reviews describe our current understanding of amyloid fibril structure [94, 28], mechanism of toxicity [113, 28] and the aggregation process [115]. An excellent overview of historical contributions to kinetic and thermodynamic descriptions of protein aggregation are given by Morris et al [83], and several current mathematical models of protein aggregation were reviewed in [42]. Although mathematical models of protein aggregation have been explored in related prion disease [94, 83], they have hitherto been scarce in Alzheimers's and dementia - but see [84, 1, 42, 10, 36, 37] and a thorough review [14]. Since aggregation models involve detailed reaction kinetics, their parameters are typically learned from *in vitro* aggregation experiments.
Recent researches suggest that processes of misfolding with subsequent prion-like spreading of the pathological alterations and aggregation affect also τ-protein [60].
The latter is abundant in neurons of the central nervous system and less common elsewhere. Its physiological function is related to the regulation of the stability of the axonal microtubules by promoting the assembly of tubulin. Studies reveal that monomeric tau protein is a soluble natively unfolded protein with low capacity to form filaments *in vitro* [102]. However, in disease conditions, the microtubule-associated tau protein undergoes a series of alterations including hyperphosphorylation and structural modifications; thus, its capacity to perform its stabilizing function is prejudiced and the misfolded protein starts diffusing through the neuronal pathways and to coagulate, first in longer polymers and then in the form of insoluble fibrils into so-called *neurofibrillary tangles*. Neurofibrillary τ tangles appear first in locus coeruleus, then entorhinal cortex, then spreads into hippocampus, amygdala, temporal lobe, basal forebrain and association areas, in that order [11]. A wealth of evidence suggests that metastable, soluble oligomers formed early in the aggregation process and small fibril fragments are the predominant toxic species. Further details on the process of tau phosphorylation and tangles' formation will be provided in Chapter 3.
However, at the current state of research, the cause-effect mechanisms by which various oligomeric τ species are produced, aggregate and disseminate, and how they cause neurodegeneration and symptomatology, are not completely known. Many important questions in AD research remain unresolved: how does protein aggregation and subsequent spread lead to stereotyped progression in the AD brain? Why do misfolded τ oligomers selectively target certain specific structures? Can mathematically precise models that describe these processes recapitulate *in vivo* measurements in human

brains? Despite advent of biophysical models of protein aggregation, it remains unknown whether they are capable of recapitulating human disease *in vivo*. Most previous aggregation models were restricted to local processes, without accounting for spatial or network spread. Some early work was done to incorporate classical spatial diffusion in prion aggregation models [87], in truncated Smoluchowski equations [10] and in NPM model [82]. The latter in particular also explored a kind of network spread, but relied on "toy" connectomes and did not compare model outputs to real *in vivo* data [82]. A network model loosely based on protein aggregation as a process of epidemic spread was proposed and validated on amyloid PET data of AD patients [59].

1.2 Introducing a novel joint Aggregation-Network-Diffusion model

In this chapter we develop and empirically validate the mathematical machinery capable of encapsulating the entire gamut of neurodegenerative etiology and progression, using bottom-up biophysical modeling. We propose a parsimonious model of all three processes: τ monomer production; subsequent aggregation into oligomers and then into tangles; and the spatiotemporal progression of misfolded τ as it ramifies into neural circuits. We hypothesize that this model, which we call Aggregation-Network-Diffusion (AND) model, can explain many experimental findings in AD. The model incorporates the following key elements, based on experimental evidence:

- Initial production of misfolded monomeric τ occurs at a specific site in the medial temporal cortex, especially the entorhinal cortex, based on histopathology findings from Braak [11].

- Monomeric τ progressively aggregates into dimers, oligomers, and finally into immobile fibrils, giving neurofibrillary tangles. Each oligomeric species has a different propensity to aggregate and to spread.

- Subsequent spread of above protein species is modeled by a (potentially directional) transmission process whereby anatomic connections govern the rate at which two distant but connected brain regions might transfer pathologic entities. The pathological underpinnings of networked spread are given by "prion-like" trans-neuronal transmission, whereby proteins misfold, trigger misfolding of adjacent same-species proteins, and thereupon cascade along neuronal pathways

[17, 38, 56, 65]. Trans-neuronal transmission implies spread along axonal projections rather than spatially. Hence networked spread is a natural model, as substantiated by neuroimaging [88, 91, 92, 125, 59].

Using these facts we formulate the AND model that is capable of predicting the spatiotemporal evolution of AD-associated τ in human brains, separately resolving the progression of all oligomeric species as they aggregate, spread and deposit in brain regions. Following the model studied in [1], [10], [36], [37], we describe the aggregation of τ polymers by means of Smoluchowski equation [98], a system of infinite discrete differential equations (without diffusion) for the study of rapid coagulation of aerosols. Smoluchowski's theory was previously extended to cover polymerization, aggregation of colloidal particles, formation of stars and planets as well as biological populations and behavior of fuel mixtures in engines. Smoluchowski equation was successfully applied to the agglomeration of $A\beta$ amyloid first in [84] and then in [1]. We combine Smoluchowski aggregation theory, applied here to τ oligomers, with a mathematical model of their trans-neuronal spread. For the latter purpose, we extend the previous Network-Diffusion model [91, 92], which was shown to recapitulate the classic spatial patterns of AD-related atrophy. This model approximates the trans-neuronal transmission of misfolded proteins as simple diffusive spread along axonal projections. Hence, the proposed AND model combines these elements into a complete model of τ progression in AD, starting from a healthy brain with no pathology.

We hypothesize that this model will recapitulate not only the spatiotemporal evolution of τ, but also predict the time course of the evolution of various oligomeric species. We implement the AND model on brain "connectomes" or connectivity networks obtained from healthy subjects' diffusion-weighted MRI, and validate it against empirical data from AD patients' regional atrophy and tau-PET scans. We evaluate several formulations of how the kinetics of protein aggregation and network diffusion varies according to oligomer size, and show that for each formulation, there exist parameter ranges within which the AND model recapitulate empirical spatio-temporal patterns of AD.

To our knowledge, this is the first report of an empirically-validated complete biophysical model of both protein aggregation and trans-neuronal spread in Alzheimer's disease. Such mathematical models can serve as critical test-beds for assessing etiologic and mechanistic hypotheses of neurodegeneration, and can be tested directly on *in*

vivo neuroimaging data. Clinically, this approach might serve as a computational biomarkers of τ progression in patients.

1.3 Description of the model

In this work, we combine network diffusion and Smoluchowski aggregation theory into a complete model of AD-associated and progression, starting from a completely healthy brain with no pathology to begin with. We propose to model jointly the network-wide ramification of τ , whose production and network dissemination are two separate processes. Since we are interested in expanding the aggregation processes to include graph-based diffusion, we will replace the spatial diffusion term in the eq. (1.9) in Appendix 1.8.1 with a graph diffusion process. We denote by $\tau_m(x_i, t)$, the molar concentration of soluble τ polymers of length m at i-th vertex x_i (i.e at the i-th grey matter structure) at time t, with $1 \leq m < M$ and $i = 1, \ldots, h$. The concentration of clusters of oligomers of length $\geq M$ (fibrils) is denoted by $\tau_M(x_i, t)$ and may be thought as tangles, clinically observable throughT807-PET [120] or AV1451-PET [49] or MRI-derived regional atrophy [111, 116]. We will also cap the infinite series (1.11) in Appendix 1.8.1 to a realistic scenario whereby once aggregates reach a certain size they become tangles and exit reaction kinetics. Finally, we will lump nearby aggregate sizes into a smaller number of "bins" in order to reduce the equations to a manageable number. These choices are described in detail in the next section.

The proposed model has the following components:

(a) Initial intra-cellular phosphorylation of τ produce monomeric misfolded τ, mislocating from its native axonal compartment to pathologic somatodendritic intra-cellular compartment. In this paper the sites of monomeric τ production are predetermined, based on extensive bench studies, to be located at the entorhinal cortex.

(b) Misfolded τ monomers undergo *in situ* agglomeration into small oligomers and progressively into tangles, which are assumed to be immobile and non-participants in the ongoing aggregation processes.

(c) These production and aggregation processes are followed by Network-wide transmission of the misfolded oligomeric τ proteins as they ramify through the neural pathways via trans-neuronal transmission [17, 38, 56, 65]. The spread process is modeled here via the Network Diffusion Model [91, 92]. Diffusivity of each oligomer species is allowed to be different, controlled by the diffusivity constants d_m for the m-th oligomer.

Fist of all, following the approach proposed in [91], we represent the human brain by means of a finite weighted graph $G = \{V, E\}$, in which the vertices $x_i \in V = \{x_1, .., x_h\}$ represent the i-th cortical or subcortical gray matter structure, while the edges $e_{i,j} \in E$ represent the connections by white-matter fiber pathways between the i-th structure and the j-th structure. Coherently, we introduce a family of coefficients $w_{i,j} > 0$ that measure "how much" the i-th structure and the j-th structure are connected. The coefficients $w_{i,j}$ are said the "connectivity weights" of the graph G. In this way we build a "brain network" in which the vertices x_i comes from the parcellation of brain MRI and the connectivities $w_{i,j}$ are measured by fiber tractography (see section 1.4.1). On this graph we define the so called graph Laplacian Δ_G denoted as the *positive* standard weighted Laplacian associated with the graph G, whose formal definition is given in section 3.2.2 of Appendix 1.
In addiction, an introduction to the Laplace operator on graphs, as well as its main properties can be found in Appendix 1.

Let us see, now, how the components (a) – (c) reflect in our mathematical model.

(a-b) We denote by $\tau_m(\cdot, t) : V \to [0, \infty)$ the molar concentration of misfolded τ-oligomers of length $m = 1, \ldots, M-1$ at the time $t \geq 0$. In addition, $\tau_M(\cdot, t) : V \to [0, \infty)$ will design the concentration of τ-tangles.

The production of monomeric misfolded τ will be represented by the source term f_τ, with

$$f_\tau(\cdot, t) : V \to [0, \infty)$$

for $t \geq 0$, where $f_\tau(x_j, \cdot)$ is a continuous function for all $j = 1, \ldots, h$. In this study we chose the production term to be a Gamma-shaped function $f_\tau(\cdot, t) = \frac{t}{\sigma_f} \exp\left(-\frac{t}{\sigma_f}\right)$, and chose $\sigma_f = 15$ to approximate a 15-year monomer production process - an arbitrary but realistic choice based on the expected time course of AD progression.

(c) Diffusion and agglomeration of oligomers through neural pathways is described by a Smoluchowski system with diffusion in G. For the sake of universality and parsimony, we assume that throughout the brain the protein species aggregate and ramify along neural pathways in the same way and at the same rate. However, it is well known that rates of trans-membrane diffusion, axonal transport and aggregation are all dependent on protein species and oligomer length. Hence we impose a simple scaling behavior on these processes such that the aggregation is controlled by the joint aggregation constants a_{mj} for oligomers of size m and

j aggregating to form a oligomer of size $m + j$. Here, we use two plausible expressions for a_{mj}: (1) based on thermodynamic arguments,

$$a_{mj} = \frac{\sigma_{agg}^2}{mj}$$

and (2) based on empirical in vitro fitting data on amyloids, a Gamma-shaped expression [42]

$$a_{mj} = \frac{mj}{\sigma_{agg}^2} \exp\left(-\frac{mj}{\sigma_{agg}^2}\right),$$

where the σ_{agg} is a positive constant that controls the scale of the Gamma function for aggregation. Assumption (c) above (tangles are non-participants in the ongoing aggregation processes) reads as $a_{m,M} = 0 \ \ \forall m$. Based on similar arguments, we define a scaling behavior of the diffusivity rates as:

$$d_m = 1/m \qquad \text{and} \qquad d_m = \frac{m}{\sigma_{diff}} \exp\left(-\frac{m}{\sigma_{diff}}\right).$$

where σ_{diff} is a scale parameter. Since by assumption (c), tangles are assumed to be immobile, hence the diffusivity rate of τ_M should vanish; here, instead of imposing a hard constraint, we rely on the above Gamma functions to ensure that at large m the diffusivity rate decays to close to zero.

We can now write extensively the system satisfied by $\tau = (\tau_1, \ldots, \tau_M)$.

The evolution of the concentration of τ is described by Smoluchowski equations on G.

If $t \geq 0$ and $x_i \in V$, $i = 1, \ldots, h$, then the equation for monomers is

$$\frac{\partial \tau_1(x_i,t)}{\partial t} = -d_1 \Delta_G \tau_1(x_i,t) - c_1 \tau_1(x_i,t) \sum_{j=1}^{M} a_{1,j} \tau_j, (x_i,t) + c_2 f_\tau(x_i,t), \tag{1.1}$$

where Δ_G denotes the *positive* weighted Laplacian associated with the graph G, d_1 is the diffusivity constant for $m = 1$, and c_1, c_2 are two positive constants that control the relative rates at which network diffusion is related to aggregation and monomer production, respectively.

The equation for polymers is

$$\frac{\partial \tau_m(x_i,t)}{\partial t} = -d_m \Delta_G \tau_m(x_i,t) + c_1 \left[\frac{1}{2} \sum_{j=1}^{m-1} a_{j,m-j} \tau_j(x_i,t) \tau_{m-j}(x_i,t) - \tau_m(x_i,t) \sum_{j=1}^{M} a_{m,j} \tau_j(x_i,t)\right] \tag{1.2}$$

for $1 \leq m < M$ and $x_i \in V$, $i = 1, \ldots, h$.

Finally, the evolution of tangles is described by the equation

$$\frac{\partial \tau_M(x_i,t)}{\partial t} = \frac{c_1}{2} \sum_{j+k \geq M; k,\, j<M} a_{j,k} \tau_j(x_i,t) \tau_k(x_i,t). \tag{1.3}$$

where $x_i \in V$, $i = 1, \ldots, h$.

Equations (1.1), (1.2), (1.3) must be associated with initial data at $t = t_0$. We assume that $\tau_m(x_i, t_0) = \tau_{0,m}(x_i)$ for $1 \leq m \leq M$ and $x_i \in V$, $i = 1, \ldots, h$.

A brief review on Smoluchowski aggregation theory can be found in section 1.8.1.

The actual numbers of oligomer length of τ are under study and a range of plausible values have been proposed, typically 20 to 40. It is not necessary for the purpose of understanding the aggregation and diffusion dynamics to consider such a large number of oligomer length. Hence for the sake of computational load and interpretability, here we have lumped oligomers into only 5 bins, such that m can take the following values: 1 (monomer), 2, 3, 4, and 5 (tangle). Each of these values should be considered a lumped average of several adjacent lengths, such that, for example, $m = 4$ can be considered to be an average of oligomers of length 30 to 40.

1.4 Methods

1.4.1 Extracting anatomic connectivity graph

Connectomes were extracted from a dataset of healthy subjects' structural MRI (T1) and diffusion-righted MRI (dMRI) scans acquired under a previous study at our institution. This connectome cohort consisted of 69 subjects. The diffusion weighted MRI (dMRI) data were processed with a custom pre-processing connectomics pipeline following [72, 92]. This study design, where the connectivity graph is extracted from healthy rather than AD subjects, allows us to test the proposed graph-based model in a manner that is not affected by impaired anatomic connectivity frequently seen in AD patients. This processing pipeline is well established in our laboratory. In short, T1 images were normalized into MNI space and segmented using the Freesurfer software tool [34] using their unified coregistration and segmentation scheme. Using the Desikan-Killarney atlas with 86 hand-labeled parcellated regions [23], the subject-specific T1 images, after coregistration and segmentation, were parcellated into 86 regional volumes corresponding to 68 cortical and 18 subcortical structures covering the entire cerebral gray matter.

The dMRI data was processed using spherical deconvolution to yield orientation distribution functions in each voxel. The resulting output was fed into a probabilistic fiber tracking algorithm, to produce fiber tracts in terms of streamlines. Details of the connectome data acquisition and processing pipeline can be found in [72]. Each voxel at each region's gray-white interface was seeded with 100 streamlines and the resulting tracts were traced probabilistically. A streamline count was kept for every pair of brain regions. The number of streamlines found to go from region i to region j and vice versa, were averaged and this value was recorded as the connectivity $w_{i,j}$ between the two regions. The full connectivity matrix was then formed as per $W = \{w_{i,j}\}$. Connectivity matrices from individual healthy subjects were found to be largely similar, and a mean over all subjects was taken in order to obtain a canonical healthy connectivity matrix W, which was used in all subsequent analysis.

1.4.2 AD subject scans

Imaging data used in this study was obtained from two sources: the public Alzheimer's Disease Neuroimaging Initiative (ADNI); and a previously published study at Yonsei University, South Korea, whose details are contained elsewhere [49]. In brief: 128 consecutive patients (53 patients with probable AD dementia, 52 patients with amnestic mild cognitive impairment, aMCI; and 23 patients with nonamnestic MCI, naMCI) were prospectively recruited after clinical diagnosis at the Memory Disorder Clinic of Gangnam Severance Hospital. Sixty-seven age-matched cognitively normal volunteers were included as healthy controls (HCs). All participants underwent 2 PET scans (18F-florbetaben for $A\beta$ and 18F-AV1451 for τ pathology), high resolution T1-weighted brain MRI, and neuropsychological tests. This study was approved by the institutional review board of the Gangnam Severance Hospital, and written informed consent was obtained from all participants. All PET images were acquired using a Biograph mCT PET/computed tomography (CT) scanner (Siemens Medical Solutions, Malvern, PA). Subjects were intravenously injected with 281.2MBq of AV1451 for tau PET and 297.9MBq of florbetaben for amyloid PET. Prior to the PET scans, a head holder was applied to minimize head motion and brain CT images were acquired for attenuation correction. At 80 minutes after the injection of AV1451 and at 90 minutes after the injection of florbetaben, PET images were acquired for 20 minutes. After correcting for attenuation, scatter, and decay, PET images were finally reconstructed with the ordered subsets expectation maximization algorithm in a $256 \times 256 \times 223$ matrix with $1.59 \times 1.59 \times 1$ mm voxel size. Axial T1-weighted brain magnetic resonance (MR) images were obtained with 3D spoiled gradient recalled sequences: repetition time

8.28 ms, echo time 1.6 to 11.0 ms, flip angle 20, matrix size 512×512, voxel size $0.43 \times 0.43 \times 1$ mm in a 3T MR scanner (Discovery MR750; GE Medical Systems, Milwaukee, WI).

ADNI is a public-private private, large multisite longitudinal study with the goal of tracking Alzheimer's disease biomarkers and accelerate prevention and treatment of the disease. The ADNI data used here consisted of early and late MCI (EMCI and LMCI, resp.) and AD groups, and included all ADNI 2 and ADNI GO subjects from early 2011 to mid–2015. Demographics and imaging details are contained in our previous publication [105]. MRI-derived group atrophy patterns were obtained for each of the EMCI,LMCI,AD groups in the ADNI study. After Freesurfer processing and quality checks, a total of 117 AD subjects, 156 LMCI and 148 EMCI subjects were available for this study.

1.4.3 Regional volumes and PET tracer uptake

Individual AD and MCI subjects' T1-MRI scans were processed using the Freesurfer tool to obtain the 86-region gray matter parcellation described above. From each parcellated region, regional volume (number of voxels) and thickness (number of vertices) was recorded. Subjects' AV1451-PET data, an empirical measurement of regional τ, were processed in the same way, as follows. PET images were resampled to uniform voxel resolution, normalized to the same common space as the Desikan atlas, and the latter's regional parcellations applied to the former. For each region, the average of voxel-wise PET uptake was recorded. Regional PET uptake values were divided by cerebellar PET uptake value in order to normalize each subject's PET uptake.

1.4.4 Description of the statistical analysis and model validation on empirical neuroimaging data

We applied the AND model on the 86×86 connectivity matrix described above. The starting pattern of tau was set to zero everywhere except a single "seed" region. AND model was numerically solved using MATLAB's *ode45* solver, which implements a numerical integration technique using Euler iterations of order (4,5). The time increment was set at 0.01. The simulation data were compared against empirical imaging-derived regional data (Korea cohort for tau-PET and ADNI cohort for atrophy), each of size $86x1$. The metric of validation was the Pearson's correlation statistic R and its associated p-value. We note that, for rigorous definitions about the statistical methods

used in that work, we address to section 1.8.2.
The AND model would be considered validated if, for some combination of model parameters, it is strongly correlated with regional pattern of group atrophy and/or tau uptake, at significance of $p < 0.05$. Since the current thrust is on model development, minute or rigorous parameter fitting was not attempted. Instead, we selected model parameters by a simple grid search technique, and evaluated the AND model at all model time values, recording only the best Pearson's R over model time. Our goal was to show that there exists a reasonable range of parameter choices and other model choices that results in strong match to empirical data. For instance, we evaluated several formulations of how the kinetics of protein aggregation and network diffusion varies according to oligomer size, i.e. d_m and $a_{m,j}$ defined above, giving 4 possible models. We ran model simulations across these various aspects and over a large range of model parameters. Without further detailed reaction kinetic data these formulations must be considered as heuristic choices at this stage.

1.5 Results

1.5.1 Mathematical proofs

The proposed aggregation-network diffusion (AND) model combines previously available but disparate ideas. Therefore, in light of its novelty, first we prove various results involving the AND theory, consisting in the fact that the proposed model has various desirable properties like existence and uniqueness of solutions, and boundedness of their values.

We notice that the system for $\tau = (\tau_1, \dots, \tau_M)$ is nothing but a system of MN ODEs for the MN unknown functions $\tau_m(x_i, \cdot)$, $i = 1, \dots, N$, $m = 1, \dots, M$.

Classical Peano-Picard-Lindelöf theorem (see [50], Chapter 2) guarantees the existence of a maximal solution in $[t_{min}, t_{max}]$ for the system (1.1)–(1.3) with Cauchy data at $t = t_0$. The following lemma states that, if the components of the solutions are strictly positive at $t = t_0$, then they remain strictly positive as long as they exist.

Lemma 1.5.1. *If $\tau_m(x_i, t_0) > 0$ and $f_\tau(x_i, t) > 0$ for all $x_i \in V$ and for $1 \le m \le M$, the maximal solution of the system (1.1), (1.2), (1.3) is positive on all the interval of existence, i.e. $\tau_m(x_i, t) > 0$ for $t_{min} < t < t_{max}$ for all $x_i \in V$ and for $1 \le m \le M$.*

Proof. Suppose by contradiction the statement fails to hold, and set

$$t^* = \sup\{t \in (t_0, t_{max}), \tau_1(x_j, t) > 0 \; \forall \; x_j \in V\} < t_{max}.$$

We claim that there exists a vertex $\bar{x}_j$ such that $\tau_1(\bar{x}_j t^*) = 0$. In fact, if $\tau_1(x_j, t^*) > 0$ for all $x_j \in V$, we would have $\tau_1(x_j, t) > 0$ for all $x_j \in V$ and for $t^* < t < t^* + \delta$ (since the number of vertices is finite). This contradicts the definition of t^*. Moreover, if $\tau_1(x_j, t^*) < 0$ for all x_j, for the same reason we would have $\tau_1(x_j, t) < 0$ for all x_j and for $t^* - \delta < t < t^*$, yielding again a contradiction.

Let us show now that $\frac{\partial \tau_1}{\partial t}(\bar{x}_j, t^*) \leq 0$. Arguing again by contradiction, suppose $\frac{\partial \tau_1}{\partial t}(\bar{x}_j, t^*) > 0$. Since $\tau_1(\bar{x}_j, t^*) = 0$ we would have $\tau_1(\bar{x}_j, t) < 0$ for $t^* - \delta < t < t^*$, contradicting once more the definition of t^*. Thus, if we write the equation (1.1) at $t = t^*$ and $x_j = \bar{x}_j$, we have:

$$0 \geq \frac{\partial \tau_1}{\partial t}(\bar{x}_j, t^*) = -d_1 \Delta_G \tau_1(\bar{x_j}, t^*) + f_\tau(\bar{x_j}, t^*).$$

Therefore:

$$-d_1 \Delta_G \tau_1(\bar{x_j}, t^*) \leq -f_\tau(\bar{x_j}, t^*),$$

and, keeping in mind that as $f_\tau(x_j, t) > 0$ for all $x_j \in V$ and $t > 0$, we have eventually that

$$-\Delta_G \tau_1(\bar{x_j}, t^*) < 0 \tag{1.4}$$

On the other hand, as $\tau_1(\bar{x_j}, t^*) = 0$, we have

$$-\Delta_G \tau_1(\bar{x_j}, t^*) = \sum_{x_i \sim \bar{x}_j} (\tau_1(x_i, t^*) - \tau_1(\bar{x_j}, t^*)) w_{ij} = \sum_{x_i \sim \bar{x}_j} w_{ij} \tau_1(x_i, t^*),$$

so that

$$\sum_{x_i \sim \bar{x}_j} w_{ij} \tau_1(t^*, x_i) < 0 \tag{1.5}$$

This means that there exists a vertex $\bar{x}_i \in V$, $\bar{x}_i \sim \bar{x}_j$ such that $\tau_1(\bar{x}_i, t^*) < 0$ and consequently $\tau_1(\bar{x}_i, t) < 0$ for $t^* - \delta < t < t^*$, This contradicts the fact that $\tau_1(x_i, t) > 0$ for all $x_i \in V$ and for $t < t^*$. This proves that $\tau_1(x_j, t) > 0$ for all $x_j \in V$ and for $t_{min} < t < t_{max}$. We prove now by induction that $\tau_m(x_j, t) > 0$ when $1 \leq m \leq M$. We have already proved that the assertion is true for $m = 1$. Let now $1 < m \leq M$ be fixed, and assume $\tau_{m-1}(t, x_j) > 0$ for all $x_j \in V$ and for $t_{min} < t < t_{max}$. We want to show that the same assertion holds for $\tau_m(\cdot, t)$. To this end, assume by contradiction there exists a vertex $x_i \in V$ and a time $t < t_{max}$ such that $\tau_m(x_i, t) \leq 0$. As above, we can put

$$t^* = \sup\{t \in (t_0, t_{max}), \tau_m(x_j, t) > 0 \; \forall \; x_j \in V\} < t_{max}.$$

Again as above, it must exist a vertex $\bar{x}_j$ such that $\tau_m(\bar{x}_j, t^*) = 0$ and $\frac{\partial \tau_m}{\partial t}(\bar{x}_j, t^*) \leq 0$. Writing equation (1.2) at $t = t^*$, $x_j = \bar{x_j}$, we have

$$0 \geq \frac{\partial \tau_m}{\partial t}(\bar{x}_j, t^*) =$$

$$d_m \sum_{x_i \sim \bar{x}_j} (\tau_m(x_i, t^*) - \tau_m(\bar{x_j}, t^*)) w_{ij} - \tau_m(\bar{x}_j, t^*) \sum_{j=1}^{M} a_{1,j} \tau_j(\bar{x}_j, t^*) + \frac{1}{2} \sum_{j=1}^{m-1} a_{j,m-j} \tau_j(\bar{x}_j, t^*) \tau_{m-j}(\bar{x}_j, t^*)$$

and hence

$$-d_m \sum_{x_i \sim \bar{x}_j} \tau_m(x_i, t^*) w_{ij} \geq \frac{1}{2} \sum_{j=1}^{m-1} a_{j,m-j} \tau_j(\bar{x}_j, t^*) \tau_{m-j}(\bar{x}_j, t^*) > 0$$

where in the last inequality we use the inductive hypothesis; therefore:

$$\sum_{x_i \sim \bar{x}_j} \tau_m(x_i, t^*) w_{ij} < 0$$

As above, this means that there exists a vertex $\bar{x_i} \in V$ such that $\tau_m(\bar{x_i}, t^*) < 0$ and consequently $\tau_m(\bar{x_i}, t) < 0$ for $t^* - \delta < t < t^*$, contradicting the definition of t^*. The case $m = M$ can be handled in the same way, using equation (1.3).

□

Theorem 1.5.2. *Suppose $\tau_m(x_j, t_0) > 0$ and $f_\tau(x_j, t) > 0$ for all $x_j \in V$, $t \geq 0$, and for $1 \leq m \leq M$. Let*

$$\tau = \tau(x, t) : V \times (t_{min}, t_{max}) \longrightarrow \mathbb{R}^{NM}$$

be the maximal solution of the Cauchy problem (1.1), (1.2), (1.3). *Then $t_{max} = +\infty$ and $t_{min} = -\infty$.*

Proof. Let us prove that $t_{max} = +\infty$. By a classical result (see, e.g., [50], Corollary 3.1), if, by contradiction, $t_{max} < +\infty$, then we would have $\lim_{t \to t_{max}} |\tau(\cdot, t)| = +\infty$. Thus, to prove the assertion we have but to show that, if $t_{max} < +\infty$, then $\tau(\cdot, t)$ is bounded when t belongs to a left neighborhood of t_{max}.

By Lemma 1.5.1, for all $x_k \in V$ we have:

$$\begin{aligned} \frac{\partial \tau_1}{\partial t}(x_k, t) &= -d_1 \Delta_G \tau_1(x_k, t) - \tau_1(x_k, t) \sum_{j=1}^{M} a_{1,j} \tau_j(x_k, t) + f_\tau(x_k, t) \\ &< -d_1 \Delta_G \tau_1(x_k, t) + f_\tau(x_k, t). \end{aligned} \tag{1.6}$$

Again by Lemma 1.5.1 we can multiply (1.6) by $\tau_1(x_k,t)$. Summing up over all $x_k \in V$ we get

$$\sum_{x_k\in V} \tau_1(x_k,t)\frac{\partial \tau_1}{\partial t}(x_k,t) < \sum_{x_k\in V} \tau_1(x_k,t)(-d_1\Delta_G\tau_1(x_k,t) + f_\tau(x_k,t)).$$

Therefore

$$\begin{aligned}\frac{1}{2}\,\frac{\partial|\tau_1(\cdot,t)|^2}{\partial t} &< -d_1 \sum_{x_i\sim x_k} (\tau_1(x_k,t)-\tau_1(x_i,t))^2 w_{ik} + \sum_{x_k\in V}\tau_1(x_k,t)f_\tau(x_k,t)\\ &\le \sum_{x_k\in V}\tau_1(x_k,t)f_\tau(x_k,t) \le \frac{1}{2}\,|\tau_1(\cdot,t)|^2 + \frac{1}{2}\,|f_\tau(\cdot)|^2,\end{aligned}$$

and, eventually

$$|\tau_1(\cdot,t)|^2 \le |\tau_1(\cdot,t_0)|^2 + \int_{t_0}^t |f_\tau(\cdot,s)|^2\,ds + \int_{t_0}^t |\tau_1(\cdot,s)|^2\,ds$$

for $t_0 < t < t_{max}$. By Gronwall inequality (see e.g. [50], Theorem 1.1) it follows eventually that

$$|\tau_1(\cdot,t)|^2 \le \Big(|\tau_1(\cdot,t_0,)|^2 + (t_{max}-t_0)\max_{t_0\le s\le t_{\max}} |f_\tau(\cdot,s)|^2\Big)\Big(1+\int_{t_0}^t \exp(s-t_0)\,ds\Big). \quad (1.7)$$

This proves that $\tau_1(t,\cdot)$ is bounded in $[t_0,t_{max})$.

We want to prove now that for $1 \le m \le M$ there exists C_m such that

$$|\tau_m(\cdot,t)| \le C_m \qquad \text{for } \ t_0 < t < t_{max}\ . \quad (1.8)$$

If $m = 1$ assertion (1.8) has been just proved. Take $1 < m < M$ and suppose (1.8) holds for $m-1$. If $x_k \in V$ is fixed, by Lemma 1.5.1, we have

$$\frac{\partial \tau_m}{\partial t}(x_k,t) \le -d_m\Delta_G\tau_m(x_k,t) + \frac{1}{2}\sum_{j=1}^{m-1} a_{j,m-j}\tau_j(x_k,t)\tau_{m-j}(x_k,t).$$

Again by Lemma 1.5.1 we can multiply the previous inequality by $\tau_m(x_k,t)$. Summing up over all $x_k \in V$, by the inductive hypothesis we get

$$\frac{1}{2}\,\frac{\partial|\tau_m(\cdot,t)|^2}{\partial t} \le \frac{1}{2}|\tau_m(\cdot,t)|\sum_{j=1}^{m-1} a_{j,m-j}C_jC_{m-j} \le \frac{1}{4}|\tau_m(\cdot,t)|^2 + C$$

and (1.8) follows as in the case $m = 1$. The case $m = M$ can be handled in the same way. This achieves the proof of the theorem.

□

Theorem 1.5.3. *Suppose* $\tau_m(t_0, x_j) \geq 0$ *and* $f_\tau(x_j, t) \geq 0$ *for all* $x_j \in V$, $t \geq 0$, *and for* $1 \leq m \leq M$. *Then our Cauchy problem for* (1.1), (1.2), (1.3) *admits a solution*

$$\tau = \tau(x, t) : V \times \mathbb{R} \longrightarrow \mathbb{R}^{NM}$$

such that $\tau_m(x_k, t) \geq 0$ *for all* $t \in \mathbb{R}$, $x_k \in V$ *and* $1 \leq m \leq M$.

Proof. If $\eta > 0$, consider the Cauchy problem (1.1), (1.2), (1.3) where $f_\tau(x_k, t)$ is replaced by $f_{\tau,t}(x_k) + \eta$ and $\tau_1(x_k, t_0)$ by $\tau_1(x_k, t_0) + \eta$ for all $x_k \in V$. By Theorem 1.5.2 and Lemma 1.5.1, this approximate problem admits a positive solution defined for all times t. Then we can conclude letting $\eta \to 0$ by the continuous dependence of the solutions of a Cauchy problem on the data (see e.g. [50], Theorem 3.2). □

1.5.2 Model validation results

In this section, we compare the tau patterns achieved by numerical simulations against empirical imaging-derived regional data (Korea cohort for tau-PET and ADNI cohort for atrophy).
In that validation results, our primary validation metric - a similarity measure between model and empirical data - is the Pearson's correlation R-statistic, unless otherwise stated.

Figure 1.1 show the temporal evolution of τ oligomers over time, totaled over the entire brain, for oligomers of length $m = 1, 2, 3, 4, 5$. Please note that $M = 5$ is considered "tangle" and does not further interact with any other oligomeric species. Recall also that only $m = 1$ (monomer) are assumed to be produced at local sites, here, the entorhinal cortex. The left panel of the figure shows the evolution of $\tau_m, m = 1 \dots 5$ oligomers over model time. Although the model time was hand-tweaked in order to correspond roughly to the 10-15 year time span of typical AD cases, its units should be considered arbitrary in absence of a calibration strategy that can in the future convert it to the unit of years. As expected, the monomer levels are the first to rise (blue curve), followed by oligomers of length $m = 2, 3, 4$. Each monomeric and oligomeric species exhibits a distinct plateau effect, and eventually begins to decline. The decline is due to two factors. First, the monomer production itself declines as given by the Gamma-shaped production function $f_\tau(t)$, which accounts for the fact that eventually

misfolding is limited by the availability of intact protein in tissue and the loss of neurons, both of which serve to limit the available pool of cleavable protein. Second, as oligomers aggregate via Smoluchowski processes, larger oligomers form progressively. Eventually, tangles form at $m = 5$, which takes active oligomers out of circulation. This is why the tangle species shows a monotonic increase (green curve), without undergoing reduction at any stage. These aspects closely track the empirical data currently available on CSF-derived total τ [106, 61, 24].

In the middle panel, we show the similarity measure computed between the regional distribution of each oligomer and the empirical regional τ pattern obtained from the Korea study. As described in Methods section, the similarity score is the Pearson correlation between the model vector at model time t and the (static) empirical AV1451-PET uptake vector. In this manner, the similarity score is independent of the overall scale of both the model and the empirical uptake value. Each curve represents a single oligomer in the AND model, and shows a peak in similarity at an intermediate time between $t = 0$ and $t = t_{max} = 10$. The temporal sequencing of peak similarity strongly follows the sequence of oligomer length, such that monomer ($m = 1$) is the first to peak, followed by $m = 2, 3, 4, 5$, in order. The tangle curve (green) has a distinct shape in comparison to the oligomer curves, confirming that the behavior of the end product of Smoluchowski aggregation should have different dynamics than intermediate oligomers. The empirical group used here is the aMCI group in the Korea study, chosen because it has the best match with the model (see next figure). Clinically, there are reasons to believe that this stage, immediately before full-blown AD, should be a suitable empirical group for τ pathology comparisons; see below. In the right panel, similarity curves are shown for the comparison of the model against regional atrophy of the ADNI cohort, this time on the LMCI group. Curves for AD groups in both studies give similar results and are not shown. The above figure corresponds to the default choice in the Smoluchowski model based on empirical *in vitro* fitting data on amyloids, where a Gamma-shaped expression [42] $a_{mj} = \frac{mj}{\sigma_{agg}^2} \exp\left(-\frac{mj}{\sigma_{agg}^2}\right)$ was used to model the behavior of the aggregation rate constants for various oligomer lengths. We also tested the behavior of the thermodynamically-inspired choice $a_{mj} = \frac{\sigma_{agg}}{mj}$, shown in Figure 1.2. Interestingly, AND dynamics did not change appreciably, although further exhaustive exploration of different formulations was not attempted. We also implemented two different formulations for diffusivity rate constants: $d_m = \frac{m}{\sigma_{diff}} \exp\left(-\frac{m}{\sigma_{diff}}\right)$ (above Figure 1.1) and $d_m = \sigma_{diff}/m$ (Figure 1.3). In the latter case, AND model evolution of different oligomers was seen to be somewhat different, but the overall correspondence with empirical data was quite comparable in all three cases.

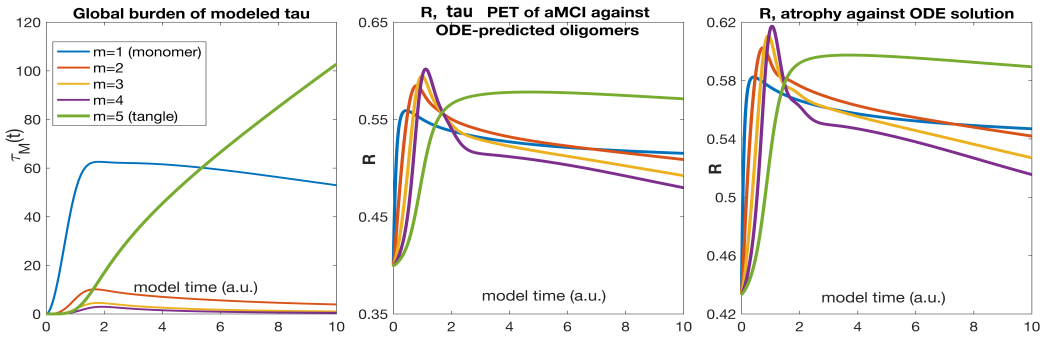

Figure 1.1 Left: Temporal evolution of τ oligomers over time, totaled over the entire brain, for oligomers of length $m = 1, 2, 3, 4, 5$. As designed, monomers are the first to rise from zero, slowly giving way to higher oligomers. Tangles ($m = 5$ here) are the last to develop, and last to reach steady state or fall back. The temporal sequencing of peak deposition clearly and strongly follows the sequence of oligomer length: $m = 1, 2, 3, 45$. Middle: Similarity index (Pearson's R) of the AND model against Korea study's empirical aMCI τ distribution, over model time t. Right: Similarity index of the AND model against ANDI study's empirical LMCI atrophy distribution, over model time t.

Figure 1.4 shows "glass brain" rendering of the evolution of the regional distribution of the theoretic AND-predicted τ oligomers over time. For the purpose of this illustration, the last oligomeric species (assumed to be tangles, $m = 5$) is shown, since AV1451 binds mainly to the tangles rather than to soluble oligomers. Each brain region is represented by a sphere placed at the region's centroid.

For comparison empirical τ distribution from AV1451-PET scans in the Korea study are shown in the middle column. A similar comparison between the spatio-temporal evolution of τ predicted by the model and empirical regional atrophy data from the ADNI study is given in the right column. Note that regional atrophy is being used here as a close surrogate of τ deposition, since there is mounting evidence from neuroimaging and mouse model studies that the two are strongly associated [111, 116]. Sphere color is by lobe: blue = frontal, purple = parietal, red = occipital, green = temporal, black = sub-cortical, cyan = cingulate. The sphere diameter is proportional to effect size: model value or empirical (PET binding SUVR or MRI-derived atrophy

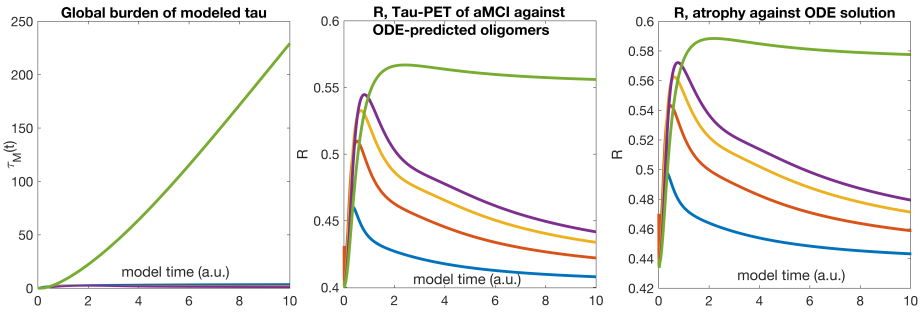

Figure 1.2 Temporal evolution of τ oligomers over time for a different definition of aggregation rates: $a_{mj} = \frac{\sigma_{agg}}{mj}$. The temporal evolution and sequencing of peak times are similar to the earlier case.

t-statistic). The key observation from this figure is that the AND model successfully recapitulates the spatiotemporal time course of τ progression at all stages of the disease, whereby: starting in the entorhinal cortex, we see increasing amounts of theoretical pathology in adjoining temporal cortices, followed by subcortical pathology, in particular hippocampus and amygdala. Thus, initial monomers generated in the entorhinal cortex undergo the process of aggregation and subsequently their networked spread causes deposits to occur in temporal, parietal and posterior cortices. The temporal behavior predicted by the model is roughly in agreement with the ordered stages of AD progression (naMCI/EMCI to aMCI/LMCI to AD). Visually, the AND model gives strikingly similar regional patterns against both empirical τ as well as atrophy data.

Similarity scores between model and empirical distributions are shown as a function of model time t. Similarity curves in the top row show that the model increasingly fits empirical regional patterns as network diffusion proceeds, with the best fits achieved for the stages preceding full-blown dementia (aMCI in the Korea cohort and LMCI in the ADNI cohort). AD patients also show high model fits, but the naMCI and EMCI

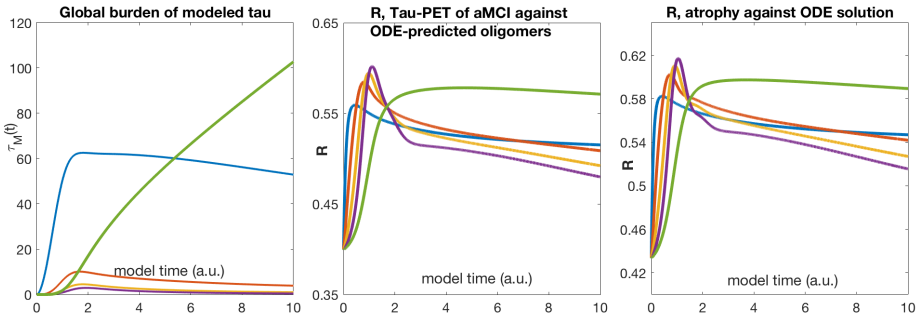

Figure 1.3 Temporal evolution of τ oligomers over time for a different definition of diffusivity rates: $d_m = \sigma_{diff}/m$. The temporal evolution and sequencing of peak times are somewhat different from the earlier case, suggesting that the exact nature of how diffusivity scales with oligomer length might be an important mediator of large-scale behavior of AND dynamics.

cohorts show poor fits, consistent with the fact that the latter are either very early in the disease process or are on track for non-amnestic dementia. That aMCI and LMCI data are fit better than AD suggests that the AND model is capturing phases where active pathology transmission is ongoing; many recent authors have suggested that by the time of onset of full AD, pathology might have reached a plateau, with further changes relating only to cell loss and functional deficits [61]. At the peak of the R-t curves, all fits are significant at $p = 0.05$. At late time points the similarity curves reaches a plateau even though the tangle pathology keeps rising, since the similarity measure here is Pearson correlation, which is insensitive to overall scale.

In section SI-1 we explore whether parameter choices strongly affect the match between the AND model and empirical data, selecting 3 key parameters from the model - $\sigma_{agg}, \sigma_{diff}, c_1$ - for detailed exploration and keeping the rest fixed. Figure S1 shows that model performance is quite insensitive to a wide range of model parameters, yet some parameters are better than others. This indicates that AND is an identifiable

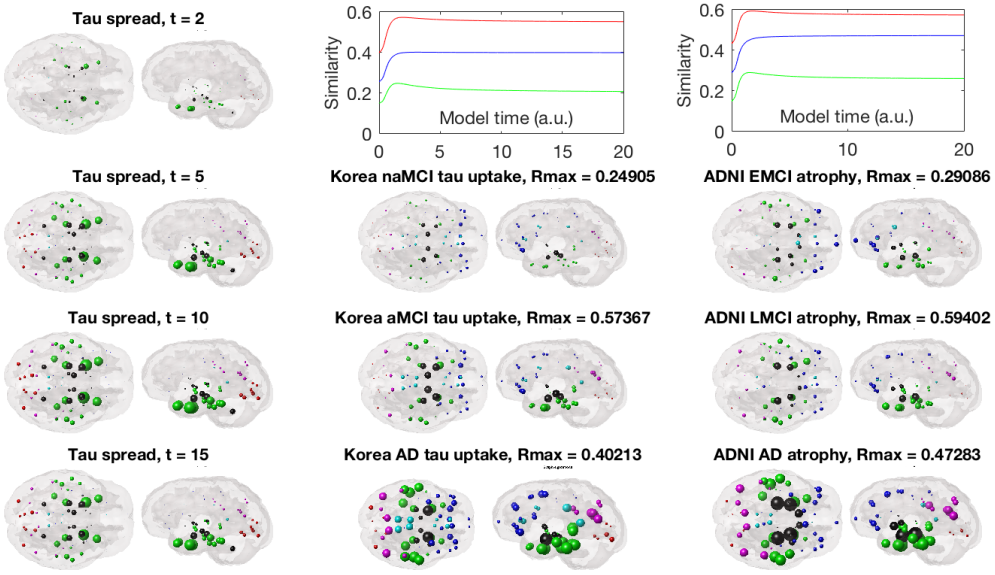

Figure 1.4 Glass brain rendering of theoretical AND-predicted regional τ distribution (left column) and its comparison with empirical τ measured from regional AV1451-PET scans of patients (middle column) and regional atrophy obtained from a different cohort of patients in the ADNI study (right column). Sphere color is by lobe: blue = frontal, purple = parietal, red = occipital, green = temporal, black = sub-cortical, cyan = cingulate. Similarity scores (Pearson's R) between the model and empirical data are shown as a function of model time t in the top row (green = naMCI and EMCI; red = aMCI and LMCI; blue = AD). At late time points the similarity curves reaches a plateau even though the tangle pathology keeps rising.

model. We repeated this analysis for 4 combinations of model choices noted earlier, arising from the two definitions of aggregation constants a_{mj} and diffusivity rates d_m. All choices are capable of yielding similar performance at some parameter value. Current *in vivo* data only measure tangle loads, hence further detailed experimental data on reaction kinetics and the ability to observe all oligomeric concentrations will be needed to thoroughly evaluate these model choices.

Although the above results relied on the well established seeding of entorhinal cortex, it possibly a different seeding location might be closer to empirical data. Although we did not explore this issue exhaustively, in Supplementary section 1.7.2 we show a results from an alternative seeding scheme: seeding the AND model at the putamen, which, as part of the striatum, is not in fact considered a plausible site of pathology initiation in AD. Instead the putamen is a common location of frontotemporal and other dementias. As expected, putamen-seeding was found not to be a good model of τ patterns in mature AD subjects ($R = 0.16$ with putamen seeding, versus $R = 0.40$

for EC-seeding), (Figure S2). This provides a null reference for the above results, and suggests that the AND model seeded at EC is not only sensitive but may also be specific to AD. But putamen seeding was somewhat better for early MCI and mixed etiology groups, where many subjects might have a different, frontal or striatal etiologic origin.

1.6 Discussion

1.6.1 Summary of key results

We propose a parsimonious mathematical model of the three pathological processes involved in the progression of τ proteins throughout the Alzheimer brain: monomer production; aggregation into oligomers and then into tangles; and the spatiotemporal progression of misfolded τ as it ramifies into neural circuits along white matter projections. Initial production of misfolded monomeric τ is assumed to occur specifically at the entorhinal cortex, based on histopathological Braak staging. The pathological underpinnings of protein aggregation and networked spread are given by mounting evidence for "prion-like" trans-neuronal transmission, whereby proteins misfold, trigger misfolding of adjacent same-species proteins, and thereupon cascade along neuronal pathways [17, 38, 56, 65]. Trans-neuronal transmission implies spread along axonal projections rather than spatially. Bidirectional transmissions are assumed through projection fibers, under a previously established Network-Diffusion process whereby anatomic connections govern the rate at which two distant but connected brain regions can transfer pathologic τ. This combined model, which we call Aggregation-Network-Diffusion (AND), exhibits all hallmarks of tau progression seen in human patients can explain many experimental findings in AD. The model is specifically effective when seeded at the entorhinal cortex, since another AND model seeded at the putamen failed to recapitulate mature Alzheimer-related τ patterning. The presented AND model unifies structural biochemical processes at the microscopic scales with local and long range trans-neuronal transmission processes at the macroscopic scales in a single, quantitatively testable model. To our knowledge, this is the first theoretical model of protein aggregation and transmission to be developed or tested on a macroscopic, whole brain scale.

1.6.2 Applications and implications

The presented AND model unifies structural biochemical processes at the microscopic scales with local and long range trans-neuronal transmission processes at the macroscopic scales in a single, quantitative and testable model. Therefore this approach can serve as an effective bridge between theoretical studies, bench science and human imaging studies. Several hitherto inaccessible possibilities emerge.

First, current models of protein aggregation involve kinetic and aggregation parameters that must be estimated from detailed in vitro experimental data on reaction kinetics. Unfortunately, kinetics in solution or suspension do not frequently capture the complex environments and the pathological milieu of proteins in tissue in vivo. This makes it very difficult if not impossible to realistically assess model parameters. Our AND model, by allowing fitting to in vivo data, can provide a new opportunity to obtain parameter fits to real in vivo human and animal brain data. In particular, there are several transgenic mouse studies from which highly detailed data on reaction and aggregation times can be deduced. When combined with detailed mesoscopic connectivity data in mice, the application of the AND model becomes possible on mouse tau studies. Second and related, the AND model can open up the possibility of testing competing models of protein aggregation in terms of their ability to reproduce not only in situ kinetics of oligomerization, but also the brain-wide ramification via trans-neuronal transmission. Although the present work considered Smoluchowski aggregation theory, several alternative models have been proposed, including the classic nucleation models. As noted above, testing these models on in vitro reaction kinetic data frequently suffers from lack of a neuropathological milieu. The proposed AND model can fill this gap. Third, the AND model provides a realistic avenue for understanding the pathophysiological progression of degenerative pathologies in a wide array of degenerative diseases, including Alzheimer's, Parkinson's, ALS, frontotemporal dementia, etc. This is because almost all these diseases involve one or more of a small number of misfolded protein species. Although in human cases we do not have access to various oligomeric species, we frequently are able to measure plaques and tangles. Thus, a model like ours, that is able to provide a mathematical link between monomeric and oligomeric species to measurable plaques and tangles, can be important addition to the burgeoning field of neurodegeneration.

1.6.3 Assumptions, limitations and future work

Several issues and applications require further investigation. The presented model incorporates the Smoluchowski aggregation theory, but in practice other models of protein misfolding and aggregation are also plausible. Although extensive experimental data are available on the basis of which the suitability of various aggregation models has previously been assessed [42], these data typically come from *in vitro* reactions and it is unclear whether the same conclusions can be reached using *in vivo* data. Hence the question of which is the best aggregation model remains open, and can only be addressed by extensive validation on human neuroimaging or animal model histopathology data - part of our future planned work. Our use of MRI-derived atrophy as a surrogate for underlying τ distribution is well borne out by the fact that ante-mortem MRI-derived atrophy correlates strongly with post-mortem histopathologic τ [111, 116]. Therefore we reported not only AV1451-PET data but also MRI-derived regional atrophy as a close surrogate for τ deposition. In this study, we used DTI-derived human connectomes, which by design cannot infer directionality of connections. In reality, protein transmission is likely to be a directional process, whether anterograde or retrograde. The incorporation of directionality of transmission can be trivially achieved by a simple modification of the presented approach.

Another important limiting assumption is that τ misfolding is generated only in the entorhinal cortex. Although the role of EC as the most likely seed region is based on pathological studies by Braak and others, and is widely accepted, this assumption precludes systematic exploration of hypotheses regarding why certain areas serve as seeds in the first place. We report in SI-2 the predictions obtained from seeding the putamen - a region not involved in Alzheimer-type pathology but a common location of frontotemporal and other dementias. In future work we will explore mathematical models that make no assumptions about seed regions. Our previous work [91] suggests that perhaps network eigenmodes can predispose certain regions to early accumulation of monomeric seeds. Finally, an important area yet to be addressed is, in diseases involving more than one protein species (e.g. $A\beta$ and τ in Alzheimer's disease), how do they interact. Future studies can extend the proposed AND model to multiple proteins, and allow interaction terms between them.

1.7 Appendix A: Additional Experiments

1.7.1 Effect of AND model parameters and choice of diffusivity / aggregation rate relationships

Here we explore whether parameter choices strongly affect the match between the AND model and empirical data, an important issue due to the presence of several *a priori* unknown parameters. These results are contained in Figure S1. We selected 3 key parameters from the model - $\sigma_{agg}, \sigma_{diff}, c_1$ - and kept the network spread rate β_τ, c_2 and the monomer generation function f_τ fixed. Recall that theses relationships are governed by the scale parameters σ_{agg} and σ_{diff}, and for convenience we impose $\sigma_{agg} = \sigma_{diff}$ in order to reduce the parameter set by one. For each set of parameter choices, we computed the Pearson's R (our preferred similarity metric) between the AND model and group τ-PET pattern from the Korean amnestic MCI cohort, chosen for its relevance to the proposed model. R was calculated at all model times t, and the maximum over t was retained as the model evidence, as has been previously described. Our goal was to assess how strongly model performance depends on parameter choice, and to help select an optimal parameter set. As shown in Figure S1, performance is quite insensitive to a wide range of model parameters, except for the outer limits. We think this might be due to two reasons: a) Pearson's R is insensitive to scale and shift changes, and b) almost all model parameters are some sort of time constant, hence by maximizing over all model times, many choices of these parameters will yield similar performance. We repeated this analysis for all 4 combinations of model choices, arising from the two definitions of aggregation constants a_{mj} and diffusivity rates d_m, defined in Methods section.

1.7.2 AND Model with different seeding location than Entorhinal cortex

Here we demonstrate that the AND model does not give better results when seeding it at a location different from entorhinal cortex. When we seed the putamen, which is not known as an early site of AD-related τ, we get very different spatial patterning of tau evolution, primarily in the frontal, striatal and orbitofrontal regions – see Figure S1. The model fits poorly to empirical AD and aMCI Korea tau data, as well as to the ADNI atrophy data, both visually and using the quantitative similarity measure (Pearson's R). Interestingly, putamen seeding matches the Korea tau data of the naMCI cohort, who are MCI subjects who do not display classic AD-like cognitive deficits. This

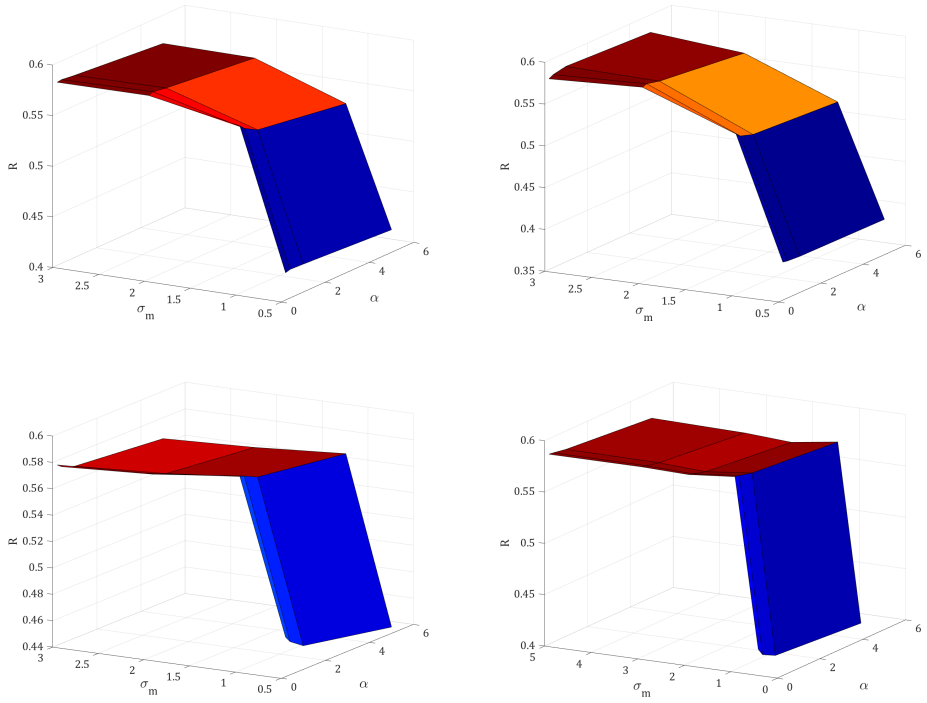

Figure S1: Optimization of AND model parameters. We selected 3 key parameters from the model - $\sigma_{agg} = \sigma_{diff} = \sigma_m$, $c_1 = \alpha$ - which are specific to the aggregation model, and kept other model parameters fixed. For each parameter choice, we computed the Pearson's R between AND model and group τ-PET pattern from the Korean amnestic MCI cohort, at all model times t, and the maximum over t was retained. We repeated this analysis for 4 combinations of model choices, arising from the two definitions of aggregation constants a_{mj} and diffusivity rates d_m. A: $a_{mj} = \frac{\sigma_{agg}^2}{mj}$, $d_m = 1/m$ B: $a_{mj} = \frac{mj}{\sigma_{agg}^2} \exp\left(-\frac{mj}{\sigma_{agg}^2}\right)$, $d_m = 1/m$ C: $a_{mj} = \frac{\sigma_{agg}^2}{mj}$, $d_m = \frac{m}{\sigma_{diff}} \exp\left(-\frac{m}{\sigma_{diff}}\right)$ D: $a_{mj} = \frac{mj}{\sigma_{agg}^2} \exp\left(-\frac{mj}{\sigma_{agg}^2}\right)$, $d_m = \frac{m}{\sigma_{diff}} \exp\left(-\frac{m}{\sigma_{diff}}\right)$.

points to an important aspect of early MCI cohorts, in that they exhibit substantial inter-subject heterogeneity, which is actually higher when looking at their likely seed regions, as demonstrated in the publication [105]. Although putamen seeding gives a good match for tau in early disease, it fails at al stages when predicting atrophy in the ADNI cohorts. This might be due to the fact that atrophy is downstream of tau, hence the etiologic heterogeneity evident in the above tau fit is not apparent in the atrophy fit.

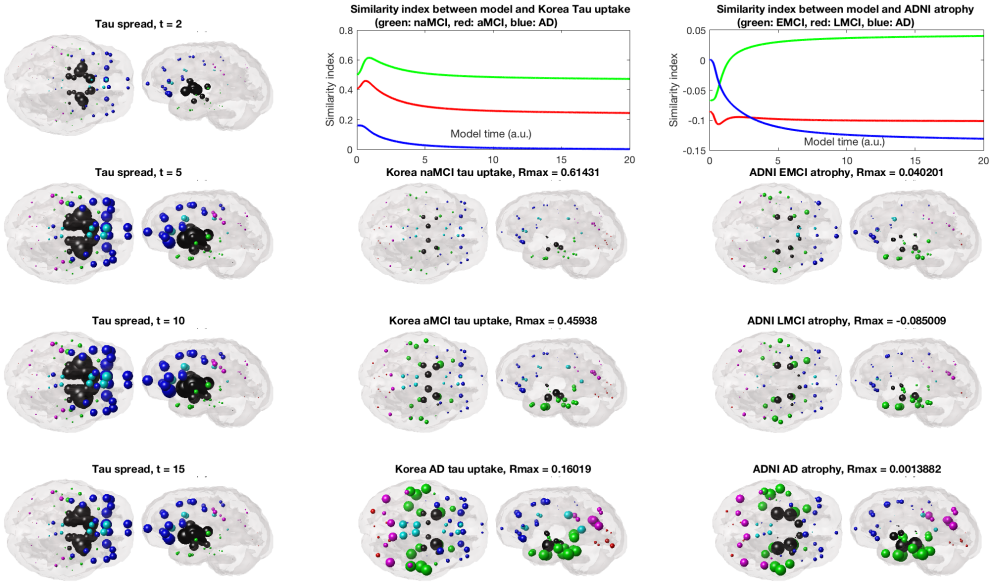

Figure S2: Glass brain rendering of theoretical AND-predicted regional τ distribution seeded at the putamen (left column) and its comparison with empirical τ measured from regional AV1451-PET scans of patients (middle column) and regional atrophy obtained from a different cohort of patients in the ADNI study (right column). Similarity scores (Pearson's R) between the model and empirical data are shown as a function of model time t in the top row (green = naMCI and EMCI; red = aMCI and LMCI; blue = AD). The AND model seeded at the putamen is not a good model of τ patterns in the AD, LMCI or aMCI groups, but gives a surprising correlation with the (non-amnestic) MCI group.

1.8 Appendix B: Notation and Theory

1.8.1 Smoluchowski aggregation theory

Following the the model studied in [1, 10, 36, 37], we describe the aggregation of the τ-polymers by means of Smoluchowski equation, following previous treatment in [84, 1] for $A\beta$. Originally, in [98] Smoluchowski introduced a system of infinite discrete differential equations (without diffusion) for the study of rapid coagulation of aerosols. Smoluchowski's theory was successively extended to cover different physical situations. In fact, this type of equations, describing the evolving densities of diffusing particles that are prone to coagulate in pairs, models various physical phenomena, such as, e.g. polymerization, aggregation of colloidal particles, formation of stars and planets as well as biological populations, behavior of fuel mixtures in engines. We refer to [26] for a exhaustive historical account. As far as we know, Smoluchowski equation first appears in the description of the agglomeration of Aβ amyloid in [84] and then in [1].

For $k \in \mathbb{N}$, let P_k denote a polymer of length k, that is a set of k identical particles (monomers) that is clustered but free to move collectively in a given medium. In previous usage in [1], [10], [36], P_k is a $A\beta$-polymer of length k; here we will reformulate this for τ. In the course of time polymers diffuse and, if they approach each other sufficiently close, with some probability they merge into a single polymer whose size equals the sum of the sizes of the two colliding polymers. By convention, we admit only binary reactions. This phenomenon is called coalescence and we write formally

$$P_k + P_j \longrightarrow P_{k+j},$$

for the coalescence of a polymer of size k with a polymer of size j. For sake of simplicity, polymer diffusion is assumed to result only from Brownian movement or diffusion (thermal coagulation). Under these assumptions, the discrete diffusive coagulation of a polymer $u_m(x,t) \geq 0$ of size $m \in \mathbb{N}$ is given under suitable initial and boundary conditions by

$$\frac{\partial u_m}{\partial t}(x,t) - d_m \triangle_x u_m(x,t) = Q_m(u) \quad \text{ in } [0,T] \times \Omega, \tag{1.9}$$

where the second term represents spatial diffusion, and the third term represents the net gain/loss of polymer due to aggregation $Q_m(u) = Q_{g,m}(u) - Q_{l,m}(u),\ m \geq 1$, with the gain ($Q_{g,m}$) and loss ($Q_{l,m}$) terms given by

$$Q_{g,m} = \frac{1}{2} \sum_{j=1}^{m-1} a_{m-j,j}\, u_{m-j}\, u_j \tag{1.10}$$

$$Q_{l,m} = u_m \sum_{j=1}^{\infty} a_{m,j}\, u_j. \tag{1.11}$$

where $u = (u_m)_{m\geq 1}$. The coagulation rates $a_{m,j}$ are non negative constants such that $a_{m,j} = a_{j,m}$ and d_m denotes the diffusion coefficient of an m-cluster, $d_m > 0 \quad \forall m \geq 1$. The kinetic coefficient $a_{m,j}$ represents reaction in which an $(m+j)$-cluster is formed from an m-cluster and a j-cluster. The term $Q_{g,m}$, given by (1.10), describes the creation of polymers of size m by coagulation of polymers of size j and $m-j$. The term $Q_{l,m}$, given by (1.11), corresponds to the depletion of polymers of size m after coalescence with other polymers. Since the size of clusters is not limited a priori, Eq. (1.9) describes a non-linear evolution equation of infinite dimension.

1.8.2 Statistical methods

In statistical analysis, it is frequently of interest to establish if there is a relationship between two variables, i.e. to see if they are correlated.
When a variable increases, according to what happens to the other variable we can speak of:

- *positive correlation*, if the other variable show a tendency to increase
- *negative correlation*, if the other variable show a tendency to decrease
- *no correlation*, if the other variable does not tend to either increase or decrease .

Correlation coefficients are introduced to measure how strong a relationship between two variables is. Statisticians are often interested in finding linear relationship between variables.
The Pearson's correlation coefficient is a statistical measure of the strength of a linear relationship between two variables.
In statistics, a population is a set of similar items or events which is of interest for an experiment.

Definition 1.1. The Pearson's population correlation coefficient $\rho_{X,Y}$ between two random variables X, Y with expected values μ_X, μ_Y and standard deviations σ_X, σ_Y is given by:

$$\rho_{X,Y} = \frac{cov(X,Y)}{\sigma_X \sigma_Y} = \frac{E[(X-\mu_X)(Y-\mu_Y)]}{\sigma_X \sigma_Y} \tag{1.12}$$

We observe that the Pearson's coefficient is defined if both standard deviations are non zero. If we consider a sample, that is a set of data selected or collected from a statistical population the Pearson's coefficient can be defined as follows:

Definition 1.2. Let x_i and y_i, for $i = 1, \ldots, n$, denote respectively the series of n measurements of X and Y. Then, the Pearson's correlation coefficient for a sample is defined as:

$$R = \frac{\sum_{i=1}^{n}(x_i - \bar{x})(y_i - \bar{y})}{\sqrt{\sum_{i=1}^{n}(x_i - \bar{x})^2}\sqrt{\sum_{i=1}^{n}(y_i - \bar{y})^2}} \tag{1.13}$$

where n is the sample size, $\bar{x} = \frac{1}{n}\sum_{i=1}^{n} x_i$ and $\bar{y} = \frac{1}{n}\sum_{i=1}^{n} y_i$(sample mean).

We note that the above formula can be obtained from equation(1.12) by substituting expressions of the covariance and standard deviations for a sample.
In the statistical analysis presented in that work (see section 1.4.4), we use Pearson's correlation coefficient, as given by (1.13), as similarity measure between model and empirical data.
By Cauchy-Schwarz inequality we have that $|R| \leq 1$ and, for istance $-1 \leq R \leq 1$.
Positive values of the Pearson's correlation coefficient denote positive linear correlation, while negative values denote negative linear correlation. A value of 0 expresses the absence of correlation. The closer the value of R is to 1, more confident we are of a positive linear correlation. Analogously, the closer the value of R is to -1, more confident we are of a negative linear correlation.

Remark 1. The existence of strong correlation does not imply necessarily a causal link between variables.

Let X a sample space and $\mathbf{P} = \{P_\theta : \theta \in \Theta\}$ a family of probability distributions on X. Points in X are the mathematical representations of possible observations, the family $\{P_\theta\}$ represents the possible descriptions of the variability in the observational situation being considered; it is supposed that one member of this family is the true description, though which one is unknown.
We define hypothesis $\bar{P}$ a subset of $\mathbf{P}$, i.e. $\bar{P} = \{P_\theta : \theta \in \bar{\Theta}, \bar{\Theta} \subset \Theta\}$.
In other words, a hypothesis is a statement that implies that the true probability distribution describing the variability in an observational situation belongs to a proper subset of the family of possible probability distributions.

Remark 2. Alternatively, we can say that a hypothesis implies that the true parameter θ belongs to a proper subset of the parameter space Θ. Moreover, sometimes it can be convenient to identify the hypothesis with the subset, to talk about the hypothesis $\bar{\Theta}$, where $\bar{\Theta} \subset \Theta$.

According to classical theory (whose key ideas were provided by Neyman and Pearson in the period 1928-1933), in a hypothesis-testing problem, two hypothesis are involved: the hypothesis of primary interest and the complementary hypothesis. The first of these is called null-hypothesis $H_0 := \{P_\theta : \theta \in \Theta_0, \Theta_0 \subset \Theta\}$, while the second one is said alternative hypothesis $H_1 := \{P_\theta : \theta \in \Theta_1, \Theta_1 = \Theta \setminus \Theta_0\}$.

Let T be a random variable, said statistic test, defined on the sample space X. Suppose to observe $T(x) = t^{obs}$. Then

$$p = \sup_{P \in H_0} P(T(x) \geq t^{obs})$$

is said the observed level of significance or p-value.

In order to decide if, based upon the sample, there is any or no evidence to suggest that linear correlation is present in the population, we perform a significance test. More precisely, we test the null hyphotesis H_0, that there is no linear correlation in the population, i.e. the true correlation coefficient ρ is equal to zero, based on the value of the sample correlation coefficient R, against the alternative hyphotesis H_1 that there is linear correlation, i.e. $\rho \neq 0$. If the p-value achieved by the significance test is such that $p > 0.05$, the empirical evidence is not sufficiently in disagreement with the null hypotesis that, for istance, can not be refused. On the other hand, if $p \leq 0.05$, the empirical evidence is strongly in disagreement with the null hyphosesis H_0, that has to be refused and we have strong confirmation to believe that the alternative hyphotesis H_1 is true.

Chapter 2

A polymerization model for the formation of NFTs in Alzheimer's Disease

In this chapter we present a polymerization model for the process of transport and aggregation of hyperphosphorylated tau protein first into fibrils and eventually up to neurofibrillary tangles. Our purpose is to investigate the formation of tangles in neurodegenerative processes by mathematically characterizing them in terms of a sol-gel phase transition.

2.1 Biological setting. Phosphorylation of tau protein and the formation of neurofibrillary tangles

Tau is a highly soluble microtubule-associated protein (MAP). In humans, it is usually found in neurons of the central nervous system and less common elsewhere. It is largely accepted [102], [96], [70] that its physiological function consists in facilitating the tubulin assembly and in stabilizing the axonal microtubules, although some recent studies seem to go towards the opposite direction, as they suggest that the actual function of tau might consist in preventing microtubules from being stabilized to keep them in constant motion [90].
In physiological conditions, and possibly to modulate its binding to microtubules or to the membrane, tau protein undergoes phosphorylation, i.e. a process, catalyzed

by enzymes said kinases, consisting in the acquisition of a phosphoryl group from a surrounding molecule. The phenomenon is higher in fetal neurons and decreases with age during development. However, it is widely believed that in pathological conditions (including Alzheimer's disease) a huge increment in tau phosphorylation takes place [102], [79]. More precisely, under homeostatic conditions a kinase is able to modify only a specific site of tau molecule and this site is different from one tau isoform to another; conversely, in diseased state a single tau isoform can be phosphorylated at an increased number of sites of the protein up to saturation [6]. Hypophosphorylated tau protein exhibits high affinity in binding to microtubules, while in hyperphosphorylated tau this capacity is reduced in significant way [63], [102], [76]. The enzyme GSK3 seems to play an important role in regulating tau phosphorylation [6], [7], [8].

The β-amyloid peptide (Aβ) is also involved in enhancing the phosphorylation of tau, particularly in its oligomeric form [102], [2]. The way in which this process takes place is not completely understood. It seems, however, that over activity of enzyme GSK3 not only accounts for tau hyperphosphorylation but also increases β-amyloid production [54]. On the other hand, it has been reported that beta-amyloid competes with insulin for binding to the insulin receptor [121]; this process contributes to GSK3 activation [57], [55] and subsequent promotion of tau phosphorylation [2]. Interestingly, these considerations could also explain the occurrence of impaired glucose metabolism as a characteristic event in the pathology of AD [121].
Several proteins called phosphatases can reverse the phosphorylation of tau. In particular, PP2A has been shown to dephosphorylate hyperphosphorylated tau [45]. However, in pathological conditions, changes of the biochemical environment lead PP2A not to function properly. Besides, the inhibition of phosphatase function is further increased by structural alterations of tau protein associated with hyperphosphorylation itself [6], [102]. An exhaustive description about the nature of the biochemical pathways involved in the process of tau hyperphosphorylation, is contained in [6].

Once a tau molecule is hyperphosphorylated, it detaches from the microtubules and self-aggregates [71]. It is largely accepted that the action of GSK3 on tau protein facilitates its assembly into polymers [7], [8], [6]. In addition, tau oligomers may act as templates for the misfolding of native tau, seeding the propagation of the modified species of the protein [41]. The spreading of non-homeostatic tau aggregates takes place first intracellularly and later extracellularly and intercellularly [39],[18]. Indeed, misfolded tau oligomers form primarily inside the neuron, where they can induce

changes to native tau molecules [102]. Subsequently, oligomers can be transported through cytoplasmic flow to the nerve terminals and may be released to neighboring neurons, where they trigger a similar process [15]. Furthermore, such aggregates can embed themselves into the cell membrane with consequent alteration of its permeability that leads to the release of the aforesaid oligomers to the extracellular space, where they can reach the surrounding neurons, thereby propagating this process to unaffected regions [15], [17].
There is experimental evidence about the fact that oligomers of hyperphosphorylated tau (and also of beta amyloid) have a key role in mental deficits associated with AD [28], [47], [96] . Indeed, they are known to be damaging for neurons, as they inhibit microtubules assembly [58], promote synaptic dysfunction [47], interfere with normal activities of the cell and are responsible of memory impairment [74].
From the biological point of view, "tau pathologies" begin in specific brain regions (i.e. entorhinal cortex) but ultimately involve much larger areas (i.e. hippocampus), a fact that has been related with an intercellular transfer of non-homeostatic tau species through the neural pathways from one cerebral area to another [18, 17, 38, 56, 65]. Once oligomers are formed, they eventually can continue to aggregate in paired helical filaments (PHF), giving rise to neurofibrillary tangles (NTFs). Studies in which an antibody that does not react with PHF 's tau is used to recognize specific compounds on tau protein, support the idea that tau phosphorylation occurs before its assembly [52]. Tangles are mainly intraneuronal structures; however, tau aggregates (including tangles) may be released to the extracellular space as a consequence of neuronal death [44].

As of today, the role of tau tangles in neurodegeneration is not completely clear. A common view is that such formations are harmful for brain's health and are considered a key factor in the destruction of neurons. In addition, the number and the localization of NFTs have been correlated with the severity of dementia [29], although they have been also found in brains of healthy people. Several studies reveal that tau in form of paired helical filaments compromises microtubules stability and their capacity to function properly and disrupts intracellular structures that are essential for normal metabolism and living functions of the cell [53], [71].
However, the correlation between NFTs presence and the incidence of the disease does not necessarily correspond to a cause-effect relationship [76]. For instance, there is evidence that neurons bearing NFTs may survive for decades [32] and that neuronal loss exceeds, by large, the amount of tau tangles detected [30], suggesting that the

latter may occur many years before neuronal death. In addition, the destruction of affected brain's areas does not seem strictly correlated with tangles' formation. Actually, it has been proposed that the role of neurofibrillary tangles is to protect cellular components from the attack by reactive oxygen species (ROS)[97]. Therefore, the process of aggregation of tau protein in tangles could be seen as a part of a multifaceted immune response of the brain against pathogen agents.A complete description about how this compensatory response might take place can be found in [76].
On the other hand, recent studies concerning mouse models suggest that the hyperphosphorylation of tau occurs in order to protect neurons from toxicity and damage caused by beta-amyloid oligomers. Further details can be found in [31].
In the light of these considerations, we cannot firmly ascertain if NFTs are a pathologic process that should be interrupted or a reaction of the organism facing disease's aggression. The mathematical model that we will present in the next section, aims at describing the formation of NFTs resulting from two mechanisms: tau polymerization and an external source of beta amyloid oligomers. We hope that this model may eventually shed light into the actual impact of NFTs on AD progression.

2.2 Description of the model

In this section, we will present a mathematical model for the formation of neurofibrillary tangles in human brain, that accounts for initial local accumulation of non-homeostatic tau protein followed by coagulation and intercellular spreading of pathologically modified tau clusters. We assume that beta amyloid acts as source of aggregation of tau monomers [102], [2], which in turn coagulate according to specific rates characteristic of classical polymerization problems, and that the transfer of assembled tau forms from one cerebral area to another occurs through the neural pathways between them by interneuronal transmission [17, 38, 56, 65, 18, 15]. In agreement with the approach proposed in chapter one, we represent the human brain by means of a finite weighted undirected graph $G = \{V, E\}$, where $V = \{x_1, .., x_h\}$ is the set of the vertices and $E = \{(x_i, x_j) \ : \ x_i \sim x_j\}$ is the set of the edges. We thus consider a functional approximation of the brain as consisting of i $(1 \leq i \leq h)$ anatomical structures located at the graph vertices and we describe the connections by white-matter fiber pathways between the i-th and the j-th region by the edge $(x_i, x_j) \in E$, $i, j = 1, \ldots, h$. In second place, we introduce a family of coefficients $w_{i,j} \geq 0$ that express the strength of connection between the i-th and the j-th structure. The coefficients $w_{i,j}$ are said the" connectivity weights" of the graph G and represent the weight function associated

with the graph.
In our model, we consider aggregation of pathologically modified tau monomers and subsequent coagulation in longer polymers in each brain structure and transport of toxic tau clusters along the connections from one structure to another. In addition, we do not distinguish between intra-neuronal and extra-neuronal space. Indeed, in our brain network single vertices denote large aggregates of neurons; in fact, our level of approximation is not as fine as to allow us to see the borders from one neuron to other and the distinction between neuronal processes from extra-neuronal ones is not relevant at the scale of our model.
We next describe the evolution of concentration of phosphorylated τ-polymers in human brain by means of a Smoluchowski-type system(including mass transfer, which will be denoted as diffusion in the sequel, and monomers production) defined on a finite graph $G = \{V, E\}$. More precisely, we consider the following system of reaction-diffusion equations:

$$\frac{\partial u_1}{\partial t} = -d_1 \Delta_G u_1 - u_1 \sum_{j=1}^{\infty} a_{1,j} u_j + f(x) \tag{2.1}$$

$$\frac{\partial u_i}{\partial t} = -d_i \Delta_G u_i + \frac{1}{2} \sum_{j=1}^{i-1} a_{j,i-j} u_j u_{i-j} - u_i \sum_{j=1}^{\infty} a_{m,j} u_j \tag{2.2}$$

to be satisfied when $x \in V$ and $t > 0$.
In system (2.1)-(2.2), the variable u_i represents the concentration of i-clusters, i.e. aggregates made of i identical monomers; Δ_G denotes the *positive* standard weighted Laplacian associated with the graph G (as defined in section 3.2.2 of Appendix 1); the coefficients $a_{i,j}$ are the coagulation rates and the source term $f = f(x)$ is a positive function on the vertices of the graph. Finally, the non negative constants d_i, $i \in \mathbb{N}$ are usually termed as the diffusion coefficients of the i-th cluster.
Equations (2.1) and (2.2) are completed with initial values:

$$u_i(x, 0) = U_i(x) \qquad i \in \mathbb{N} \tag{2.3}$$

where $x \in V$.
Written on the x_m vertex of G, equations (2.1), (2.2) become:

$$\frac{\partial u_1(x_m, t)}{\partial t} = -d_1 \Delta_G u_1(x_m, t) - u_1(x_m, t) \sum_{j=1}^{\infty} a_{1,j} u_j(x_m, t) + f(x_m) \tag{2.4}$$

$$\frac{\partial u_i(x_m,t)}{\partial t} = -d_i\Delta_G u_i(x_m,t)+\frac{1}{2}\sum_{j=1}^{i-1} a_{j,i-j}u_j(x_m,t)u_{i-j}(x_m,t)-u_i(x_m,t)\sum_{j=1}^{\infty} a_{m,j}u_j(x_m,t)\ . \tag{2.5}$$

with initial values:

$$u_i(x_m,0) = U_i(x_m)\,. \tag{2.6}$$

It is worth observing that the coagulation rates $a_{i,j}$ measure how polymers of length i are prone to aggregate with polymers of length j to create polymers of length $i+j$. In fact, we suppose that the aggregation process follows the law of mass action according to which the rate of a chemical reaction is directly proportional to the product of the concentrations of the reactants. Hence, the coagulation of i clusters with j clusters to give rise to clusters of length $i+j$ is described through terms of the form $a_{i,j}u_iu_j$, where $a_{i,j}$ are corresponding reaction rates. These coefficients are assumed to be nonnegative constants such that $a_{i,j} = a_{j,i}$ for all $i,j \in \mathbb{N}$. In this view, the i-th equation in (2.1) and (2.2) describes the rate of change of concentration of i-clusters due to coagulation of polymers of length less than i to form i-clusters and due to coagulation of i-clusters with other clusters (of possible length from one to infinity) to form larger aggregates. Unlike the model discussed in Chapter one, equations (2.1), (2.2) describe a problem in which the possible size of polymers is not limited a priori; thus an infinite number of variables (and equations) is introduced.

In the light of the biological setting described above, the function $u_i(x_m,t)$ represents the concentration of hyper-phosphorylated τ clusters of length $i \in \mathbb{N}$ at the m-th vertex of the graph, that is the m-th cerebral structure identified by that vertex. Instead, the source term $f(x_m)$, $m = 1,\dots,h$ represents the induction of phosphorylated tau protein by beta-amyloid clusters. For simplicity, the action of beta amyloid on tau phosphorylation is assumed to be constant in time at each vertex of the network.

At this point, we introduce some notation. We call *sol* the set of reacting i-clusters, $i \in \mathbb{N}$:

$$\{u_i(x_m,\cdot)\}_{i\in\mathbb{N},\ m=1,\dots,h}\ ,$$

while the total mass concentration of sol at a vertex $x_m \in V$, $m = 1,\dots,h$, is defined as:

$$M_1(x_m,t) = \sum_{i=1}^{\infty} iu_i(x_m,t) \quad \text{for } t>0\ . \tag{2.7}$$

The total mass concentration of sol at any vertex x_m, $m = 1, \ldots, h$ is assumed to be finite at time $t = 0$ that is:

$$M_1(x_m, 0) = \sum_{i=1}^{\infty} iU_i(x_m) < \infty \, . \tag{2.8}$$

The total mass concentration over the entire set of vertices is given by:

$$M_1(t) = \sum_{x_m \in V} \sum_{i=1}^{\infty} iu_i(x_m, t) \quad \text{for} \;\; t > 0 \, . \tag{2.9}$$

and

$$M_1(0) = \sum_{x_m \in V} \sum_{i=1}^{\infty} iU_i(x_m) \tag{2.10}$$

Analogously, we can define the second moment of the solution at a vertex $x_m \in V$, $m = 1, \ldots, h$, as:

$$M_2(x_m, t) = \sum_{i=1}^{\infty} i^2 u_i(x_m, t) \quad \text{for} \;\; t \geq 0 \, . \tag{2.11}$$

while over the entire set of vertices the corresponding quantity takes the form:

$$M_2(t) = \sum_{x_m \in V} \sum_{i=1}^{\infty} i^2 u_i(x_m, t) \quad \text{for} \;\; t \geq 0 \, . \tag{2.12}$$

If there are not sinks or sources in the system, we could expect that the total mass of clusters remains constant in time. This property is known as total mass conservation. However, it is not obvious that such property should hold true for any time. In fact, when the rate of production of large clusters is fast enough, a part of the total mass of the system is quickly transferred to larger aggregates, eventually giving rise to a hypercluster, said gel, which is made of an infinite number of monomers and removes polymers fractions from the medium, not to allow them to return to the sol fraction. The effect produced by the breakdown in a finite time of mass conservation is referred to in physics literature as *sol-gel phase transition* or *gelation* and the time at which this occurs is known as the *gelation time* [99],[78].
The occurrence of gelation for systems related to (2.1)-(2.3) depends on the assumptions made on coagulation coefficients. In the diffusionless case $d_i = 0$ the total mass conservation is known to hold if

$$0 \leq a_{i,j} \leq A(i + j) \;\; \text{for some} \;\; A > 0 \text{ and for } i, j \geq 1 \, . \tag{2.13}$$

(see [9]). A similar result also holds when diffusion is included, under some additional hypotheses on diffusion coefficients [118]. Classical theory of polymerization [99] provides a description of the interaction between two polymers under the assumption that polymer molecules do not form loops and in each monomer there are exactly σ functional groups (i.e. σ active spots for chemical bunding). The form of coagulation coefficients corresponds to the product of the number of free active spots in two interacting polymers; so that the coefficients are given by:

$$a_{i,j} = ((\sigma - 2)i + 2)((\sigma - 2)j + 2) \text{ for some } \sigma \in \mathbb{N} . \tag{2.14}$$

A way of taking this fact into account consists in setting:

$$a_{i,j} \sim i^{\alpha} j^{\alpha} \text{ for } i, j \geq 1 \text{ for some } \alpha \ : \ 0 < \alpha \leq 1 .$$

Since $i^{\frac{1}{2}} j^{\frac{1}{2}} \leq \frac{1}{2}(i + j)$, for any $i, j \geq 1$, one can guess that the case $\alpha = \frac{1}{2}$ in the above expression should be a borderline one with respect to (2.13). In fact, when $d_i = 0$ for all $i \in \mathbb{N}$, it has been proven in [35] that for $\frac{1}{2} < \alpha \leq 1$, there exist global solutions that do not preserve the total mass in time. According to this perspective, sol-gel phase transition is expected to occur when $\frac{1}{2} < \alpha \leq 1$.
Bearing in mind (2.14) and our previous remarks, we shall be mainly concerned here with the case $\alpha = 1$, i.e.:

$$a_{i,j} = ij \quad \text{for } \ i, j \in \mathbb{N} . \tag{2.15}$$

We finally recall an important result concerning the standard graph Laplacian described in Appendix 1 that we will repeatedly use in this chapter: if $u = u(x)$ is a real-valued function on $V = \{x_1, .., x_h\}$, then

$$\sum_{x_i \in V} \Delta_G u(x_i) = 0 \tag{2.16}$$

2.3 Main results

In this section, we will discuss the main results of this chapter, namely:

1. The existence of solutions for system (2.1), (2.2), (2.3). More precisely, we prove the existence of a global weak solution and a local in time classical solution.

2. The onset of a sol gel transition for sufficiently large times.

2.3.1 Existence of generalized solutions

Following [119], we can introduce the definition of a weak solution to (2.1),(2.2), (2.3). In the sequel, we shall write $u_i(x,t) = (u_i(x_1,t),\dots,u_i(x_h,t))$ for any $i \in \mathbb{N}$.

Definition 2.1. A weak solution to (2.1)-(2.3) on $[0,T_*)$, $T_* \in (0,+\infty]$, is a mapping $u = (u_i(x,t))_{i\geq 1}$ such that for any $T \in (0,T_*)$, $\sum_{i=1}^{\infty} iu_i \in L^\infty((0,T)\times V)$ and for each $i \geq 1$, for each $x_m \in V$ there holds:

- $u_i(x_m,\cdot) \in C([0,T],\mathbb{R})$ and $u_i(x_m,\cdot) \geq 0$, $\forall t \in [0,T]$
- $\sum_{j=1}^{\infty} a_{i,j}u_i(x_m,\cdot)u_j(x_m,\cdot) \in L^1((0,T))$
- u_i satisfies for each $t \in [0,T]$

$$u_i(t) = \exp(-td_i\Delta_G)U_i + \int_0^t \exp((s-t)d_i\Delta_G)(\frac{1}{2}\sum_{j=1}^{i-1} a_{i-j,j}u_{i-j}(s)u_j(s) - u_i(s)\sum_{j=1}^{\infty} a_{i,j}u_j(s) + f(x))ds\,. \tag{2.17}$$

We will focus now on the meaning of some terms in equation 2.17. Let $\{\phi_j\}_{j=1}^h$ be an orthonormal basis of eigenfunctions of the graph laplacian Δ_G with eigenvalues $\lambda_1,\dots,\lambda_h$ (see Appendix 1). Then for each $i \geq 1$:

$$\exp(-td_i\Delta_G)U_i = \sum_{j=1}^{h} \exp(-td_i\lambda_j)\langle\phi_j, U_i\rangle\phi_j,$$

where $U_i = [U_i(x_1,0),\dots,U_i(x_h,0)]$ is the vector of the initial data and for each $i \geq 1$

$$\langle\phi_j, U_i\rangle = \sum_{m=1}^{h} \phi_j(x_m)U_i(x_m,0) \text{ for } j = 1,\dots,h\,.$$

In addition, for each $x_m \in V$ and for each $i \geq 1$ we define:

$$F_i(x_m,s) = (\frac{1}{2}\sum_{j=1}^{i-1} a_{i-j,j}u_{i-j}(x_m,s)u_j(x_m,s) - u_i(x_m,s)\sum_{j=1}^{\infty} a_{i,j}u_j(x_m,s) + f(x_m))\,.$$

For simplicity, we set for each $i \geq 1$ $F_i(s) = (F_i(x_1,s),\dots,F_i(x_h,s))$; then

$$\exp(sd_i\Delta_G)F_i(s) = \sum_{j=1}^{h}\langle\phi_j, F_i(s)\rangle\exp(sd_i\lambda_j)\phi_j,$$

where for each $i \geq 1$

$$\langle \phi_j(\cdot), F_i(\cdot, s) \rangle = \sum_{m=1}^{h} \phi_j(x_m) F_i(x_m, s) \text{ for } j = 1, \ldots, h \, .$$

Definition 2.2. A classical solution to (2.1)-(2.3) on $[0, T_*)$, $T_* \in (0, +\infty]$, is a mapping $u = (u_i(x,t))_{i \geq 1}$ such that for any $T \in (0, T_*)$

- $u_i(x_m, t) \in C^1([0,T], \mathbb{R})$ $\forall x_m \in V$, $\forall i \geq 1$;
- $\sum_{j=1}^{\infty} a_{i,j} u_j(x_m, \cdot)$ converges uniformly in $[0,T]$, $\forall x_m \in V$, $\forall i \geq 1$.

and that satisfies (2.1)-(2.3) for each $t \in [0,T]$.

Remark 3. It easy to see that a classical solution is a weak solution.

Following [118], solutions of the infinite system are constructed by approximating the full system (2.1), (2.2) by the following systems $(\mathbf{S}^N)$ of $2N$ equations defined for any integer $N \geq 1$ as follows:

$$\frac{\partial u_1^N}{\partial t} = -d_1 \Delta_G u_1^N - u_1^N \sum_{j=1}^{N} a_{1,j} u_j^N + f(x) \tag{2.18}$$

$$\frac{\partial u_i^N}{\partial t} = -d_i \Delta_G u_i^N + \frac{1}{2} \sum_{j=1}^{i-1} a_{j,i-j} u_j^N u_{i-j}^N - u_i^N \sum_{j=1}^{N} a_{i,j} u_j^N \qquad \text{for } i = 2, \ldots N, \tag{2.19}$$

and

$$\frac{\partial u_i^N}{\partial t} = -d_i \Delta_G u_i^N + \frac{1}{2} \sum_{j=i-N}^{N} a_{j,i-j} u_j^N u_{i-j}^N \tag{2.20}$$

for $N+1 \leq i \leq 2N$. The functions u_i^N are subject to initial conditions as in (2.3). This system corrisponds to the first $2N$ equations of the system (2.1), (2.2) where $a_{ij} = 0$ for $i > N$ or $j > N$.
We recall that a solution of $(\mathbf{S}^N)$ is a function

$$u^N = u^N(x,t) : V \times \mathbb{R}^+ \longrightarrow \mathbb{R}^{2Nh} \, .$$

We shall also write

$$u^N(t) := u^N(\cdot, t) = \left(u_1^N(\cdot, t), \ldots, u_{2N}^N(\cdot, t) \right),$$

whereas, for $x = (x_1, \ldots, x_h) \in G$,

$$u_i^N(x,t) := \left(u_i^N(x_1, t), \ldots, u_i^N(x_h, t) \right) \qquad \text{for } i = 1, \ldots, 2N.$$

Existence of solution of the finite dimesional problem has been discussed in chapter one and is guaranteed in some interval $[0, t_{max}]$ by classical Peano-Picard-Lindelöf Theorem. In addition, suitable estimates of the norm $\|u_i(\cdot,t)^N\|_2$ for $i = 1, \ldots, 2N$, where $\|u_i^N(\cdot,t)\|_2 = \left(\sum_{x_m \in V} u_i^N(x_m,t)\right)^{\frac{1}{2}}$ allow us to extend the solution of problem $(\mathbf{S}^N)$ to $[0, +\infty)$ (see theorem 1.5.2).
Definition 2.1 of weak solution is motivated by the fact that not much information is avaible about the regularity of the terms $u_i \sum_{j=1}^{\infty} a_{i,j} u_j$ when $i \geq 1$. Thus, we can not take advantage of classical regularity results for ordinary differential equations and conclude that each equation in (2.1),(2.2) holds in classical sense.
To proceed further we take up an argument introduced in [86]. Namely, on multiplying the i-th equation in $(\mathbf{S}^N)$ by an arbitrary real number g_i and then adding up all the equations, we obtain the following useful identity written on the vertex x_m of G:

$$\begin{aligned} &\sum_{i=1}^{2N} g_i \frac{\partial u_i^N(x_m,t)}{\partial t} + \sum_{i=1}^{2N} g_i d_i \Delta_G u_i^N(x_m,t) \\ &\quad = \frac{1}{2} \sum_{i=1}^{N} \sum_{j=1}^{N} (g_{i+j} - g_i - g_j) a_{ij} u_i^N(x_m,t) u_j^N(x_m,t) + g_1 f(x_m) \end{aligned} \tag{2.21}$$

If we choose $g_i = i$ for $i = 1, \ldots, 2N$, we have:

$$\sum_{i=1}^{2N} i \frac{\partial u_i^N(x_m,t)}{\partial t} + \sum_{i=1}^{2N} i d_i \Delta_G u_1^N(x_m,t) = f(x_m)$$

Summing up over all $x_m \in V$ and integrating between 0 and t, by (2.16) we see that:

$$\begin{aligned} \sum_{x_m \in V} \sum_{i=1}^{2N} i u_i^N(x_m,t) &= \sum_{x_m \in V)} \sum_{i=1}^{2N} i U_i(x_m) + t \sum_{x_m \in V} f(x_m) \\ &\leq M_1(0) + \|f(\cdot)\|_\infty h t \end{aligned} \tag{2.22}$$

where h is the number of vertices of the graph G.

We will prove the existence of a positive global weak solution in the sense precised by Definition 2.1 for a wider range of coagulation coefficients. Specifically, we prove the existence of that solution for (2.1)-(2.3) under the assumption on cofficients

$$\lim_{j \to \infty} \frac{a_{i,j}}{j} = 0 \text{ for } i \in \mathbb{N} \tag{2.23}$$

or

$$\underline{A} i j \leq a_{ij} \leq \bar{A} i j \text{ for } \underline{A}, \bar{A} > 0 \text{ for any } i, j \geq 1 \,. \tag{2.24}$$

We first prove the existence of a non negative local in time weak solution and then we extend it to $[0,\infty)$. Thus, we are able to prove the following results:

Theorem 2.3.1. *Suppose* (2.23) *holds and let* $T>0$ *be an arbitrary time. Then there exists a non negative weak solution* $\{u_i\}_{i=1}^{\infty}$ *of* (2.1), (2.2),(2.3) *defined on* $V\times[0,T]$, *such that:*

$$M_1(t)\leq M_1(0)+\|f(\cdot)\|_\infty hT \quad \textit{for } t\in[0,T]. \tag{2.25}$$

where h *is the number of verteces of* G.

Before indroducing the proof of Theorem 2.3.1, we will state a preliminary Lemma.

Lemma 2.3.2. *Solutions of* ($\boldsymbol{S}^N$) *are classical and global in time. For any* $0\leq t<T$ *the following estimates hold:*

$$\|u_1^N(\cdot,t)\|_\infty\leq\|u_1^N(\cdot,t)\|_2\leq K_1:=\Big(\Big(\|u_1^N(\cdot,0)\|_2^2+T\|f(\cdot)\|_2^2\Big)\exp\{T\}\Big)^{\frac{1}{2}} \tag{2.26}$$

$$\|u_i^N(\cdot,t)\|_\infty\leq\|u_i^N(\cdot,t)\|_2\leq K_i:=\left(\Big(\|u_i^N(\cdot,0)\|^2+\frac{T}{2}(\sum_{j=1}^{i-1}a_{j,i-j}K_jK_{i-j})^2\exp\{\frac{T}{2}\}\right)^{\frac{1}{2}} \tag{2.27}$$

for $1<i\leq N$, *and*

$$\|u_i^N(\cdot,t)\|_\infty\leq\|u_i^N(\cdot,t)\|_2\leq K_i:=\left(\Big(\|u_i^N(\cdot,0)\|^2+\frac{T}{2}(\sum_{j=i-N}^{N}a_{j,i-j}K_jK_{i-j})^2\exp\{\frac{T}{2}\}\right)^{\frac{1}{2}} \tag{2.28}$$

for $N+1\leq i\leq 2N$.

Proof. The proof is analogous to Theorem 1.5.2 in Chapter 1. □

Remark 4. If $a_{i,j}=o(j)$, for $j\to\infty$, for each $i\geq1$, it follows that for each i there exists a constant $\bar{c}_i$ such that

$$a_{i,j}\leq\bar{c}_i j$$

for $j\geq1$. For $x_m\in V$ let $\{u_j^N(x_m,t)\}_{j=1}^{2N}$ be the solution restricted to $[0,T]$ of the approximating system ($\mathbf{S}^N$) (2.18)-(2.20) Hence, by (2.22), for $t\leq T$ it holds:

$$\begin{aligned}\sum_{j=1}^{N}a_{ij}u_j^N(x_m,t)&\leq\sum_{x_m\in V}\sum_{j=1}^{2N}a_{i,j}u_j^N(x_m,t)\leq\bar{c}_i\sum_{x_m\in V}\sum_{j=1}^{2N}ju_j^N(x_m,t)\\&\leq\bar{c}_i(\sum_{x_m\in V}M_1(x_m,0)+\|f(\cdot)\|_\infty hT)\end{aligned} \tag{2.29}$$

Proof of Theorem 2.3.1. The proof will be made of several steps.
Step 1: Let denote the reaction terms in the ith equation of $(\mathbf{S}^N)$ by

$$F_i^N = f_i^N - u_i^N g_i^N$$

where

$$\begin{cases} f_i^N = \frac{1}{2}\sum_{j=1}^{i-1} a_{j,i-j} u_j^N u_{i-j}^N \\ g_i^N = \sum_{j=1}^{N} a_{ij} u_j^N \qquad\qquad \text{if } i \leq N \end{cases} \tag{2.30}$$

and

$$\begin{cases} f_i^N = \frac{1}{2}\sum_{j=i-N}^{N} a_{j,i-j} u_j^N u_{i-j}^N \\ g_i^N = 0 \qquad\qquad\qquad\qquad \text{if } N < i \leq 2N\ . \end{cases} \tag{2.31}$$

Let consider for each $1 \leq i$, the sequence of functions $\{u_i^N(x_m,t)\}_{N=i}^{\infty}$ in $C([0,T])$. By (2.26) and (2.27), $u_i^N(x_m,t) \leq K_i$ for each $x_m \in V$ and $0 \leq t \leq T$, with K_i that does not depend on N. Thus, for each $i \leq N$, $\{u_i^N(x_m,t)\}_{N=i}^{\infty}$ is a equi bounded sequence of functions in $C([0,T])$. In addition, we can show that for any $i \in \mathbb{N}$, for any $x_m \in V$ $\{u_i^N(x_m,t)\}_{N=i}^{\infty}$ is equi-Lipschitz that implies equicontinous. For each $N \geq 1$, by(2.29) , the first equation of the N-th system gives that for any $t \in [0,T]$,

$$\begin{aligned} |\frac{\partial u_1^N}{\partial t}(x_m,t)| &\leq |d_1 \sum_{x_j \sim x_m} (u_1^N(x_j,t) - u_1^N(x_m,t)) w_{m,j}| + |u_1^N(x_m,t)||\sum_{j=1}^{N} a_{1,j} u_j^N(x_m,t)| + \|f(\cdot)\|_\infty \\ &\leq d_1 |\sum_{x_j \sim x_m} u_1^N(x_j,t) w_{m,j}| + d_1 |deg(x_m) u_1(x_m,t)| + |u_1^N(x_m,t)||\sum_{j=1}^{N} a_{1,j} u_j^N(x_m,t)| + \|f(\cdot)\|_\infty \\ &\leq d_1 \sum_{x_j \sim x_m} \|u_1^N(\cdot,t)\|_\infty w_{m,j} + d_1 deg(x_m) \|u_1^N(\cdot,t)\|_\infty + |u_1^N(x_m,t)||\sum_{j=1}^{N} a_{1,j} u_j^N(x_m,t)| + \|f(\cdot)\|_\infty \\ &\leq 2 d_1 deg(x_m) \|u_1^N(\cdot,t)\|_\infty + \|u_1^N(\cdot,t)\|_\infty \bar{c}_1 (M_1(0) + \|f(\cdot)\|_\infty h T) + \|f(\cdot)\|_\infty\ . \end{aligned} \tag{2.32}$$

where $deg(x_m) = \sum_{x_j \sim x_m} w_{m,j}$ is the degree of the vertex x_m. As (2.32) holds for all $x_m \in V$, it follows that for $t \in [0,T]$:

$$\begin{aligned} \|\frac{\partial u_1^N}{\partial t}(\cdot,t)\|_\infty &\leq D_1 \|u_1^N(\cdot,t)\|_\infty + \|f(\cdot)\|_\infty \\ &\leq D_1 \int_0^t \|\frac{\partial u_1^N}{\partial t}(\cdot,t)\|_\infty + D_1 \|u_1^N(\cdot,0)\|_\infty + \|f(\cdot)\|_\infty \end{aligned} \tag{2.33}$$

where

$$D_1 = 2 d_1 \max_{x_m \in V} \{deg(x_m)\} + \bar{c}_1 (M_1(0) \|f(\cdot)\|_\infty h T) + \|f(\cdot)\|_\infty$$

. Thus, by Gronwall's inequality we obtain that :

$$\|\frac{\partial u_1^N}{\partial t}(\cdot,t)\|_\infty \leq \Big(D_1\|u_1^N(\cdot,0)\|_\infty + \|f(\cdot)\|_\infty\Big)\exp\{D_1 t\} \quad \text{for any } t\in[0,T]\ . \tag{2.34}$$

We prove now that for every $i\in\mathbb{N}$ and for every $N\geq i$

$$\|\frac{\partial u_i^N}{\partial t}\|_{L^\infty(V\times[0,T])} \leq \mathbf{C}_i\ . \tag{2.35}$$

The proof will be carried out by induction on i. Indeed, the assertion is true for $i=1$, since (2.34) holds.
Suppose the assertion (2.35) holds for $i-1$. Then, for any $t\in[0,T]$:

$$\begin{aligned}|\frac{\partial u_i^N}{\partial t}(x_m,t)| &\leq 2d_i deg(x_m)\|u_i^N(\cdot,t)\|_\infty + \|u_i^N(\cdot,t)\|_\infty \bar{c}_i(M_1(0)+\|f(\cdot)\|_\infty hT)\\ &\quad + \frac{1}{2}\sum_{j=1}^{i-1} a_{j,i-j}\|u_j^N(\cdot,t)\|_\infty\|u_{i-j}^N(\cdot,t)\|_\infty\end{aligned}$$

$$\begin{aligned}&\leq D_i\|u_i^N(\cdot,t)\|_\infty\\ &\quad + \frac{1}{2}\sum_{j=1}^{i-1} a_{j,i-j}(\|u_j^N(\cdot,t)-u_j^N(\cdot,0)\|_\infty + \|u_j^N(\cdot,0)\|_\infty)(\|u_{i-j}^N(\cdot,t)-u_{i-j}^N(\cdot,0)\|_\infty + \|u_{i-j}^N(\cdot,0)\|_\infty)\end{aligned}$$

$$\begin{aligned}&\leq D_i\|u_i^N(\cdot,t)\|_\infty\\ &\quad + \frac{1}{2}\sum_{j=1}^{i-1} a_{j,i-j}\left(\int_0^t \|\frac{\partial u_j^N}{\partial t}(\cdot,t)\|_\infty + \|u_j^N(\cdot,0)\|_\infty\right)\left(\int_0^t \|\frac{\partial u_{i-j}^N}{\partial t}(\cdot,t)\|_\infty + \|u_{i-j}^N(\cdot,0)\|_\infty\right)\end{aligned}$$

$$\leq D_i\int_0^t \|\frac{\partial u_i^N}{\partial t}(\cdot,t)\|_\infty + D_i\|u_i^N(\cdot,0)\|_\infty + \frac{1}{2}\sum_{j=1}^{i-1} a_{j,i-j}\Big(\mathbf{C}_j T + \|u_j^N(\cdot,0)\|_\infty\Big)\Big(\mathbf{C}_{i-j}T + \|u_{i-j}^N(\cdot,0)\|_\infty\Big) \tag{2.36}$$

where

$$D_i = 2d_i\max_{x_m\in V}\{deg(x_m)\} + \bar{c}_i(M_1(0)+\|f(\cdot)\|_\infty hT).$$

As (2.32) holds for all $x_m\in V$, using Gronwall's inequality we obtain that :

$$\|\frac{\partial u_i^N}{\partial t}(\cdot,t)\|_\infty \leq \left(D_i\|U_i(\cdot)\|_\infty + \frac{1}{2}\sum_{j=1}^{i-1} a_{j,i-j}\left(\mathbf{C}_j T + \|U_j(\cdot)\|_\infty\right)\left(\mathbf{C}_{i-j}T + \|U_{i-j}(\cdot)\|_\infty\right)\right)\exp\{D_i t\}\ . \tag{2.37}$$

for any $t \in [0,T]$.
Thus, the $\mathbf{C}_i$'s in (2.35) are given recursively by:

$$C_1 = (D_1\|U_1(\cdot)\|_\infty + \|f(\cdot)\|_\infty)\exp\{D_1T\}$$

and

$$\mathbf{C}_i = \left(D_i\|U_i(\cdot)\|_\infty + \frac{1}{2}\sum_{j=1}^{i-1} a_{j,i-j}\left(\mathbf{C}_jT + \|U_j(\cdot)\|_\infty\right)\left(\mathbf{C}_{i-j}T + \|U_{i-j}(\cdot)\|_\infty\right)\right)\exp\{D_iT\} \text{ for } i \geq 2\,.$$

In particular, $\mathbf{C}_i$ is indipendent of N for $i = 1, 2, \ldots$.
For any $i \in \mathbf{N}$, $\{u_i^N(x_m,\cdot), N \geq i\}$ is equicontinuous in $[0,T]$ for $m = 1, \cdots, h$. Thus, by Ascoli-Arzelà theorem, for any $i \in \mathbf{N}$ there exists a subsequence $u_i^{N_\ell^i}(x_m,\cdot)$ that converges uniformly in $[0,T]$ to $u_i(x_m,\cdot)$ for $m = 1, \cdots, h$. Without loss of generality, we may assume $(N_\ell^2)_{\ell\in\mathbf{N}}$ is a subsequence of $(N_\ell^1)_{\ell\in\mathbf{N}}$, $(N_\ell^3)_{\ell\in\mathbf{N}}$ is a subsequence of $(N_\ell^2)_{\ell\in\mathbf{N}}$ and so on. The construction can be summarised as follows: there exists a sequence of sequences $(u_i^{N_\ell^i})_{\ell\in\mathbb{N}}$, $i = 1, 2, \ldots$ such that

- $u_i^{N_\ell^i} \to u_i$ as $\ell \to \infty$;
- $(N_\ell^{i+1})_\ell$ is a subsequence of $(N_\ell^i)_\ell$ and $N_\ell^i \geq i$.

Notice that $N_\ell^{i+1} \geq N_\ell^i$. Indeed, by definition, $N_\ell^{i+1} = N_{k_\ell}^i$. Since $(N_\ell^i)_\ell$ is increasing and $k_\ell > \ell$, the assertion follows. For sake of simplicity, set now $M_\ell := N_\ell^\ell$. We have $M_{\ell+1} = N_{\ell+1}^{\ell+1} > N_\ell^{\ell+1} \geq N_\ell^\ell$. Hence, $(u_i^{M_\ell})_{\ell\in\mathbb{N}}$ is a subsequence of $(u_i^{N_\ell^i})_{\ell\in\mathbb{N}}$ for $i = 1, 2, \ldots$ and

$$u_i^{M_\ell}(x_m,t) \to u_i(x_m,t) \tag{2.38}$$

uniformly $\forall i = 1, 2, \ldots$. In addition, $u_i(x_m,t) \in C([0,T])$, for all $i \geq 1$ and for all $x_m \in V$. By the fact that $u_i^{M_\ell}(x_m,t) \geq 0$, for all $\ell \in \mathbb{N}$, for any $i \geq 1$, for any $x_m \in V$, for any $t \in [0,T]$, it follows $u_i(x_m,t) \geq 0$ for any $i \geq 1$, for any $x_m \in V$, for any $t \in [0,T]$.
Finally, $\|u_i\|_{V\times[0,T]} \leq K_i$ for any $i \geq 1$, where K_i are given by 2.26 and 2.27.

We will discuss at this point the convergence of the series $\sum_{i=1}^\infty iu_i(x_m,t)$ for $t \in [0,T]$ and for $x_m \in V$. If $P \in \mathbb{N}$, set $S_P(t) = \sum_{i=1}^P iu_i(x_m,t)$. Consider now the sequence $\{u_i^{M_\ell}\}_{\ell\in\mathbb{N}}$ for $i = 1, 2, \ldots$ built previously. By construction, for each fixed M_ℓ, $\{u_i^{M_\ell}\}_{i=1}^{2M_\ell}$ is the solution restricted to the interval $[0,T]$ of the approximating system $(\mathbf{S}^{M_\ell})$ (2.18)-(2.20).

Then, for $1 \leq P < 2M_\ell$ and for each $t \in [0,T]$ we have:

$$\sum_{i=1}^{P} i u_i^{M_\ell}(x_m,t) \leq \sum_{i=1}^{2M_\ell} i u_i^{M_\ell}(x_m,t) \leq M_1(0) + \|f(\cdot)\|_\infty hT \tag{2.39}$$

where in the last inequality we use (2.22). Passing to the limit for $\ell \to \infty$, by (2.38), we obtain for each $t \in [0,T]$

$$\sum_{i=1}^{P} i u_i(x_m,t) = \lim_{l\to\infty} \sum_{i=1}^{P} i u_i^{M_\ell}(x_m,t) \leq \limsup_{l\to\infty} \sum_{i=1}^{2M_\ell} i u_i^{M_\ell}(x_m,t) \leq M_1(0) + \|f(\cdot)\|_\infty hT\ . \tag{2.40}$$

Hence, for each $t \in [0,T]$ the partial sums $S_P(t)$ are equibounded from above. Since $\sum_{i=1}^{\infty} i u_i(x_m,t)$ is a series with non negative terms, then it converges in $[0,T]$ and from (2.40), it holds that for each $t \in [0,T]$:

$$\sum_{i=1}^{\infty} i u_i(x_m,t) = \lim_{P\to\infty} \sum_{i=1}^{P} i u_i(x_m,t) \leq M_1(0) + \|f(\cdot)\|_\infty hT\ . \tag{2.41}$$

In addition, for $1 \leq P < 2M_\ell$ and for each $t \in [0,T]$ again by (2.22) we also have:

$$\sum_{x_m\in V} \sum_{i=1}^{P} i u_i^{M_\ell}(x_m,t) \leq \sum_{x_m\in V} \sum_{i=1}^{2M_\ell} i u_i^{M_\ell}(x_m,t) \leq M_1(0) + \|f(\cdot)\|_\infty hT\ . \tag{2.42}$$

Thus, passing to the limit for $\ell \to \infty$, by (2.38) we have that for each $t \in [0,T]$:

$$\begin{aligned} \sum_{x_m\in V} \sum_{i=1}^{P} i u_i(x_m,t) &= \lim_{l\to\infty} \sum_{x_m\in V} \sum_{i=1}^{P} i u_i^{M_\ell}(x_m,t) \\ &\leq \limsup_{l\to\infty} \sum_{x_m\in V} \sum_{i=1}^{2M_\ell} i u_i^{M_\ell}(x_m,t) \leq M_1(0) + \|f(\cdot)\|_\infty hT\ . \end{aligned} \tag{2.43}$$

Inequality (2.25) follows, passing to the limit for $P \to \infty$.

Step 2:

In the previous step we proved the existence of a mapping $u = (u_i(x,t))_{i\geq 1}$, obtained as limit of solutions of the approximating sistem (2.18)-(2.20), where $u_i(x,t) = (u_i(x_1,t),\ldots,u_i(x_h,t)$ and such that for each $x_m \in V$ $u_i(x_m,\cdot) \in C([0,T])$ and $u_i(x_m,\cdot) \geq 0$, $\forall t \in [0,T]$. We will prove now that the functions u_i satisfy for each $t \in [0,T]$ equation (2.17) for $i = 1,2\ldots$.

We observe that for fixed ℓ and $i < M_\ell$ the function $u_i^{M_\ell}$ is the solution given by the

Duhamel formula:

$$u_i^{M_\ell}(t) = \exp^{-td_i\Delta_G} U_i + \int_0^t \exp^{(s-t)d_i\Delta_G}(f_i^{M_\ell}(s) - u_i^{M_\ell}(s)g_i^{M_\ell}(s) + f(x))ds \qquad (2.44)$$

with $t \leq T$.
In order to pass to the limit in (2.44) we show preliminarly that for each i and for each $x_m \in V$

$$\int_0^T |g_i^{M_\ell}(x_m, s) - \sum_{j=1}^{\infty} a_{i,j}u_j(x_m, s)|ds \to 0 \qquad \text{for } \ell \to \infty \ ; \qquad (2.45)$$

in other words that:

$$\int_0^T |\sum_{j=1}^{M_\ell} a_{i,j}u_j^{M_\ell}(x_m, s) - \sum_{j=1}^{\infty} a_{i,j}u_j(x_m, s)|ds \to 0 \qquad \text{for } \ell \to \infty \ ; \qquad (2.46)$$

and

$$\int_0^T |\frac{1}{2}\sum_{j=1}^{i-1} a_{j,i-j}(u_j^{M_\ell}(x_m, s)u_{i-j}^{M_\ell}(x_m, s) - u_j(x_m, s)u_{i-j}(x_m, s))|ds \to 0 \ \text{ for } \ell \to \infty \ . \qquad (2.47)$$

First, we notice that (2.47) follows from (2.38) by dominated convergence theorem, since $u_j^{M_\ell}(x_m, s)u_{i-j}^{M_\ell}(x_m, s) \leq K_j K_{i-j}$, for $0 \leq s \leq T$.
In order to show (2.46), we observe that by (2.22) for each fixed ℓ and for $s \leq T$ we have:

$$\sum_{j=1}^{2M_\ell} j u_j^{M_\ell}(x_m, s) \leq \sum_{x_m \in V} \sum_{j=1}^{2M_\ell} j u_j^{M_\ell}(x_m, s) \leq M_1(0) + \|f(\cdot)\|_\infty hT \ .$$

In addition, if $\lambda \leq \ell$, for $1 \leq M_\lambda < M_\ell$

$$\begin{aligned} \sum_{j=M_\lambda}^{M_\ell} a_{i,j}u_j^{M_\ell}(x_m, s) &\leq \sup_{j>M_\lambda} \frac{a_{ij}}{j} \sum_{j=M_\lambda}^{M_\ell} j u_j^{M_\ell}(x_m, s) \\ &\leq \sup_{j>M_\lambda} \frac{a_{ij}}{j} \sum_{j=1}^{2M_\ell} j u_j^{M_\ell}(x_m, s) \\ &\leq \sup_{j>M_\lambda} \frac{a_{ij}}{j}(M_1(0) + \|f(\cdot)\|_\infty hT) \end{aligned} \qquad (2.48)$$

and consequently,

$$\int_0^T \sum_{j=M_\lambda}^{M_\ell} a_{i,j}u_j^{M_\ell}(x_m, s)ds \leq \sup_{j>M_\lambda} \frac{a_{ij}}{j}(M_1(0) + \|f(\cdot)\|_\infty hT)T \ . \qquad (2.49)$$

By (2.23) for fixed i and arbitrary ϵ there exists an ℓ_0 such that for any $\ell > \ell_0$,

$$\int_0^T \sum_{j=M_{\ell_0}}^{M_\ell} a_{i,j} u_j^{M_\ell}(x_m, s) ds \leq \sup_{j > M_{\ell_0}} \frac{a_{ij}}{j} (M_1(0) + \|f(\cdot)\|_\infty hT) T < \frac{\epsilon}{3} . \tag{2.50}$$

Hence, we can write:

$$|\sum_{j=1}^{M_\ell} a_{i,j} u_j^{M_\ell}(x_m, s) - \sum_{j=1}^{\infty} a_{i,j} u_j(x_m, s)| =$$

$$|\sum_{j=1}^{M_{\ell_0}-1} a_{i,j} u_j^{M_\ell}(x_m, s) + \sum_{j=M_{\ell_0}}^{M_\ell} a_{i,j} u_j^{M_\ell}(x_m, s) - \sum_{j=1}^{\infty} a_{i,j} u_j(x_m, s)|$$

$$\leq \sum_{j=1}^{M_{\ell_0}-1} a_{i,j} |u_j^{M_\ell}(x_m, s) - u_j(x_m, s)| + |\sum_{j=M_{\ell_0}}^{M_\ell} a_{i,j} u_j^{M_\ell}(x_m, s)| + |\sum_{j=M_{\ell_0}}^{\infty} a_{i,j} u_j(x_m, s)| . \tag{2.51}$$

Thus, we want to prove now that there exists an $\bar{\ell} \geq \ell_0$ such that for any $\ell > \bar{\ell}$:

$$\int_0^T \sum_{j=1}^{M_{\ell_0}-1} a_{i,j} |u_j^{M_\ell}(x_m, s) - u_j(x_m, s)| + |\sum_{j=M_{\ell_0}}^{M_\ell} a_{i,j} u_j^{M_\ell}(x_m, s)| + |\sum_{j=M_{\ell_0}}^{\infty} a_{i,j} u_j(x_m, s)| < \epsilon . \tag{2.52}$$

By (2.38), there exists an $\ell_1 \geq \ell_0$ such that for any $\ell > \ell_1$

$$\int_0^T \sum_{j=1}^{M_{\ell_0}-1} a_{i,j} |u_j^{M_\ell}(x_m, s) - u_j(x_m, s)| ds < \frac{\epsilon}{3} . \tag{2.53}$$

Hence, keeping into account (2.50), it remains to be proven that

$$\int_0^T \sum_{j=M_{\ell_0}}^{\infty} a_{i,j} u_j(x_m, s) ds < \frac{\epsilon}{3} . \tag{2.54}$$

We observe preliminary that $\sum_{j=1}^{\infty} a_{i,j} u_j(x_m, s)$ converges for all $s \in [0, T]$. In fact, by hypothesis, for each $i \geq 1$, there exists a constant $\bar{c}_i$ such that

$$a_{i,j} \leq \bar{c}_i j$$

for each $s \in [0,T]$, so that

$$\sum_{j=1}^{\infty} a_{i,j} u_j(x_m,s) \le \bar{c}_i \sum_{j=1}^{\infty} j u_j(x_m,s) < \infty. \tag{2.55}$$

We prove now (2.54).
For $P^{'} \in \mathbb{N}$, such that $M_{\ell_0} \le P^{'} < 2M_\ell$, for each fixed i and for each $s \in [0,T]$ we have:

$$\sum_{j=M_{\ell_0}}^{P^{'}} a_{i,j} u_j^{M_\ell}(x_m,s) \le \sum_{j=M_{\ell_0}}^{2M_\ell} a_{i,j} u_j^{M_\ell}(x_m,s) \le \sup_{j>M_{\ell_0}} \frac{a_{ij}}{j} (M_1(0) + \|f(\cdot)\|_\infty hT)$$

where in the last inequality we use (2.48).
Thus, integrating in time and passing to the limit for $\ell \to \infty$, by (2.38), we obtain :

$$\begin{aligned} \int_0^T \sum_{j=M_{\ell_0}}^{P^{'}} a_{i,j} u_j(x_m,s) ds &= \lim_{\ell\to\infty} \int_0^T \sum_{j=M_{\ell_0}}^{P^{'}} a_{i,j} u_j^{M_\ell}(x_m,s) ds \\ &\le \limsup_{\ell\to\infty} \int_0^T \sum_{j=M_{\ell_0}}^{2M_\ell} a_{i,j} u_j^{M_\ell}(x_m,s) ds \\ &\le \sup_{j>M_{\ell_0}} \frac{a_{ij}}{j} (M_1(0) + \|f(\cdot)\|_\infty hT) T \, . \end{aligned} \tag{2.56}$$

Finally, by monotone convergence theorem, (2.56), (2.50), there holds:

$$\int_0^T \sum_{j=M_{\ell_0}}^{\infty} a_{i,j} u_j(x_m,s) = \lim_{P^{'}\to\infty} \int_0^T \sum_{j=M_{\ell_0}}^{P^{'}} a_{i,j} u_j(x_m,s) \le \sup_{j>M_{\ell_0}} \frac{a_{ij}}{j} (M_1(0) + \|f(\cdot)\|_\infty hT) T < \frac{\epsilon}{3} \, . \tag{2.57}$$

Putting togheter (2.57),(2.53), (2.50) it follows that for $\ell > \ell_1 \ge \ell_0$

$$\int_0^T |\sum_{j=1}^{M_\ell} a_{i,j} u_j^{M_\ell}(x_m,s) - \sum_{j=1}^{\infty} a_{i,j} u_j(x_m,s)| ds < \epsilon \, . \tag{2.58}$$

We will show, now, that for each i and for each $x_m \in V$

$$\int_0^T |u_i^{M_\ell}(x_m,s) \sum_{j=1}^{M_\ell} a_{i,j} u_j^{M_\ell}(x_m,s) - u_i(x_m,s) \sum_{j=1}^{\infty} a_{i,j} u_j(x_m,s) ds| \to 0 \quad \text{for } \ell \to \infty \, .$$

Using the fact that the series $\sum_{j=1}^{\infty} a_{i,j}u_j(x_m,s)$ converges in $[0,T]$, it holds:

$$\int_0^T |u_i^{M_\ell}(x_m,s)\sum_{j=1}^{M_\ell} a_{i,j}u_j^{M_\ell}(x_m,s) - u_i^{M_\ell}(x_m,s)\sum_{j=1}^{\infty} a_{i,j}u_j(x_m,s) + u_i^{M_\ell}(x_m,s)\sum_{j=1}^{\infty} a_{i,j}u_j(x_m,s) - u_i(x_m,s)\sum_{j=1}^{\infty} a_{i,j}u_j(x_m,s)|ds$$

$$\leq \int_0^T u_i^{M_\ell}(x_m,s)|\sum_{j=1}^{M_\ell} a_{i,j}u_j^{M_\ell}(x_m,s) - \sum_{j=1}^{\infty} a_{i,j}u_j(x_m,s)|ds + \int_0^T |u_i^{M_\ell}(x_m,s) - u_i(x_m,s)|\sum_{j=1}^{\infty} a_{i,j}u_j(x_m,s)ds$$

$$\leq K_i\int_0^T |\sum_{j=1}^{M_\ell} a_{i,j}u_j^{M_\ell}(x_m,s) - \sum_{j=1}^{\infty} a_{i,j}u_j(x_m,s)|ds + \int_0^T |u_i^{M_\ell}(x_m,s) - u_i(x_m,s)|\sum_{j=1}^{\infty} a_{i,j}u_j(x_m,s)ds$$

where in the last inequality we use Lemma 2.3.2.
Letting $\ell \to \infty$ the first term of the last inequality goes to zero by (2.58).
It remains to show that

$$\int_0^T |u_i^{M_\ell}(x_m,s) - u_i(x_m,s)|\sum_{j=1}^{\infty} a_{i,j}u_j(x_m,s)ds \to 0 \quad \text{for } \ell \to \infty\,. \tag{2.59}$$

We observe prelimirary that by (2.55), (2.41)

$$\int_0^T \sum_{j=1}^{\infty} a_{i,j}u_j(x_m,s)ds \leq \int_0^T \bar{c}_i\sum_{j=1}^{\infty} ju_j(x_m,s)ds \leq \bar{c}_i(M_1(0) + \|f(\cdot)\|_\infty hT)T\,.$$

Thus, $\sum_{j=1}^{\infty} a_{i,j}u_j(x_m,s) \in L^1[0,T]$ and

$$|u_i^{M_\ell}(x_m,s) - u_i(x_m,s)|\sum_{j=1}^{\infty} a_{i,j}u_j(x_m,s) \leq 2K_i\sum_{j=1}^{\infty} a_{i,j}u_j(x_m,s)$$

by Lemma 2.3.2. Hence, (2.59) follows from (2.38) by dominated convergence theorem.

Let $\varphi_i^{M_\ell}(s) = f_i^{M_\ell}(s) - u_i^{M_\ell}(s)g_i^{M_\ell}(s) + f(x)$ for each $i = 1, 2, \ldots$; previously, we have shown that

$$\varphi_i^{M_\ell} \to \varphi_i \qquad \text{for } \ell \to \infty$$

in $L^1(0,T)$, where

$$\varphi_i(s) = f_i(s) - u_i(s)g_i(s) + f(x) = \frac{1}{2}\sum_{j=1}^{i-1} a_{j,i-j}u_j u_{i-j} - u_i \sum_{j=1}^{\infty} a_{ij}u_j + f(x)\ .$$

Therefore, it remains to show that

$$\exp(sd_i\Delta_G)\varphi_i^{M_\ell} \to \exp(sd_i\Delta_G)\varphi_i \qquad \text{for } \ell \to \infty$$

in $L^1(0,T)$, i.e. that the operator $\mathbf{A} := \exp(sd_i\Delta_G) : L^1(0,T) \to L^1(0,T)$ is continuous. Hence, we have to prove that $\mathbf{A}$ is limited, i.e. there exists a real number $C \geq 0$ such that

$$|\exp(sd_i\Delta_G)\bar{\varphi}|_{L^1(0,T)} \leq C|\bar{\varphi}|_{L^1(0,T)} \tag{2.60}$$

for every $\bar{\varphi} \in L^1(0,T)$.
Let $\{\phi_j\}_{j=1}^h$ be an orthonormal basis of eigenfunctions of Δ_G. If $s \in [0,T]$, we can write

$$\bar{\varphi}(s) = \sum_{j=1}^{h} \langle \bar{\varphi}(s), \phi_j\rangle \phi_j,$$

and

$$|\bar{\varphi}(s)|^2 = \sum_{j=1}^{h} \langle \bar{\varphi}(s), \phi_j\rangle^2.$$

Since

$$\exp(sd_i\Delta_G)\bar{\varphi}(s) = \sum_{j=1}^{h} \langle \bar{\varphi}(s), \phi_j\rangle \exp(sd_i\lambda_j)\phi_j,$$

then

$$|\exp(sd_i\Delta_G)\bar{\varphi}(s)|^2 = \sum_{j=1}^{h} \langle \bar{\varphi}(s), \phi_j\rangle^2 \exp^{(2sd_i\lambda_j)} \leq C|\bar{\varphi}(s)|^2\ .$$

where $C = \max_{j=1,\ldots,h} \exp\{2Td_i\lambda_j\}$.
Integrating between 0 and t, (2.60) follows.
Step 3: We observe that the term $\sum_{j=1}^{\infty} a_{i,j}u_i(x_m,\cdot)u_j(x_m,\cdot) \in L^1(0,T)$, for each $x_m \in V$. In fact, for each $\ell \geq 1$ by (2.29) and by Lemma 2.3.2 we have that:

$$\int_0^T u_i^{M_\ell} \sum_{j=1}^{M_\ell} a_{i,j}u_j^{M_\ell}(x_m,t) \leq \int_0^T K_i\bar{c}_i(M_1(0) + \|f(\cdot)\|_\infty hT) < \infty\ .$$

Hence, we have that $\{u_i^{M_\ell} \sum_{j=1}^{M_\ell} a_{i,j} u_j^{M_\ell}(x_m,t)\}_{\ell\in\mathbf{N}}$ is a sequence of functions in $L^1(0,T)$. In addition, it holds that:

$$\int_0^T |u_i^{M_\ell}(x_m,s)\sum_{j=1}^{M_\ell} a_{i,j}u_j^{M_\ell}(x_m,s) - u_i(x_m,s)\sum_{j=1}^{\infty} a_{i,j}u_j(x_m,s)|ds \to 0 \qquad \text{for } \ell\to\infty\ ; \tag{2.61}$$

thus, $\sum_{j=1}^{\infty} a_{i,j}u_i(x_m,\cdot)u_j(x_m,\cdot) \in L^1(0,T)$, due to the fact that $L^1(0,T)$ is a Banach space.

Finally, the term $\sum_{i=1}^{\infty} iu_i \in L^\infty((0,T)\times V)$, as by (2.41), we have that for each $x_m \in V$ and for each $t\in[0,T]$

$$\sum_{j=1}^{\infty} ju_j(x_m,t) \le M_1(0) + \|f(\cdot)\|_\infty hT\ .$$

hence:

$$\sup_{(x_m,t)\in V\times(0,T)} \sum_{i=1}^{\infty} iu_i(x_m,t) < \infty\ .$$

We have shown that $(u_i(x,t))_{i\in\mathbb{N}}$ is a weak solution of (2.1)-(2.3) in sense of Definition 2.1. □

The solutions obtained in the previous result are then shown to hold true for arbitrarly large times. More precisely:

Theorem 2.3.3. *Under the hypothesis of the Theorem 2.3.1, there exists a non negative weak solution* $\{u_i\}_{i=1}^{\infty}$ *of* (2.1), (2.2),(2.3) *defined on* $V\times[0,\infty)$

Proof. We can construct a solution of (2.1), (2.2),(2.3) defined on $V\times[0,\infty)$ in the following way. Let $\{T_n\}_{n=1}^{\infty}$ be any increasing sequence of positive numbers such that $T_n\to\infty$, as $n\to\infty$. Using the result of Theorem 2.3.1, there exists a sequence $\{M_\ell^1\}_{l=1}^{\infty}$ such that for each $i=1,2,\dots$ a solution $u_i^1(x_m,t)$ to (2.4), (2.5),(2.6) on the interval $[0,T_1]$ is defined as the limit of $\{u_i^{M_\ell^1}(x_m,t)|_{[0,T_1]}\}_{l=1}^{\infty}$. Let $\{M_{\ell_k}^2\}_{k=1}^{\infty}$ be a subsequence of $\{M_\ell^1\}_{l=1}^{\infty}$ such that $\{u_i^{M_{\ell_k}^2}(x_m,t)|_{[0,T_2]}\}_{k=1}^{\infty}$ tends to a solution $u_i^2(x_m,t)$ defined on $[0,T_2]$. By the uniqueness of the solution of the finite dimensional Cauchy problem,

$$u_i^{M_{\ell_k}^2}(x_m,t) \equiv u_i^{M_{\ell_k}^1}(x_m,t) \qquad \text{on } [0,T_1],$$

so that u_i^1 and u_i^2 coincide on $[0,T_1]$. To avoid cumbersome notations, we denote $\{M_{\ell_k}^2\}_{k=1}^{\infty}$ by $\{M_\ell^2\}_{\ell=1}^{\infty}$.

Arguing in an iterative way we define a sequence $\{M_\ell^n\}_{l=1}^{\infty}$ for any $n>1$. Notice that $(M_\ell^{n+1})_\ell$ is a subsequence of $(M_\ell^n)_\ell$ and $M_\ell^{n+1} \ge M_\ell^n$. Indeed, by definition,

$M_\ell^{n+1} = M_{k_\ell}^n$. Since $(M_l^n)_l$ is increasing and $k_\ell > \ell$, the assertion follows. We consider now $Z_\ell := M_\ell^\ell$. We have $Z_{\ell+1} = M_{\ell+1}^{\ell+1} > M_\ell^{\ell+1} \geq M_\ell^\ell$. Hence, the solution $u_i(x_m, t)$ of (2.4), (2.5),(2.6) on $[0, \infty)$ is obtained upon passing to the limit in $\{u_i^{M_\ell^\ell}(x_m, t)\}_{\ell=1}^\infty$ where $\{M_\ell^\ell\}_{\ell=1}^\infty$ is diagonal subsequence. For each $i = 1, 2, \ldots$, the vector $(u_i(x_1, t), u_i(x_2, t), \ldots, u_i(x_h, t))$ thus provides a solution of (2.1), (2.2),(2.3) defined on $V \times [0, \infty)$. □

We also have:

Theorem 2.3.4. *Under the assumption* (2.24) *there exists a non negative weak solution* $\{u_i\}_{i=1}^\infty$ *of* (2.1), (2.2),(2.3) *defined on* $V \times [0, \infty)$ *that satisfies* (2.25).

We postpone the proof of Theorem 2.3.4 to Appendix C at the end of the chapter.

2.3.2 Existence of classical solutions and phase transitions

As we observed in the introduction of this chapter, in the absence of monomer injection, it is natural to expect that the total mass in (2.9) should remain constant in time. Indeed, this has been proved for systems related to (2.1), (2.2),(2.3) defined in open subsets of the euclidean space $\mathbb{R}^N$ when coagulation coefficients $a_{i,j}$ are constant [119] or sublinear, that is :

$$0 \leq a_{i,j} \leq A(i + j) \text{ for some } A > 0 \text{ and for } i, j \geq 1 ,$$

(see [118]).
Moreover, for choices of coagulation coefficients like (2.24) and under the additional hypothesis (H_1) it has been proved in [118], that mass conservation holds only until some finite time.
In addition, when $a_{i,j} \cong ij$ it is well known that a sol-gel phase transition occurs at some finite $t = t_g$. Indeed, the total mass is preserved only until time t_g and it decreases in time for $t > t_g$ (see [80]). The mechanism leading to the formation of the gel is triggered by a high rate of production of large clusters involving a transfer of a portion of the total mass of system to larger and larger aggregates. Summarizing, according to classical theory of gelation, in absence of monomers injection a sol-gel phase transition can be considered as associated with the breakdown in finite time of mass conservation and has the following features:

- the total mass decreases for $t > t_g$, where t_g is the gelation time
- moreover, the second moment of the solution blows up at finite time $t = t_g$.

In the case we are dealing with, we expect that the total mass will increase in time due to the presence of source term $f(x)$. More precisely, we expect to have the following relation :

$$M_1(t) = M_1(0) + t \sum_{x_m \in V} f(x_m) \quad \text{for } t > 0 \, . \tag{2.62}$$

We then say that a sol-gel transition for our system (2.1)-(2.3) occurs if equation (2.62) fails to hold in a finite time. In Theorem 2.3.5 below, we show that, under the choice of coefficients (2.24) and the assumption that diffusion coefficients are basically independent on i, equation (2.62) is true until a finite time t_*. In addition, if the initial mass is sufficiently large, we will show that we can find a time t^* and a time T such that the total mass decreases under its initial value in the interval $[t^*, T]$ that is:

$$M_1(t) < M_1(0) \quad \text{for } \; t^* \leq t \leq T \, .$$

This is the content of Theorem 2.3.8. Hence, t^* represents an upper bound for the gelation time t_g.
We next proceed to state in detail the result just sketched. To begin with, we have:

Theorem 2.3.5. *Suppose that:*

- *there exists an integer n and $d > 0$ such that $d_i = d$ for $i \geq n$*
- *$a_{i,j} \leq \bar{A} ij$ for $i, j \geq 1$, $\bar{A} > 0$*
- *$\| \sum_{i=1}^{\infty} i^2 U_i(\cdot) \|_{\infty} \leq const.$*

Then, the weak solution $\{u_i\}_{i=1}^{\infty}$ of (2.1),(2.2), (2.3) achieved in Theorem 2.3.4 satisfies:

$$M_1(t) = M_1(0) + t \sum_{x_m \in V} f(x_m) \quad \textit{for all } t \in [0, t_*) \tag{2.63}$$

where

$$t_* = \frac{\arctan\left(\left(\frac{\sqrt{\bar{A}} M_2(0)}{\sqrt{\sum_{x_m \in V} f(x_m)}}\right)^{-1}\right)}{\sqrt{\bar{A} \sum_{x_m \in V} f(x_m)}} \, , \tag{2.64}$$

with $M_2(0) = \sum_{x_m \in V} \sum_{i=1}^{\infty} i^2 U_i(x_m)$.

We next derive a result concerning the existence of local (in time) classical solutions. More precisely, there holds:

Theorem 2.3.6. *Suppose that:*

- *there exists an integer* n *and* $d > 0$ *such that* $d_i = d$ *for* $i \geq n$
- $a_{i,j} = ij$ *for* $i, j \geq 1$,
- $\| \sum_{i=1}^{\infty} i^2 U_i(\cdot) \|_{\infty} \leq const.$

then, the weak solution $\{u_i\}_{i=1}^{\infty}$ *of* (2.1),(2.2), (2.3) *obtained in Theorem 2.3.4 is a classical solution of* (2.1)-(2.3) *for any* $0 \leq t < t_*$, *where* t_* *is given by*

$$t_* = \frac{\arctan((\frac{M_2(0)}{\sqrt{\sum_{x_m \in V} f(x_m)}})^{-1})}{\sqrt{\sum_{x_m \in V} f(x_m)}} \, . \tag{2.65}$$

Proof of theorem 2.3.5. Let $\{u_i^N\}_{i=1}^{2N}$ be the solution of the approximating system $(\mathbf{S}^N)$ definited by (2.18), (2.19), (2.20). We now argue as in Lemma 2.3 of [118]. On setting in (2.21) $g_i = i^2$ for $i = 1, \cdots, 2N$ we obtain:

$$\sum_{i=1}^{2N} i^2 \frac{\partial u_i^N(x_m,t)}{\partial t} + \sum_{i=1}^{2N} i^2 d_i \Delta_G u_1^N(x_m,t) = \sum_{k \leq i,j \leq N} ij a_{ij} u_i^N(x_m,t) u_j^N(x_m,t) + f(x_m) \, . \tag{2.66}$$

Summing up over all $x_m \in V$, it follows by (2.16):

$$\begin{aligned} \sum_{x_m \in V} \sum_{i=1}^{2N} i^2 \frac{\partial u_i^N(x_m,t)}{\partial t} &\leq \bar{A} \sum_{x_m \in V} (\sum_{i=1}^{2N} i^2 u_i^N(x_m,t))^2 + \sum_{x_m \in V} f(x_m) \\ &\leq \bar{A} \left(\sum_{x_m \in V} \sum_{i=1}^{2N} i^2 u_i^N(x_m,t) \right)^2 + \sum_{x_m \in V} f(x_m) \end{aligned} \tag{2.67}$$

and

$$\frac{\partial}{\partial t} \left(\sum_{x_m \in V} \sum_{i=1}^{2N} i^2 u_i^N(x_m,t) \right) \leq \bar{A} \left(\sum_{x_m \in V} \sum_{i=1}^{2N} i^2 u_i^N(x_m,t) \right)^2 + \sum_{x_m \in V} f(x_m) \, . \tag{2.68}$$

Setting $\rho^N(t) = \sum_{x_m \in V} \sum_{i=1}^{2N} i^2 u_i^N(x_m,t)$, (2.68) becomes:

$$\frac{\partial \rho^N}{\partial t} \leq \bar{A} (\rho^N)^2 + \sum_{x_m \in V} f(x_m) \tag{2.69}$$

Let $z : [0, t_*) \to \mathbb{R}$ be the maximal solution of the o.d.e.

$$\frac{\partial z}{\partial t} = \bar{A} z^2 + \sum_{x_m \in V} f(x_m) \tag{2.70}$$

with initial data $z(0) = \sum_{x_m \in V} \sum_{i=1}^{\infty} i^2 U_i(x_m) \equiv M_2(0)$. As $\rho^N(0) \leq z(0)$, we have that $\rho^N(t) \leq z(t)$ in $[0, t_*)$. We observe that $z(0)$ is finite by hypothesis. In fact, $\sum_{x_m \in V} \sum_{i=1}^{\infty} i^2 U_i(x_m) \leq h \| \sum_{i=1}^{\infty} i^2 U_i(\cdot) \|_{\infty} < \infty$.
We now introduce the following change of variables:

$$\begin{aligned} \frac{\sqrt{\bar{A}}}{\sqrt{\sum_{x_m \in V} f(x_m)}} z &= v \\ \frac{\sqrt{\bar{A}}}{\sqrt{\sum_{x_m \in V} f(x_m)}} z' &= v' \ . \end{aligned} \tag{2.71}$$

Hence (2.70) becomes:

$$\frac{v'}{\sqrt{\bar{A} \sum_{x_m \in V} f(x_m)}(v^2 + 1)} = 1$$

which upon integration gives:

$$\frac{1}{\sqrt{\bar{A} \sum_{x_m \in V} f(x_m)}} \int_{v(0)}^{v(t)} \frac{dv}{(v^2 + 1)} = t \ .$$

Thus,

$$v(t) = \tan \left(\sqrt{\bar{A} \sum_{x_m \in V} f(x_m)} t + \arctan(v(0)) \right)$$

and

$$z(t) = \frac{\sqrt{\sum_{x_m \in V} f(x_m)}}{\sqrt{\bar{A}}} \tan \left(\sqrt{\bar{A} \sum_{x_m \in V} f(x_m)} t + \arctan(\frac{\sqrt{\bar{A}}}{\sqrt{\sum_{x_m \in V} f(x_m)}} M_2(0)) \right) \ . \tag{2.72}$$

Hence, for $t < t_*$,

$$\sum_{x_m \in V} \sum_{i=1}^{2N} i^2 u_i^N(x_m, t) \leq z(t) \ . \tag{2.73}$$

We observe that:

$$\tan \left(\sqrt{\bar{A} \sum_{x_m \in V} f(x_m)} t + \arctan(\frac{\sqrt{\bar{A}}}{\sqrt{\sum_{x_m \in V} f(x_m)}} M_2(0)) \right) < \infty$$

if and only if

$$\sqrt{\bar{A} \sum_{x_m \in V} f(x_m)} t + \arctan(\frac{\sqrt{\bar{A}}}{\sqrt{\sum_{x_m \in V} f(x_m)}} M_2(0)) < \frac{\pi}{2} \ ,$$

from which it follows that:

$$\tan\left(\sqrt{\bar{A}\sum_{x_m\in V} f(x_m)}t + \arctan(\frac{\sqrt{\bar{A}}}{\sqrt{\sum_{x_m\in V} f(x_m)}}M_2(0))\right) < \infty$$

if and only if

$$t < \frac{\arctan((\frac{\sqrt{\bar{A}}}{\sqrt{\sum_{x_m\in V} f(x_m)}}M_2(0))^{-1})}{\sqrt{\bar{A}\sum_{x_m\in V} f(x_m)}}\ .$$

Hence,

$$t_* = \frac{\arctan((\frac{\sqrt{\bar{A}}M_2(0)}{\sqrt{\sum_{x_m\in V} f(x_m)}})^{-1})}{\sqrt{\bar{A}\sum_{x_m\in V} f(x_m)}}\ . \tag{2.74}$$

For each $\bar{t} < t_*$ it holds:

$$\sum_{i=1}^{2N} i^2 u_i^N(x_m,t) \le \sum_{x_m\in V}\sum_{i=1}^{2N} i^2 u_i^N(x_m,t) \le \mathbf{C}(\bar{t}) \quad \text{for } (x_m,t)\in V\times[0,\bar{t}]$$

where

$$\mathbf{C}(\bar{t}) = \sup_{t\in[0,\bar{t}]}\{\frac{\sqrt{\sum_{x_m\in V} f(x_m)}}{\sqrt{\bar{A}}}\tan\left(\sqrt{\bar{A}\sum_{x_m\in V} f(x_m)}t + \arctan(\frac{\sqrt{\bar{A}}}{\sqrt{\sum_{x_m\in V} f(x_m)}}M_2(0))\right)\}\ ; \tag{2.75}$$

thus, it follows that :

$$\sup_{t\in[0,\bar{t}]}\|\sum_{i=1}^{2N} i^2 u_i^N(\cdot,t)\|_\infty \le \mathbf{C}(\bar{t}) \quad \text{for all } \bar{t}\in[0,t_*)\ .$$

Let $\{M_\ell\}_{\ell=1}^\infty$ be the sequence introduced in the proof of Theorem 2.3.1. For each fixed M_ℓ, let $\{u_i^{M_\ell}\}_{i=1}^{2M_\ell}$ be the solution of the approximating system $(\mathbf{S}^{M_\ell})$ definited by (2.18), (2.19), (2.20). Hence, for each $\bar{t} < t_*$:

$$\begin{aligned}\sum_{i=k}^{2M_\ell} i u_i^{M_\ell}(x_m,t) \le \frac{\sum_{i=k}^{2M_\ell} i^2 u_i^{M_\ell}(x_m,t)}{k} &\le \frac{\sup_{t\in[0,\bar{t}]}\|\sum_{i=1}^{2M_\ell} i^2 u_i^{M_\ell}(\cdot,t)\|_\infty}{k}\\ &\le \frac{\mathbf{C}(\bar{t})}{k} \quad \text{for } (x_m,t)\in V\times[0,\bar{t}].\end{aligned} \tag{2.76}$$

In particular, for any $\epsilon > 0$, for any $t \in [0, \bar{t}]$, $\bar{t} < t_*$, there exists a large enough $\underline{k}$, such that

$$\sum_{i=\underline{k}}^{2M_\ell} i u_i^{M_\ell}(x_m, t) \leq \frac{\mathbf{C}(\bar{t})}{\underline{k}} < \epsilon \, . \tag{2.77}$$

As proved in Theorem 2.3.1, for any $x_m \in V$, the series $\sum_{j=1}^{\infty} j u_j(x_m, t)$ converges for any $t \in [0, \bar{t}]$. Hence, for any $\epsilon > 0$, for any $t \in [0, \bar{t}]$, $\bar{t} < t_*$ there exists $\bar{k}_{\epsilon,t}$ such that $\forall k \geq \bar{k}$

$$|\sum_{j=1}^{\infty} j u_j(x_m, t) - \sum_{j=1}^{k} j u_j(x_m, t)| = |\sum_{j=k+1}^{\infty} j u_j(x_m, t)| < \epsilon \, . \tag{2.78}$$

Hence, setting $k_0 = \max\{\underline{k}, \bar{k}+1\}$ by (2.38), we have that for $x_m \in V$, for each $t \in [0, \bar{t}]$, $\bar{t} < t_*$ and for any $\epsilon > 0$, there exists $\ell_\epsilon > k_0$ such that $\forall \ell > \ell_\epsilon$:

$$\begin{aligned} &|\sum_{i=1}^{\infty} i u_i(x_m, t) - \sum_{i=1}^{2M_\ell} i u_i^{M_\ell}(x_m, t)| \\ &\leq \sum_{i=1}^{k_0-1} |u_i(x_m, t) - u_i^{M_\ell}(x_m, t)| + |\sum_{i=k_0}^{\infty} i u_i(x_m, t)| + |\sum_{i=k_0}^{2M_\ell} i u_i^{M_\ell}(x_m, t)| < \epsilon \, . \end{aligned} \tag{2.79}$$

In order to show (2.63), we observe that by (2.22) it follows for any $t \in [0, \bar{t}]$, $\bar{t} < t_*$:

$$\sum_{x_m \in V} \sum_{i=1}^{2M_\ell} i u_i^N(x_m, t) = \sum_{x_m \in V} \sum_{i=1}^{2M_\ell} i U_i(x_m) + t \sum_{x_m \in V} f(x_m) \tag{2.80}$$

and, as the number of the vertex of the graph V is finite, by (2.79), we obtain that for any $t \in [0, \bar{t}]$, $\bar{t} < t_*$:

$$\begin{aligned} \sum_{x_m \in V} \sum_{i=1}^{\infty} i u_i(x_m, t) &= \sum_{x_m \in V} \lim_{\ell \to \infty} \sum_{i=1}^{2M_\ell} i u_i^{M_\ell}(x_m, t) = \sum_{x_m \in V} \lim_{\ell \to \infty} \sum_{i=1}^{2M_\ell} i U_i(x_m) + t \sum_{x_m \in V} f(x_m) \\ &= \sum_{x_m \in V} \sum_{i=1}^{\infty} i U_i(x_m) + t \sum_{x_m \in V} f(x_m) = M_1(0) + t \sum_{x_m \in V} f(x_m) \, . \end{aligned} \tag{2.81}$$

□

Proof of theorem 2.3.6. Theorem 2.3.4 and theorem 2.3.5 holds under the more restrictive hyphothesis on coagulation coefficients $a_{i,j} = ij$ for $i, j \geq 1$.

Hence, if we set $\bar{A} = 1$, from above theorem we obtain that:

$$\sup_{t\in[0,\bar{t}]} \|\sum_{i=1}^{2N} i^2 u_i^N(\cdot,t)\|_\infty \leq \mathbf{C}(\bar{t}) \quad \text{for all } \bar{t} \in [0, t_*) \ .$$

where $\mathbf{C}(\bar{t})$ is like in (2.75) and

$$t_* = \frac{\arctan((\frac{M_2(0)}{\sqrt{\sum_{x_m\in V} f(x_m)}})^{-1})}{\sqrt{\sum_{x_m\in V} f(x_m)}} \ .$$

In addition, (2.76), (2.79)and (2.81) holds.
Putting toghether (2.76) and (2.79) we have that for any $k \geq 1$, for any $t \in [0, \bar{t}]$:

$$\sum_{i=k}^{\infty} i u_i(x_m,t) = \lim_{\ell\to\infty} \sum_{i=k}^{2M_\ell} i u_i^{M_\ell}(x_m,t) \leq \frac{\mathbf{C}(\bar{t})}{k} \ ; \tag{2.82}$$

thus:

$$\sup_{t\in[0,\bar{t}]} |\sum_{i=k}^{\infty} i u_i(x_m,t)| \leq \frac{\mathbf{C}(\bar{t})}{k} \tag{2.83}$$

In particular, for any $\epsilon > 0$ there exists $k^* \in \mathbb{N}$ large enough such that:

$$\sup_{t\in[0,\bar{t}]} |\sum_{i=k^*}^{\infty} i u_i(x_m,t)| \leq \frac{\mathbf{C}(\bar{t})}{k^*} < \epsilon \ . \tag{2.84}$$

Therefore, for any $\epsilon > 0$, there exists k^* such that $\forall k \geq k^*$

$$\begin{aligned} |\sum_{j=1}^{\infty} j u_j(x_m,t) - \sum_{j=1}^{k} j u_j(x_m,t)| &= |\sum_{j=k+1}^{\infty} j u_j(x_m,t)| \\ \leq \sup_{t\in[0,\bar{t}]} |\sum_{i=k^*}^{\infty} i u_i(x_m,t)| &\leq \frac{\mathbf{C}(\bar{t})}{k^*} < \epsilon \quad \forall t \in [0,\bar{t}] \ . \end{aligned} \tag{2.85}$$

Hence, the series $\sum_{j=1}^{\infty} j u_j(x_m,t)$ converges uniformly in $[0,\bar{t}]$, $\forall \bar{t} < t_*$.
In addition, the functions $j u_j(x_m,t) \in C[0,\bar{t}]$ for all $j \in \mathbb{N}$; hence the sum $S(t) = \sum_{j=1}^{\infty} j u_j(x_m,t)$ is continuous in $[0,\bar{t}]$, $\forall \bar{t} < t_*$.
As the coagulation coefficients are of the form $a_{i,j} = ij$, for $i,j \geq 1$, we have that for any fixed $i \geq 1$ the terms $u_i(x_m,t)\sum_{j=1}^{\infty} a_{i,j} u_j(x_m,t) = u_i(x_m,t) i \sum_{j=1}^{\infty} j u_j(x_m,t)$ in equation (2.17) are continuous in $[0,\bar{t}]$, $\forall \bar{t} < t_*$.
Therefore, the global weak solution $(u_i(x,t))_{i\geq 1}$ of (2.1),(2.2),(2.3) achieved in Theorem

2.3.4 is a classical solution (in sense of definition 2.2) of (2.1)-(2.3) for any $t < t_*$, where t_* is given by (2.65). □

We next show:

Lemma 2.3.7. *Suppose* (2.24) *holds and*

$$0 < \sum_{x_m \in V} M_1(x_m, 0) < +\infty \, .$$

Set $\chi = \frac{4|V|}{\underline{A} \sum_{x_m \in V} M_1(x_m,0)}$, *where* $|V|$ *is the number of vertices of* G. *Then, if* $T > 2\chi$ *there exists* $0 \leq \delta = \delta(T) \leq \chi$ *such that the weak solution of* (2.1), (2.2), (2.3) *obtained in Theorem 2.3.4 satisfies*

$$\sum_{x_m \in V} M_1(x_m, t) \leq \sum_{x_m \in V} M_1(x_m, 0) \left(\frac{\chi}{\chi + t - \delta} + T \frac{\sum_{x_m \in V} f(x_m)}{\sum_{x_m \in V} M_1(x_m, 0)} \right)^{\frac{1}{2}} \quad \textit{for } t \in [0, T] \, . \tag{2.86}$$

Lemma 2.3.7 is instrumental in deriving our main result on the existence of a phase transition for the problem under consideration.

Theorem 2.3.8. *As in previous Lemma 2.3.7, suppose* (2.24) *holds and set* $\chi = \frac{4|V|}{\underline{A} \sum_{x_m \in V} M_1(x_m,0)}$. *If*

$$\left(\frac{|V|}{\underline{A}} \sum_{x_m \in V} f(x_m) \right)^{\frac{1}{2}} < \sum_{x_m \in V} M_1(x_m, 0) < \infty \, , \tag{2.87}$$

there exists $0 \leq \delta \leq \chi$ *so that* (2.86) *becomes*

$$\sum_{x_m \in V} M_1(x_m, t) \leq \sum_{x_m \in V} M_1(x_m, 0) \left(\frac{\chi}{\chi + t - \delta} + \frac{1}{2} \right)^{\frac{1}{2}} \quad \textit{for } t \in [0, \frac{\sum_{x_m \in V} M_1(x_m, 0)}{2 \sum_{x_m \in V} f(x_m)}] \, . \tag{2.88}$$

In addition, there exists $t^* \in (\chi, 2\chi]$ *such that*

$$\sum_{x_m \in V} M_1(x_m, t) < \sum_{x_m \in V} M_1(x_m, 0) \;\; \textit{for } t^* \leq t \leq \frac{\sum_{x_m \in V} M_1(x_m, 0)}{2 \sum_{x_m \in V} f(x_m)} \, . \tag{2.89}$$

Hence, the solution exhibits a sol-gel transition at a time $t_g \leq t^*$.

Proof of Lemma 2.3.7. For each fixed $T > 0$, let $\{u_i^N\}_{i=1}^{2N}$ be the solution of the approximating system $(\mathbf{S}^N)$. Then, we consider equation (2.21) in which we take

$g_i = i^{\frac{1}{2}}$, for $i = 1, .., N$ and $g_i = 0$ for $i > N$.
Using the following inequality

$$i^{\frac{1}{2}} + j^{\frac{1}{2}} - (i+j)^{\frac{1}{2}} \geq \frac{1}{2}(\min\{i,j\})^{\frac{1}{2}} \ ,$$

integrating in time and summing up over all $x_m \in V$ we have:

$$\int_s^t \sum_{x_m \in V} \sum_{i=1}^{N} i^{\frac{1}{2}} \frac{\partial u_i^N(x_m,\tau)}{\partial \tau} d\tau + \int_s^t \sum_{x_m \in V} d_1 \Delta_G u_1^N(x_m,\tau) d\tau \leq$$

$$\int_s^t \sum_{x_m \in V} -\frac{1}{4} \sum_{i=1}^{N} \sum_{j=1}^{N} (\min\{i,j\})^{\frac{1}{2}} a_{ij} u_i^N(x_m,\tau) u_j^N(x_m,\tau) d\tau + (t-s) \sum_{x_m \in V} f(x_m)$$

where $0 \leq s < t$. Hence:

$$\sum_{x_m \in V} \sum_{i=1}^{N} i^{\frac{1}{2}} u_i^N(x_m,t) - \sum_{x_m \in V} \sum_{i=1}^{N} i^{\frac{1}{2}} u_i^N(x_m,s) + d_1 \int_s^t \sum_{x_m \in V} \Delta_G u_1^N(x_m,\tau) \leq$$

$$\int_s^t \sum_{x_m \in V} -\frac{1}{4} \sum_{i=1}^{N} \sum_{j=1}^{N} (\min\{i,j\})^{\frac{1}{2}} a_{ij} u_i^N(x_m,\tau) u_j^N(x_m,\tau) d\tau + (t-s) \sum_{x_m \in V} f(x_m) \ .$$

Using (2.16) and (2.24) we get:

$$\int_s^t \sum_{x_m \in V} \frac{A}{4} \sum_{i=1}^{N} \sum_{j=1}^{N} (\min\{i,j\})^{\frac{1}{2}} ij u_i^N(x_m,\tau) u_j^N(x_m,\tau) d\tau \leq$$

$$\sum_{x_m \in V} \sum_{i=1}^{N} i^{\frac{1}{2}} u_i^N(x_m,s) + (t-s) \sum_{x_m \in V} f(x_m) \tag{2.90}$$

Therefore, for any k such that $1 < k < N$ it follows:

$$k^{\frac{1}{2}} \int_s^t \sum_{x_m \in V} \sum_{i=k}^{N} \sum_{j=k}^{N} ij u_i^N(x_m,\tau) u_j^N(x_m,\tau) d\tau \leq \frac{4}{\underline{A}} \sum_{x_m \in V} \sum_{i=1}^{N} i^{\frac{1}{2}} u_i^N(x_m,s) + \frac{4}{\underline{A}}(t-s) \sum_{x_m \in V} f(x_m) \ . \tag{2.91}$$

If we consider the functions $h = h(x) : V \longrightarrow \mathbb{R}^h$ such that $h(x_m) = 1 \ \forall x_m \in V$ and $g = g(\cdot,t) = (\sum_{i=1}^N i u_i^N(x_1,t), \ldots, \sum_{i=1}^N i u_i^N(x_h,t))$ By the Cauchy Schwarz inequality we get:

$$\left(\sum_{x_m \in V} h(x_m) \sum_{i=1}^{N} i u_i^N(x_m,t) \right)^2 \leq |g(\cdot,t)|^2 \cdot |h(\cdot)|^2 =$$

$$\sum_{x_m\in V}(\sum_{i=1}^{N} iu_i^N(x_m,t))^2 \sum_{x_m\in V} 1 = \sum_{x_m\in V}\left(\sum_{i=1}^{N} iu_i^N(x_m,t)\right)^2 |V|$$

where $|V|$ is the number of vertex of the graph G. Setting $k=1$ in (2.91) we have:

$$\frac{1}{|V|}\int_s^t \left(\sum_{x_m\in V}\sum_{i=1}^{N} iu_i^N(x_m,\tau)dx\right)^2 d\tau \leq \int_s^t \sum_{x_m\in V}\left(\sum_{i=1}^{N} iu_i^N(x_m,\tau)\right)^2 d\tau \leq$$

$$\frac{4}{\underline{A}}\sum_{x_m\in V}\sum_{i=1}^{N} iu_i^N(x_m,s)dx + \frac{4}{\underline{A}}(t-s)\sum_{x_m\in V} f(x_m) \leq$$

$$\frac{4}{\underline{A}}\sum_{x_m\in V}\sum_{i=1}^{N} iu_i^N(x_m,s)dx + \frac{4}{\underline{A}}T\sum_{x_m\in V} f(x_m)$$

with $T>(t-s)$. Setting

$$E_N(s) = \sum_{x_m\in V}\sum_{i=1}^{N} iu_i^N(x_m,s)$$

and $\chi = \frac{4|V|}{\underline{A}E(0)}$, where $E(0) = \sum_{x_m\in V} M_1(x_m,0) = \sum_{x_m\in V}\sum_{i=1}^{\infty} iU_i(x_m)$ we have:

$$\int_s^t E_N^2(\tau)d\tau \leq \chi E(0)E_N(s) + \chi E(0)T\sum_{x_m\in V} f(x_m)$$

and letting $t\to T$, it follows:

$$\int_s^T E_N^2(\tau)d\tau \leq \chi E(0)E_N(s) + \chi E(0)T\sum_{x_m\in V} f(x_m)\ . \tag{2.92}$$

Setting $U(s) = \int_s^T E_N^2(\tau)d\tau$ and $c=\chi E(0)$, we have $U'(s) = -E_N^2(s)$ and $E_N(s) = (-U'(s))^{\frac{1}{2}}$. It follows that

$$U(s) \leq c(-U'(s))^{\frac{1}{2}} + cT\sum_{x_m\in V} f(x_m)\ . \tag{2.93}$$

Let $V(s) = U(s) - cT\sum_{x_m\in V} f(x_m)$, then $V'(s) = U'(s)$. We have that $V(s)$ is decreasing, due to the fact that $U(s)$ is decreasing. Hence, $V(s)\leq V(0)$, for all $0<s\leq T$. Consider the case $V(0)>0$. This implies that $V(s)>0$ in a maximal interval $[0,b]$. If $b\in[T,+\infty]$, we restrict to $[0,T]$.

Going back to equation (2.93), we have that:

$$V(s) \leq c(-V'(s))^{\frac{1}{2}} \tag{2.94}$$

and

$$V(s)^2 \leq c^2(-V'(s)) \tag{2.95}$$

Integrating between 0 and z such that $0 < z \leq T$ we have:

$$\frac{z}{c^2} \leq \int_{V(0)}^{V(z)} \frac{-V'(\tau_1)}{V^2(\tau_1)} d\tau_1 \ . \tag{2.96}$$

Hence:

$$\frac{z}{c^2} \leq \left[\frac{1}{V(\tau_1)}\right]_{V(0)}^{V(z)} \tag{2.97}$$

and

$$\frac{z}{c^2} + \frac{1}{V(0)} \leq \frac{1}{V(z)} \ . \tag{2.98}$$

By (2.93), we have that $V(0) \leq cE_N(0) \leq cE(0)$. Thus, by (2.98), we have:

$$\frac{1}{V(z)} \geq \frac{z}{c^2} + \frac{1}{V(0)} \geq \frac{z}{c^2} + \frac{1}{cE(0)} = \frac{E(0)z + c}{c^2E(0)}$$

and

$$V(z) \leq \frac{c^2E(0)}{E(0)z + c} \ . \tag{2.99}$$

If $V(z) > 0$ in a maximal interval $[0, b]$, $b < T$, it follows that $V(z) \leq 0$ for $b < z \leq T$ and (2.99) is still true, due to the fact the right-hand of the inequality is positive for all $z \geq 0$. If $V(0) \leq 0$, $V(z) \leq 0$ for all $0 \leq z \leq T$, due to the fact that the function V is decreasing. Thus, also in this case (2.99) holds for all $0 \leq z \leq T$. In other terms, we have that for any $0 \leq z \leq T$:

$$\int_z^T E^2(\tau_1)d\tau_1 - cT \sum_{x_m \in V} f(x_m) \leq \frac{c^2E(0)}{E(0)z + c} \ . \tag{2.100}$$

By the mean value theorem, for $\tau \in [z, z + \lambda]$:

$$\begin{aligned} E_N^2(\tau)\lambda = \int_z^{z+\lambda} E_N^2(\tau_1)d\tau_1 &\leq \int_z^T E_N^2(\tau_1)d\tau_1 \\ &\leq \frac{\chi^2E(0)^2}{\chi + z} + \chi E(0)T \sum_{x_m \in V} f(x_m) \ . \end{aligned} \tag{2.101}$$

The first inequality in requires that $z + \lambda \leq T$. We restrict to $0 \leq z < \frac{T}{2}$. If

$$\chi < \frac{T}{2} \tag{2.102}$$

we have that $z + \chi < T$ and we can set $\lambda = \chi$.
Inequalities (2.102) implies that $T > 2\chi = 8\frac{|V|}{\underline{A}E(0)}$ and this choice is always possible, as it depends by fixed constants and T is an arbitrary large fixed finited time.
Hence, (2.101) becomes :

$$\begin{aligned} E_N^2(\tau) = \frac{1}{\chi}\int_z^{z+\chi} E_N^2(\tau_1)d\tau_1 &\leq \frac{1}{\chi}\int_z^{T} E_N^2(\tau_1)d\tau_1 \\ &\leq \frac{\chi E(0)^2}{\chi + z} + E(0)T\sum_{x_m \in V} f(x_m) \end{aligned} \tag{2.103}$$

for $\tau \in [z, z+\chi]$.
As $\tau = z + \delta$, for a $0 < \delta \leq \chi$, we have that:

$$E_N^2(\tau) \leq E(0)^2\left(\frac{\chi}{\chi + (\tau - \delta)} + \frac{T\sum_{x_m \in V} f(x_m)}{E(0)}\right) .$$

It follows that for $0 < \tau \leq T$, for $0 < \delta \leq \chi$, $\delta < \tau$:

$$E_N(\tau) \leq E(0)\left(\frac{\chi}{\chi + (\tau - \delta)} + \frac{T\sum_{x_m \in V} f(x_m)}{E(0)}\right)^{\frac{1}{2}} \tag{2.104}$$

Let $\{M_\ell\}_{\ell=1}^{\infty}$ be the sequence introduced in the proof of Theorem 2.3.1. For each fixed M_ℓ, let $\{u_i^{M_\ell}\}_{i=1}^{2M_\ell}$ be the solution of the approximating system $(\mathbf{S}^{M_\ell})$ definited by (2.18), (2.19), (2.20). For each M_ℓ, for $0 < \tau \leq T$ it holds:

$$E_{M_\ell}(\tau) \leq E(0)\left(\frac{\chi}{\chi + (\tau - \delta)} + \frac{T\sum_{x_m \in V} f(x_m)}{E(0)}\right)^{\frac{1}{2}} \tag{2.105}$$

where $E_{M_\ell}(\tau) = \sum_{x_m \in V}\sum_{i=1}^{M_\ell} iu_i^{M_\ell}(x_m, \tau)$, $\chi = \frac{4|V|}{\underline{A}\sum_{x_m \in V}\sum_{i=1}^{\infty} iU_i(x_m)}$, $0 < \delta < \chi$, $\delta < \tau$.
In addition, let $P \in \mathbb{N}$. For $1 \leq P < M_\ell$ and for each $\tau \in [0, T]$ we have:

$$\sum_{x_m \in V}\sum_{i=1}^{P} iu_i^{M_\ell}(x_m, \tau) \leq \sum_{x_m \in V}\sum_{i=1}^{M_\ell} iu_i^{M_\ell}(x_m, \tau)$$

and by (2.38) for each $\tau \in [0,T]$ it holds:

$$\sum_{x_m \in V} \sum_{i=1}^{P} iu_i(x_m,\tau) = \lim_{\ell \to \infty} \sum_{x_m \in V} \sum_{i=1}^{P} iu_i^{M_\ell}(x_m,\tau) \leq \limsup_{M_\ell \to \infty} \sum_{x_m \in V} \sum_{i=1}^{M_\ell} iu_i^{M_\ell}(x_m,\tau) \ .$$

Passing to the limit for $P \to \infty$ we get that for each $\tau \in [0,T]$:

$$\sum_{x_m \in V} \sum_{i=1}^{\infty} iu_i(x_m,\tau) = \lim_{P \to \infty} \sum_{x_m \in V} \sum_{i=1}^{P} iu_i(x_m,\tau) \leq \limsup_{M_\ell \to \infty} \sum_{x_m \in V} \sum_{i=1}^{M_\ell} iu_i^{M_\ell}(x_m,\tau) \ .$$

Therefore, passing to the limit for $\ell \to \infty$ in (2.105) we get for $0 < \tau \leq T$:

$$\sum_{x_m \in V} M_1(x_m,\tau) \leq \sum_{x_m \in V} M_1(x_m,0) \left(\frac{\chi}{\chi + (\tau - \delta)} + \frac{T \sum_{x_m \in V} f(x_m)}{\sum_{x_m \in V} M_1(x_m,0)} \right)^{\frac{1}{2}} \tag{2.106}$$

where $0 < \delta < \chi$, $\delta < \tau$, $T > 2\chi$. □

Proof of Theorem 2.3.8. In the previous lemma we have shown that for $0 < \tau \leq T$:

$$\sum_{x_m \in V} M_1(x_m,\tau) \leq \sum_{x_m \in V} M_1(x_m,0) \left(\frac{\chi}{\chi + (\tau - \delta)} + \frac{T \sum_{x_m \in V} f(x_m)}{\sum_{x_m \in V} M_1(x_m,0)} \right)^{\frac{1}{2}} \tag{2.107}$$

where $0 < \delta < \chi$, $\delta < \tau$, $T > 2\chi$. In order to simplify the notation we set $E(0) = \sum_{x_m \in V} M_1(x_m,0)$. Consider now the case when the quantity within braces in the right of (2.107) is less than one. This happens when:

$$E(0)\chi + T \sum_{x_m \in V} f(x_m)\chi + T \sum_{x_m \in V} f(x_m)(\tau - \delta) < E(0)\chi + E(0)(\tau - \delta)$$

that implies for $E(0) - T \sum_{x_m \in V} f(x_m) > 0$, (i.e. for $T < \frac{E(0)}{\sum_{x_m \in V} f(x_m)}$:

$$\frac{T \sum_{x_m \in V} f(x_m)\chi}{E(0) - T \sum_{x_m \in V} f(x_m)} < (\tau - \delta) \ . \tag{2.108}$$

We note that if $E(0) - T \sum_{x_m \in V} f(x_m) < 0$, the time $(\tau - \delta)$ is negative and this is impossible because by construction $0 < z = \tau - \delta$ (see Lemma 2.3.7).
Moreover, by construction we must have:

$$\frac{T \sum_{x_m \in V} f(x_m)\chi}{E(0) - T \sum_{x_m \in V} f(x_m)} + \delta < \tau \leq T \ . \tag{2.109}$$

Hence, we should verify that:

$$\frac{T\sum_{x_m\in V} f(x_m)\chi}{E(0)-T\sum_{x_m\in V} f(x_m)}+\delta<T \tag{2.110}$$

where $0<\delta<\chi$ that is equal to verify that:

$$\frac{T\sum_{x_m\in V} f(x_m)\chi}{E(0)-T\sum_{x_m\in V} f(x_m)}+\chi<T\ . \tag{2.111}$$

It follows that:

$$\frac{\chi E(0)}{E(0)-T\sum_{x_m\in V} f(x_m)}-T<0$$

that implies:

$$\frac{\chi E(0)-TE(0)+T^2\sum_{x_m\in V} f(x_m)}{E(0)-T\sum_{x_m\in V} f(x_m)}<0\ .$$

Assuming that $E(0)-T\sum_{x_m\in V} f(x_m)>0$, the inequality above holds for

$$T\in(\frac{E(0)-\sqrt{E(0)^2-\frac{16}{\underline{A}}|V|\sum_{x_m\in V} f(x_m)}}{2\sum_{x_m\in V} f(x_m)},\frac{E(0)+\sqrt{E(0)^2-\frac{16}{\underline{A}}|V|\sum_{x_m\in V} f(x_m)}}{2\sum_{x_m\in V} f(x_m)})\ ,$$

where

$$E(0)>4\sqrt{\frac{1}{\underline{A}}|V|\sum_{x_m\in V} f(x_m)}\ . \tag{2.112}$$

If we choose T as the midpoint of the above interval, we have $T=\frac{E(0)}{2\sum_{x_m\in V} f(x_m)}$.
We verify that $\chi<\frac{T}{2}$, that achieve $E(0)>4\sqrt{\frac{1}{\underline{A}}|V|\sum_{x_m\in V} f(x_m)}$, as in in (2.112).
Hence, (2.107) becomes:

$$\sum_{x_m\in V} M_1(x_m,\tau)\le\sum_{x_m\in V} M_1(x_m,0)\left(\frac{\chi}{\chi+\tau-\delta}+\frac{1}{2}\right)^{\frac{1}{2}}\ . \tag{2.113}$$

Setting $t^*=\frac{T\sum_{x_m\in V} f(x_m)\chi}{E(0)-T\sum_{x_m\in V} f(x_m)}+\delta$, where $0<\delta\le\chi$, our choice of T implies that $\chi<t^*\le 2\chi$. □

If $M_2(0)=\sum_{x_m\in V}\sum_{i=1}^{\infty} i^2U_i(x_m)$, we want to compare now

$t_*=\frac{\arctan\left(\left(\frac{\sqrt{\bar{A}}M_2(0)}{\sqrt{\sum_{x_m\in V} f(x_m)}}\right)^{-1}\right)}{\sqrt{\bar{A}\sum_{x_m\in V} f(x_m)}}$, with $t^*\in(\chi,2\chi]$.

We will show that $t_*<\chi$. We recall that $\chi=4\frac{|V|}{\underline{A}M_1(0)}$ where $M_1(0)=\sum_{x_m\in V}\sum_{i=1}^{\infty} iU_i(x_m)$.

We claim that:

$$\arctan(\frac{\sqrt{\sum_{x_m\in V} f(x_m)}}{\sqrt{\bar{A}}M_2(0)}) < 4\sqrt{\bar{A}\sum_{x_m\in V} f(x_m)}\frac{|V|}{\underline{A}M_1(0)}$$

To this end, we observe that:

$$\frac{\sqrt{\sum_{x_m\in V} f(x_m)}}{\sqrt{\bar{A}}M_2(0)} < 4\sqrt{\bar{A}\sum_{x_m\in V} f(x_m)}\frac{|V|}{\underline{A}M_1(0)}\ .$$

This follows from:

$$\frac{\underline{A}M_1(0)}{4\bar{A}M_2(0)} < |V|$$

due to the fact that $M_1(0) \le M_2(0)$ and $\underline{A} \le \bar{A}$ implies $\underline{A}M_1(0) \le \bar{A}M_1(0) \le \bar{A}M_2(0)$, so that the left-hand side of the inequality is less that one and the number of the nodes of the graph is a positive integer. Hence,

$$\arctan(\frac{\sqrt{\sum_{x_m\in V} f(x_m)}}{\sqrt{\bar{A}}M_2(0)}) < \arctan(4\sqrt{\bar{A}\sum_{x_m\in V} f(x_m)}\frac{|V|}{\underline{A}M_1(0)})$$

and

$$\begin{aligned}\arctan\left(\frac{\sqrt{\sum_{x_m\in V} f(x_m)}}{\sqrt{\bar{A}}M_2(0)}\right) - 4\sqrt{\bar{A}\sum_{x_m\in V} f(x_m)}\frac{|V|}{\underline{A}M_1(0)}\\ < \arctan\left(4\sqrt{\bar{A}\sum_{x_m\in V} f(x_m)}\frac{|V|}{\underline{A}M_1(0)}\right) - 4\sqrt{\bar{A}\sum_{x_m\in V} f(x_m)}\frac{|V|}{\underline{A}M_1(0)} < 0\end{aligned} \tag{2.114}$$

In the following theorem we will prove the blow up of the second moment of the solution of system (2.1)-(2.3) in a finite time.

Theorem 2.3.9. *Let*

$$M_2(t) = \sum_{x_m\in V}\sum_{i=1}^{\infty} i^2 u_i(x_m,t) \quad \textit{for } t \ge 0\ .$$

be the second moment of the solution of (2.1)-(2.3) *obtained in Theorem* (2.3.4). *Suppose that* $M_2(0) < \infty$ *and* (2.15) *is satisfied. Then* $M_2(t)$ *blows up at a finite time*

t_g such that

$$t_g \leq \hat{t} = \sqrt{\frac{h}{\sum_{x_m \in V} f(x_m)}} \arctan\left(\frac{\sqrt{h \sum_{x_m \in V} f(x_m)}}{M_2(0)}\right) .$$

In addition, $\hat{t} > t_*$, where t_* is given by (2.65).

Proof. We argue as in [101] and we introduce a new function:

$$g(x_m, z, t) = \sum_{j=1}^{\infty} \exp\{-jz\} u_j(x_m, t) \qquad \text{for } x_m \in V,\ z > 0\ , t > 0\ . \tag{2.115}$$

Multiplying the $j-th$ equation of (2.1), (2.2) by the positive function $\exp\{-jz\}$, $z > 0$ and summing up over all the equations we get:

$$\begin{aligned} \frac{\partial g(x_m, z, t)}{\partial t} =& f(x_m) \exp\{-z\} + (\frac{\partial g(x_m, z, t)}{\partial z}) \left(\sum_{j=1}^{\infty} j u_j(x_m, t)\right) \\ &+ \frac{1}{2}(\frac{\partial g(x_m, z, t)}{\partial z})^2 - \sum_{j=1}^{\infty} d_j \Delta_G u_j(x_m, t) \exp\{-jz\}\ . \end{aligned} \tag{2.116}$$

Deriving (2.116) two times in z and calculating in $z = 0$ we get that

$$\frac{\partial}{\partial t}\left(\sum_{j=1}^{\infty} j^2 u_j(x_m, t)\right) = f(x_m) + (\sum_{j=1}^{\infty} j^2 u_j(x_m, t))^2 - \sum_{j=1}^{\infty} j^2 d_j \Delta_G u_j(x_m, t) \tag{2.117}$$

Summing up over all $x_m \in V$, we get by (2.16) that

$$\frac{\partial}{\partial t}\left(\sum_{x_m \in V} \sum_{j=1}^{\infty} j^2 u_j(x_m, t)\right) = \sum_{x_m \in V} f(x_m) + \sum_{x_m \in V} (\sum_{j=1}^{\infty} j^2 u_j(x_m, t))^2\ . \tag{2.118}$$

Writing (2.118) in term of the second moment of the solution at a vertex of the graph , it follows that:

$$\begin{aligned} \frac{\partial}{\partial t}\left(\sum_{x_m \in V} M_2(x_m, t)\right) &= \sum_{x_m \in V} f(x_m) + \sum_{x_m \in V} M_2(x_m, t)^2 \\ &\geq \frac{1}{h}(\sum_{x_m \in V} M_2(x_m, t))^2 + \sum_{x_m \in V} f(x_m) \end{aligned} \tag{2.119}$$

by Cauchy-Schwarz inequality. In fact, we have:

$$\sum_{x_m\in V} y_m M_2(x_m,t) \le (\sum_{x_m\in V}(M_2(x_m,t))^2)^{\frac{1}{2}}(\sum_{x_m\in V} y_m^2)^{\frac{1}{2}}$$

where $h=|V|$ and y_m a positive function on V ; setting $y_m=1$, $m=1,\dots,h$ we get:

$$\sum_{x_m\in V} M_2(x_m,t)^2 \ge \frac{1}{h}(\sum_{x_m\in V} M_2(x_m,t))^2$$

Hence, from (2.119) it holds:

$$\frac{\partial}{\partial t}M_2(t) \ge \frac{1}{h}M_2(t)^2 + \sum_{x_m\in V} f(x_m) \tag{2.120}$$

Let $\omega:[0,\hat{t})\to\mathbb{R}$ be the maximal solution of the o.d.e.

$$\frac{\partial \omega}{\partial t} = \frac{\omega^2}{h} + \sum_{x_m\in V} f(x_m)$$

with initial data $\omega(0)=\sum_{x_m\in V}\sum_{j=1}^{\infty} j^2 U_j(x_m)\equiv M_2(0)$. Then, $M_2(t)\ge\omega(t)$ in $[0,\hat{t})$, where

$$\omega(t)=\sqrt{h\sum_{x_m\in V} f(x_m)}\tan\left(\sqrt{\frac{\sum_{x_m\in V} f(x_m)}{h}}t+\arctan(\frac{M_2(0)}{\sqrt{h\sum_{x_m\in V} f(x_m)}})\right)\ .$$

At $\hat{t}=\sqrt{\frac{h}{\sum_{x_m\in V} f(x_m)}}\arctan\left(\frac{\sqrt{h\sum_{x_m\in V} f(x_m)}}{M_2(0)}\right)$, the function ω blows up. Hence, $t_g\le\hat{t}$. Let us show that $t_*<\hat{t}$, that is:

$$\frac{\arctan((\frac{\sqrt{\sum_{x_m\in V} f(x_m)}}{M_2(0)})}{\sqrt{\sum_{x_m\in V} f(x_m)}} < \sqrt{\frac{h}{\sum_{x_m\in V} f(x_m)}}\arctan\left(\frac{\sqrt{h\sum_{x_m\in V} f(x_m)}}{M_2(0)}\right)\ .$$

We have that:

$$\frac{\sqrt{\sum_{x_m\in V} f(x_m)}}{M_2(0)} < \frac{\sqrt{h\sum_{x_m\in V} f(x_m)}}{M_2(0)}$$

by the fact $1 < \sqrt{h}$, as the number of nodes of the graph is a positive integer and the graph has at least two node. Thus this implies:

$$\begin{aligned}\frac{\arctan((\frac{\sqrt{\sum_{x_m\in V} f(x_m)}}{M_2(0)})}{\sqrt{\sum_{x_m\in V} f(x_m)}} &< \sqrt{\frac{1}{\sum_{x_m\in V} f(x_m)}}\arctan\left(\frac{\sqrt{h\sum_{x_m\in V} f(x_m)}}{M_2(0)}\right) \\ &< \sqrt{\frac{h}{\sum_{x_m\in V} f(x_m)}}\arctan\left(\frac{\sqrt{h\sum_{x_m\in V} f(x_m)}}{M_2(0)}\right).\end{aligned} \tag{2.121}$$

□

2.4 Discussion

In this work, we make use of Smoluchowski's theory to address a number of issues motivated by the study of neurodegenerative diseases. Originally, Smoluchowski's equations were introduced to study the coagulation of colloids [98] and were then used to deal with different physical problems in polymer science [99], [51], aerosol formation [123] and stars and planets formation [40] among others. To our knowledge, models similar to (2.1),(2.2), (2.3), defined in subsets of $\mathbb{R}^n$, have been only recently used in [84] and then in [1],[36], [37] for the description of the neuro-biological problem of aggregation of beta amyloid in AD brain. As far as we know, the representation of the process of polymerization of abnormally phosphorylated tau protein by means of Smoluchowski equation on finite weighted graph has been first introduced in this thesis.

In this chapter, we have dealt with conditions that assure the occurrence of a sol-gel phase transition for the coagulation-diffusion model (2.1)-(2.3). This kind of problems arises typically in chemical engineering where the onset of a gel in a reactor in which oligomers of different sizes are polymerizing is a common (and often unwanted) feature in technical processes. In this work, we study such problems in a different context, consisting in the formation of neurofibrillary tangles in AD.
More precisely, we have shown that under the choice of coagulation coefficients (2.15) the solution of system (2.1)-(2.3) exhibits a sol gel phase transition at a finite time t_g s. t. $t_* < t_g < t^*$, where t_* and t^* are given in Theorem 2.3.6 ,2.3.8. Interestingly, such transition is associated with a loss of regularity of the solution.

We next discuss on the implications of our result. The part of the total mass of the system that seems to be lost after the time t_g is associated with the formation of a gel, which has the property of removing polymers from the medium and does not allow them to return to the sol fraction. Thus, clusters of hyperphosphorylated tau protein do not contribute to the mass in (2.63) for times $t \geq t_g$, by analogy with classical gelation process, as these are expected to be transferred to larger and larger aggregates giving rise to the NFTs, whose mass would coincide with that lost, on the whole, by the system. The association between the onset of the gel and the formation of tangles allow us to advance the conjecture that clusters of hyperphosphorylated tau protein aggregate in NFTs in order to subtract highly toxic oligomers from damaging neurons. In that case, their role may be beneficial for brain cells. This view is supported by several studies (see for instance [15], [76]) according to which tangles need not be harmful for neurons, as they have been found also in healthy-aged brains, and may represent an immune response against oxidative stress and against the damage caused by oligomers, which are deemed to be the primary noxious tau species [15]. Such proposal needs, however, of additional evidence to be either proved or disproved. In the light of these considerations the estimate $t_* < t_g < t^*$ for the gelation time can be interpreted as an estimate for the time of onset of NFTs. Thus, our conjectures would imply that smaller t_g is, i.e. the sooner tangles form, the more efficiently neurons can be preserved from injury due to disease agents.

At the mathematical level, there remain several open problems related to our model. An interesting question consists in establishing in which brain regions (represented as vertices in our graph) the formation of NTFs occurs and which mass of tangles is produced in each region. Indeed, our result of the occurrence of a sol gel phase transition, mathematically expressed by a loss of total mass of tau aggregates, does not allow to describe these aspects, since the total mass is a global property of the system. Thus, in order to investigate the aforesaid issues, it would be probably necessary to add a further equation to system (2.1)-(2.3), which describes the mass density produced, in time and space, in consequence of the formation of neurofibrillary tangles.
Furthermore, in Theorem 2.3.8, we have considered the weak solution of (2.1)-(2.3) obtained in Theorem (2.3.4) in the interval $[0, \frac{\sum_{x_m \in V} M_1(x_m,0)}{2\sum_{x_m \in V} f(x_m)}]$, and we proved the occurence of a sol-gel phase transition at $t_* \leq t_g < \frac{\sum_{x_m \in V} M_1(x_m,0)}{2\sum_{x_m \in V} f(x_m)}$. However, we have seen in Theorem (2.3.4) that such solution of (2.1)-(2.3) exists globally in time. Thus, other sol-gel transitions may possibly take place at $t_g^{'} > \frac{\sum_{x_m \in V} M_1(x_m,0)}{2\sum_{x_m \in V} f(x_m)}$. In future work,

we intend to investigate the question of the occurrence of several sol-gel transitions in the solution of (2.1)-(2.3) jointly with the problem of the evolution of the disease as a result of tau agglomeration. Indeed, from a biological point of view, it would be interesting if such transitions could be regarded as a kind of beneficial immune response mounted up by brain's cells against the cerebral damage inflicted by AD. However, in order to analyze this issue, a further study is required in which the model discussed here shoud be perhaps coupled to another model specifically designed to describe the progression of the disease in connection with the formation of tau aggregates.
Tangles are measurable in human brain. If such formations would be beneficial for neurons the optimal situation would be to have a higher number of tangles in a suitable time scale, in order to sequester a higher quantity of neurodegenerative agents. It would be very interesting to find a link between the degree of the vertex and the blowing-up time of the second moment of the solution in that vertex. More precisely, it would be relevant to ascertain if the rate of connection of the nodes of the network has any influence in how quickly the sol-gel phase transition takes place.In future work, we will investigate such issues, which could open new perspectives in the field of neurodegenerative studies.

2.5 Appendix C. The proof of Theorem 2.3.4

Proof of Theorem 2.3.4. The proof follows repeating the arguments yielding Theorem 1. We only have to show that for each $i \geq 1$ and for each $x_m \in V$)

$$\int_0^T |\sum_{j=1}^{M_\ell} a_{i,j} u_j^{M_\ell}(x_m, s) - \sum_{j=1}^{\infty} a_{i,j} u_j(x_m, s)| ds \to 0 \quad \text{for } \ell \to \infty \,. \tag{2.122}$$

We observe preliminary that by (2.24), we have that for each fixed $i \geq 1$, for each $x_m \in V$ and for each $s \in [0, T]$

$$\sum_{j=1}^{\infty} a_{i,j} u_j(x_m, s) \leq \bar{A} i \sum_{j=1}^{\infty} j u_j(x_m, s) < \infty \,.$$

Thus, $\sum_{j=1}^{\infty} a_{i,j} u_j(x_m, s)$ converges for any $s \in [0, T]$ and for any $x_m \in V$.
We will provide, now, some estimates that will allow us to prove (2.122).
To this aim, denote by $\{M_\ell\}_{\ell=1}^{\infty}$ the sequence introduced in the proof of previous theorem.
We approximate the full system (2.1), (2.2), by a system $(\mathbf{S}^{M_\ell})$ of $2M_\ell$ equations

definited as in (2.18), (2.19), (2.20).
We set $g_j = j^{\frac{1}{2}}$ in (2.21) for $j = 1, .., M_\ell$, $g_j = 0$ for $M_\ell + 1 \le j \le 2M_\ell$.
Using the following inequality

$$i^{\frac{1}{2}} + j^{\frac{1}{2}} - (i+j)^{\frac{1}{2}} \ge \frac{1}{2}(\min\{i,j\})^{\frac{1}{2}} \ ,$$

integrating in time and summing up over all $x_m \in V$ we have for $t \le T$:

$$\begin{aligned} &\int_0^t \sum_{x_m \in V} \sum_{j=1}^{M_\ell} j^{\frac{1}{2}} \frac{\partial u_j^{M_\ell}(x_m, s)}{\partial s} ds + \int_0^t \sum_{x_m \in V} \sum_{j=1}^{M_\ell} j^{\frac{1}{2}} d_j \Delta_G u_j^{M_\ell}(x_m, s) ds \\ &\le \int_0^t \sum_{x_m \in V} -\frac{1}{4} \sum_{i=1}^{M_\ell} \sum_{j=1}^{M_\ell} (\min\{i,j\})^{\frac{1}{2}} a_{ij} u_i^{M_\ell}(x_m, s) u_j^{M_\ell}(x_m, s) ds + t \sum_{x_m \in V} f(x_m) \end{aligned} \tag{2.123}$$

Hence:

$$\begin{aligned} &\sum_{x_m \in V} \sum_{j=1}^{M_\ell} j^{\frac{1}{2}} u_j^{M_\ell}(x_m, t) - \sum_{x_m \in V} \sum_{j=1}^{M_\ell} j^{\frac{1}{2}} u_j^{M_\ell}(x_m, 0) + \int_0^t \sum_{j=1}^{M_\ell} \sum_{x_m \in V} j^{\frac{1}{2}} \Delta_G u_j^{M_\ell}(x_m, s) ds \\ &\qquad \le \int_0^t \sum_{x_m \in V} -\frac{1}{4} \sum_{i=1}^{M_\ell} \sum_{j=1}^{M_\ell} (\min\{i,j\})^{\frac{1}{2}} a_{ij} u_i^{M_\ell}(x_m, s) u_j^{M_\ell}(x_m, s) ds + \|f(\cdot)\|_\infty hT \ . \end{aligned} \tag{2.124}$$

Using (2.16) and (2.24) we have:

$$\begin{aligned} &\int_0^t \sum_{x_m \in V} \frac{A}{4} \sum_{i=1}^{M_\ell} \sum_{j=1}^{M_\ell} (\min\{i,j\})^{\frac{1}{2}} ij u_i^{M_\ell}(x_m, s) u_j^{M_\ell}(x_m, s) ds \\ &\qquad \le \sum_{x_m \in V} \sum_{j=1}^{M_\ell} j^{\frac{1}{2}} U_j(x_m) + \|f(\cdot)\|_\infty hT \ . \end{aligned} \tag{2.125}$$

Letting $t \to T$, we have that for any k such that $1 < k < M_\ell$:

$$\begin{aligned} k^{\frac{1}{2}} \int_0^T \sum_{x_m \in V} (\sum_{j=k}^{M_\ell} j u_j^{M_\ell}(x_m, s))^2 ds &= k^{\frac{1}{2}} \int_0^T \sum_{x_m \in V} \sum_{i=k}^{M_\ell} \sum_{j=k}^{M_\ell} ij u_i^{M_\ell}(x_m, s) u_j^{M_\ell}(x_m, s) ds \\ &\leq \int_0^T \sum_{x_m \in V} \sum_{i=k}^{M_\ell} \sum_{j=k}^{M_\ell} (\min\{i,j\})^{\frac{1}{2}} ij u_i^{M_\ell}(x_m, s) u_j^{M_\ell}(x_m, s) ds \\ &\leq \int_0^T \sum_{x_m \in V} \sum_{i=1}^{M_\ell} \sum_{j=1}^{M_\ell} (\min\{i,j\})^{\frac{1}{2}} ij u_i^{M_\ell}(x_m, s) u_j^{M_\ell}(x_m, s) ds \\ &\leq \frac{4}{\underline{A}} (\sum_{x_m \in V} \sum_{j=1}^{M_\ell} j^{\frac{1}{2}} U_j(x_m) + Th \|f(\cdot)\|_\infty) \\ &\leq \frac{4}{\underline{A}} (\sum_{x_m \in V} \sum_{j=1}^{\infty} j^{\frac{1}{2}} U_j(x_m) + Th \|f(\cdot)\|_\infty) \ . \end{aligned} \tag{2.126}$$

It follows that for any fixed $i \geq 1$:

$$\begin{aligned} &\int_0^T (\sum_{j=k}^{M_\ell} a_{i,j} u_j^{M_\ell}(x_m, s))^2 ds \\ &\quad \leq \bar{A}^2 i^2 \int_0^T (\sum_{j=k}^{M_\ell} j u_j^{M_\ell}(x_m, s))^2 ds \\ &\quad \leq \bar{A}^2 i^2 \int_0^T \sum_{x_m \in V} (\sum_{j=k}^{M_\ell} j u_j^{M_\ell}(x_m, s))^2 ds \\ &\quad \leq \frac{4\bar{A}^2 i^2}{\underline{A} k^{\frac{1}{2}}} (\sum_{x_m \in V} \sum_{j=1}^{\infty} j^{\frac{1}{2}} U_j(x_m) + Th \|f(\cdot)\|_\infty) \end{aligned} \tag{2.127}$$

and by Hölder inequality it holds:

$$\begin{aligned} &\int_0^T \sum_{j=k}^{M_\ell} a_{i,j} u_j^{M_\ell}(x_m, s)) ds \\ &\quad \leq (\int_0^T (\sum_{j=k}^{M_\ell} a_{i,j} u_j^{M_\ell}(x_m, s))^2 ds)^{\frac{1}{2}} T^{\frac{1}{2}} \\ &\quad \leq \frac{2\bar{A} i}{\underline{A}^{\frac{1}{2}} k^{\frac{1}{4}}} (M_{\frac{1}{2}}(0) + Th \|f(\cdot)\|_\infty)^{\frac{1}{2}} T^{\frac{1}{2}} \ . \end{aligned} \tag{2.128}$$

We will estimate now the term:

$$\int_0^T \sum_{j=k}^{\infty} a_{i,j} u_j(x_m, s) ds \qquad \text{for any fixed } \ k \in \mathbb{N} \, .$$

We proceed like in Theorem 2.3.1.
For any $P^{'} \in \mathbb{N}$ and for any $k \in \mathbb{N}$ such that $k \leq P^{'} < M_\ell$, for each fixed i and for each $s \in [0, T]$ we have:

$$\sum_{j=k}^{P^{'}} a_{i,j} u_j^{M_\ell}(x_m, s) \leq \sum_{j=k}^{M_\ell} a_{i,j} u_j^{M_\ell}(x_m, s) \, .$$

Thus, integrating in time and passing to the limit for $\ell \to \infty$, by (2.38) and (2.128), we obtain :

$$\begin{aligned} \int_0^T \sum_{j=k}^{P^{'}} a_{i,j} u_j(x_m, s) ds &= \lim_{\ell \to \infty} \int_0^T \sum_{j=k}^{P^{'}} a_{i,j} u_j^{M_\ell}(x_m, s) ds \\ &\leq \limsup_{\ell \to \infty} \int_0^T \sum_{j=k}^{M_\ell} a_{i,j} u_j^{M_\ell}(x_m, s) ds \\ &\leq \frac{2\bar{A} i}{\underline{A}^{\frac{1}{2}} k^{\frac{1}{4}}} (M_{\frac{1}{2}}(0) + Th \|f(\cdot)\|_\infty)^{\frac{1}{2}} T^{\frac{1}{2}} \, . \end{aligned} \tag{2.129}$$

Finally, by monotone convergence theorem and (2.129), there holds:

$$\int_0^T \sum_{j=k}^{\infty} a_{i,j} u_j(x_m, s) = \lim_{P^{'} \to \infty} \int_0^T \sum_{j=k}^{P^{'}} a_{i,j} u_j(x_m, s) \leq \frac{2\bar{A} i}{\underline{A}^{\frac{1}{2}} k^{\frac{1}{4}}} (M_{\frac{1}{2}}(0) + Th \|f(\cdot)\|_\infty)^{\frac{1}{2}} T^{\frac{1}{2}} \, . \tag{2.130}$$

By (2.38), (2.130), (2.128), we have that for any given $\epsilon > 0$ there exists k large enough such that:

$$\begin{aligned} &\int_0^T |\sum_{j=1}^{M_\ell} a_{i,j} u_j^{M_\ell}(x_m, s) - \sum_{j=1}^{\infty} a_{i,j} u_j(x_m, s)| ds \\ &\leq \int_0^T \sum_{j=1}^{k-1} a_{i,j} |u_j^{M_\ell}(x_m, s) - u_j(x_m, s)| ds + \int_0^T |\sum_{j=k}^{M_\ell} a_{i,j} u_j^{M_\ell}(x_m, s)| ds + \int_0^T \sum_{j=k}^{\infty} a_{i,j} u_j(x_m, s) ds \\ &< \epsilon \, . \end{aligned}$$

Proceeding like in Theorem 2.3.3 we can build a solution $(u_i(x_1, t), \ldots, u_i(x_h, t))$, for each $i \in \mathbb{N}$, of (2.1)-(2.3) defined on $V \times [0, \infty)$. □

Chapter 3

Appendix 1: The Laplace operator for graphs

In this chapter, we will provide an overview about graph theory and graph Laplacian, focusing on the known results that we use in the proofs of that thesis. We refer to the works [46], [93], [124].

3.1 Graphs

A graph G is a representation of a set of objects where some pairs of objects are connected by links. More precisely, it is a couple (V, E), where $V = \{x_1, \cdots x_h\}$ denotes the set of the *vertices*, that is an arbitrary set whose elements are called vertices, and E is the set of the *edges*, that is, E consists of some couples (x_i, x_j), where $x_i, x_j \in V$.
A graph (V, E) is said finite if the number of element of V is finite. In our discussion the graph is assumed to be finite. In fact, many of the well-known results fail to hold in the infinite case.
A basic relation in graph theory is the following:

Definition 3.1. If $(x_i, x_j) \in E$, x_i, x_j are said *adjacent* vertices of G. In symbols: $x_i \sim x_j$.

For each vertex x_i, define its degree

$$deg(x_i) = \#\{x_j \in V \ : \ x_i \sim x_j\} \ ,$$

that is $deg(x_i)$ is the number of the neighbors of x_i. If $deg(x_i) = 0$, x_i is said isolated vertex. A graph that has at least one edge is said non trivial.
If the edge (x_i, x_j) is identical to the edge (x_j, x_i), the graph is said *undirected*. This means that the edges have no orientation and E can be seen as the set of the unordered pairs (x_i, x_j) such that $x_i \sim x_j$. Moreover, in this case the adjacency is a symmetric binary relation.
If the edges have orientation, that is the edges (x_i, x_j) are thought as ordered pairs, the graph is said *directed* and the simmetry of the adiacency relation fails to hold. An edge that connects to the vertex at both ends is said *loop*. Two or more edges that join the same two vertices are said *multiple edges*. An undirected graph without loops or multiple edges is said *simple*. In what follows, we will deal with simple graphs.

Definition 3.2. We say that (V', E') is a subgraph of G if $V' \subset V$ and $E' \subset E$. A subgraph is said maximal if for any of its vertices the all edges that connect to it belong to the subgraph.

The are several graph classes. Some examples can be the following:

- A *k regular* graph. Each vertex has the same degree, i.e. $deg(x_i) = k \ \forall x_i \in V$.
- A *complete graph* K_h. The set of the vertices is $V = \{1, \dots, h\}$, and the edges are defined as follows: $i \sim j$ for any two distinct $i, j \in V$.
- A *complete bipartite graph* $K_{n,h}$. The set of the vertices is $V = \{1, \dots, n, n+1, \dots, n+h\}$ and the edges are defined as follows: $i \sim j$ if either $i < n$ and $j \geq n$ or $i \geq n$ and $j < n$. This means that the set of vertices is split into two groups: $V_1 = \{1, \dots, n\}$ and $V_2 = \{n+1, \dots, h\}$; the vertices are connected if and only if they belong to different groups.

3.1.1 Product of Graphs

Let (V_1, E_1) and (V_2, E_2) be two graphs. Their Cartesian product is given by:

$$(V, E) = (V_1, E_1) \square (V_2, E_2)$$

where $V = V_1 \times V_2$ is the set of pairs (x, y) such that $x \in V_1$ and $y \in V_2$. The set E of the edges is defined by:

$$(x, y) \sim (x', y) \ \text{ if } x' \sim x \quad \text{and} \quad (x, y) \sim (x, y') \ \text{ if } y' \sim y \ .$$

We have $|V| = (|V_1|)(|V_2|)$ and $deg(x, y) = deg(x) + deg(y)$ for all $x \in V_1$ and $y \in V_2$.

3.1.2 Graph Distance

Before introducing a notion of distance on simple graphs we will give some preliminary definitions:

Definition 3.3. A *path* is a finite sequence $\{x_i\}_{i=0}^n$ of vertices on a graph such that $x_i \sim x_{i+1}$ for all $i = 0, 1, \ldots, n-1$. The *length* of the path is given by the number n of edges in the path.

Definition 3.4. A graph (V, E) is said *connected* if for any pair of vertices $x, y \in V$ there is a path connecting them. This means that there exists a path $\{x_i\}_{i=0}^n$ whose endpoints are $x_0 = x$ and $x_n = y$.

Let (V, E) be a connected graph then we can define the graph distance in the following way:

Definition 3.5. The *graph distance* $d(x, y)$ between any pairs of vertices $x, y \in V$ such that $x \neq y$ is defined as the minimal length of a path that connect x and y. If $x = y$, then $d(x, y) = 0$.

Remark 5. The graph is assumed to be connected in order to assure that $d(x, y) < \infty$ for any two points. In fact, if there is not any path joining x and y, $d(x, y) = \infty$.

Lemma 3.1.1. *Let (V, E) a connected graph, then the graph distance is a metric.*

Proof. From the definition, it follows immediately that $d(x, y) \geq 0$ for all $x, y \in V$ and $d(x, y) = 0$ if and only if $x = y$.
The simmetry, that is $d(x, y) = d(y, x)$ for any pair $x, y \in V$, follows from the definition of undirected graph.
It needs to be demonstrated that for all $x, y, z \in V$, $d(x, y) \leq d(x, z) + d(z, y)$(triangle inequality).
Starting with a path that connects x and z of length $d(x, z)$ and adding a path from z to y of length $d(z, y)$, we obtain a path from x to y of length $d(x, z) + d(z, y)$. But this path can not be shorter than the *distance* $d(x, y)$, because by definition $d(x, y)$ is the length of the shortest path joining x and y. Hence, we must have

$$d(x, y) \leq d(x, z) + d(z, y) \text{ for any } x, y, z \in V \ .$$

□

It follows that for any connected graph, (V, d) is a metric space.

3.1.3 Weighted graphs

Weighted graphs are important class of graph, in which all information about the set of the edges is expressed by a non negative function associeted with the graph. More precisely, we can state the following definition:

Definition 3.6. A weighted graph $((V, E), w)$ is a graph with a weight function:

$$w : V \times V \longrightarrow \mathbb{R}$$

such that:

$$w(x_i, x_j) = w(x_j, x_i)$$

and

$$w(x_i, x_j) \geq 0 \ \forall i, j = 1, .., h \ .$$

Moreover:

$$w(x_i, x_j) > 0 \text{ if and only if } x_i \sim x_j \ .$$

Unweighted graphs are a particular case of weighted graphs in which all the weights are 0 or 1. More precisely, $w(x_i, x_j) = 1$ if $x_i \sim x_j$ and $w(x_i, x_j) = 0$ otherwise.
For each vertex $x_i \in V$, we can define its weight as:

$$\mathbf{w}(x_i) = \sum_{x_j \in V \, : \, x_j \sim x_i} w(x_i, x_j) \ . \tag{3.1}$$

In litterature, (3.1) also represents the degree of the vertex x_i ($deg(x_i)$) for a weighted graph.

3.2 Laplace Operator on graphs

3.2.1 The standard Laplacian matrix for simple unweighted graphs

The graph Laplacian is a discrete operator that can be defined in several ways.
Let $V = \{x_1, \ldots, x_h\}$ and $G = (V, E)$ be a finite simple unweighted graph with $|V| = h$. The *standard Laplacian* matrix $\Delta_{Gh \times h}$ (whose rows and columns are indexed by the vertices of the graph) is given by:

$$\Delta_G = T - A \tag{3.2}$$

where T is the degree matrix, that is an $h \times h$ diagonal matrix defined as follows:

$$T := t_{i,j} = \begin{cases} deg(x_i) & \text{if } i = j \\ 0 & \text{otherwise} \end{cases} \tag{3.3}$$

and

$$A := a_{i,j} = \begin{cases} 1 & \text{if } x_i \text{ and } x_j \text{ are adjacent} \\ 0 & \text{otherwise} \end{cases} \tag{3.4}$$

is an $h \times h$ matrix, said the adjacency matrix of the graph. Hence, the elements of Δ_G are given by:

$$\Delta_G := \Delta_{Gi,j} = \begin{cases} deg(x_i) & \text{if } i = j \\ -1 & \text{if } x_i \text{ and } x_j \text{ are adjacent} \\ 0 & \text{otherwise} \end{cases} \tag{3.5}$$

Let f be a function from V into $\mathbb{R}$. We can think of f as a vector where the i-th coordinate corresponds to the value of $f(x_i)$:

$$f \equiv \begin{pmatrix} f(x_1) \\ \vdots \\ f(x_h) \end{pmatrix} .$$

We can add functions of the vertices and scale as expected:

$$(f + g)(x_i) := f(x_i) + g(x_i) \text{ for all } x_i \in V$$

$$(cf)(x_i) := c(f(x_i)) \text{ for all } x_i \in V .$$

This gives us linearity of the functions. Hence, the functions from V into $\mathbb{R}$ form a vector space that we call $\mathtt{F}(V)$ and (that acts like)is isomorphic to $\mathbb{R}^h$. In fact, we have that $\dim \mathtt{F}(V) = |V| = h$.
In order to show this statement we observe that each element f of $\mathtt{F}(V)$ is usually written in the following form $f = \sum_{i=1}^{h} f_i v^i$, where $f_i = f(x_i)$ for each $i = 1, \ldots, h$. If we think v^i as the function from V into $\mathbb{R}$ such that

$$v^i(x_j) := \begin{cases} 1 & \text{if } i = j \\ 0 & \text{otherwise} \end{cases}$$

then $(v^1, ..., v^h)$ is a basis for $\mathtt{F}(V)$ and the sum above expresses an element f in term of the basis elements. Given two functions $f, g : V \to \mathbb{R}$, we can define the inner product $\langle f, g\rangle = \sum_{x_i \in V} f(x_i)g(x_i)$ that can be seen like the standard inner product in $\mathbb{R}^h$.
The Laplacian can be regarded like a linear operator $\Delta_G = \mathtt{F}(V) \to \mathtt{F}(V)$. For each function $f \in \mathtt{F}(V)$, we have that:

$$\Delta_G f(x_i) = \sum_{x_j \sim x_i} (f(x_i) - f(x_j)) \ . \tag{3.6}$$

We observe that the Laplacian in the Euclidean space $\mathbb{R}^h$ is a differential operator, while the Laplace operator on graphs is represented by a matrix. Hence, it is not immediate to see the connection between the continous and the discrete case. However, there is a deep link between the graph Laplacian and the Laplace operator on functions in $\mathbb{R}^2$ that we try to explain in what follows. We recall that the Laplace operator on functions in $\mathbb{R}^2$ is given by:

$$\Delta f = \frac{\partial^2 f}{\partial x^2} + \frac{\partial^2 f}{\partial y^2} \ .$$

Using the approximation of the second derivative:

$$\frac{\partial^2 f}{\partial x^2}(x, y) \approx \frac{f(x + h, y) - 2f(x, y) + f(x - h, y)}{h^2}$$

$$\frac{\partial^2 f}{\partial y^2}(x, y) \approx \frac{f(x, y + h) - 2f(x, y) + f(x, y - h)}{h^2} \ ;$$

we obtain:

$$\Delta f \approx \frac{4}{h^2} \left(\frac{f(x + h, y) + f(x - h, y) + f(x, y - h) + f(x, y + h)}{4} - f(x, y) \right) \ .$$

We restrict f to the grid $h\mathbb{Z}^2$ and we define the edges in $h\mathbb{Z}^2$ as in the product graph that is:

$$(x, y) \sim (x', y') \ \text{ if } x' = x + h \ \text{ or } \ x' = x - h \text{ and } y = y'$$

or

$$(x, y) \sim (x', y') \ \text{ if } y' = y + h \ \text{ or } \ y' = y - h \text{ and } x = x' \ .$$

Hence, the discrete Laplace operator on $h\mathbb{Z}^2$ is given by:

$$\Delta f \approx \frac{4}{h^2} \left(\frac{1}{4} \sum_{(x', y') \sim (x, y)} f(x', y') - f(x, y) \right) \ .$$

If the pair (x, y) is thought as the i-th vertex of the graph, the pairs (x', y') are thought as the vertices adjacent to the i-th vertex and $h = 1$, the expression above is equivalent to the negative graph laplacian.

3.2.2 The standard Laplacian matrix for weighted graphs

The Laplacian of a weighted graph (V, E), with $|V| = h$, is defined to be the following $h \times h$ matrix:

$$\Delta_G := \delta_{Gi,j} = \begin{cases} \sum_{x_j \sim x_i} w(x_i, x_j) & \text{if } i = j \\ -w(x_i, x_j) & \text{if } x_i \text{ and } x_j \text{ are adjacent} \\ 0 & \text{otherwise} \end{cases} \tag{3.7}$$

In particular, for a function $f : V \to \mathbb{R}$ we have:

$$\Delta f(x_i) = \sum_{x_j : x_j \sim x_i} (f(x_i) - f(x_j)) w(x_i, x_j) \text{ for each } i = 1, \ldots, h$$

We observe that definition (3.7) holds also for unweighted graph. In fact, (3.5) is a particular case of (3.7), in which the weights are in the set $\{0, 1\}$. More precisely, $w(x_i, x_j) = 1$ if $x_i \sim x_j$ and $w(x_i, x_j) = 0$ otherwise.

3.2.3 Discrete Operators on graphs

A significant way to denote the Laplacian of a function f in a euclidean space is:

$$\Delta f = \nabla \cdot \nabla f$$

where $\nabla \cdot$ is the divergence operator. A similar definition holds in the case of graph Laplacian that it is what we want to derive in this section. We will consider the general case of a weighted graph (V, E), but obviously it can be extended to unweighted graphs, as the latter are weighted graph in which all weights belong to the set $\{0, 1\}$.
Now, we will introduce some preliminar definitions.
Let $e_1, \ldots, e_{|E|}$ be the edges of the graph and let g be a function from E into $\mathbb{R}$. We can think of g as a vector where the k-th coordinate corresponds to the value of $g(e_k)$:

$$g \equiv \begin{pmatrix} g(e_1) \\ \vdots \\ g(e_{|E|}) \end{pmatrix} .$$

We can add functions of the vertices and scale as expected:

$$(g+\varphi)(e_k) := g(e_k) + h(e_k) \text{ for all } e_k \in E$$

$$(cg)(e_k) := c(g(e_k)) \text{ for all } e_k \in E\ .$$

This gives us linearity of the functions. Hence, the functions from E into $\mathbb{R}$ form a vector space that we call $\mathtt{F}(E)$. Given two functions $g, \varphi \in \mathtt{F}(E)$ we can consider the inner product

$$\langle g, \varphi \rangle = \sum_{e_k \in E} g(e_k)\varphi(e_k)$$

that can be seen like the standart inner product in $\mathbb{R}^{|E|}$. In what follows we will change notation and we denote the k-th edge by its endpoints $[x_i, x_j]$. Consider $f \in \mathtt{F}(V)$, where $\mathtt{F}(V)$ is the vector space of all functions from V to $\mathbb{R}$.

Definition 3.7. The *graph difference operator* $\nabla : \mathtt{F}(V) \to \mathtt{F}(E)$ is defined by:

$$(\nabla f)[x_i, x_j] = \sqrt{w(x_i, x_j)}(f(x_j) - f(x_i)) \text{ for all } [x_i, x_j] \in E\ . \tag{3.8}$$

Definition 3.8. The *graph divergence* is an operator $div : \mathtt{F}(E) \to \mathtt{F}(V)$ that satisfies:

$$\sum_{[x_i,x_j]\in E} (\nabla f)[x_i, x_j]\psi[x_i, x_j] = \sum_{x_i \in V(G)} f(x_i)(-(div\ \psi))(x_i) \tag{3.9}$$

for all $f \in \mathtt{F}(V),\ \psi \in \mathtt{F}(E)$.

In other words $-div$ is defined to be the adjoint of the graph difference operator. Equation (3.9) can be thought as the discrete analogue of the Stokes theorem.

Proposition 3.2.1. *The graph divergence can be computed as:*

$$(div\ \psi)(x_i) = \sum_{x_j \sim x_i} \sqrt{w(x_i, x_j)}(\psi[x_i, x_j] - \psi[x_j, x_i])\ . \tag{3.10}$$

Proof. By (3.8), we have that:

$$\begin{aligned}
&\sum_{[x_i,x_j]\in E}(\nabla f)[x_i,x_j]\psi[x_i,x_j] = \sum_{[x_i,x_j]\in E}\sqrt{w(x_i,x_j)}(f(x_j)-f(x_i))\psi[x_i,x_j]\\
&= \sum_{[x_i,x_j]\in E}\sqrt{w(x_i,x_j)}f(x_j)\psi[x_i,x_j] - \sum_{[x_i,x_j]\in E}\sqrt{w(x_i,x_j)}f(x_i)\psi[x_i,x_j]\\
&= \sum_{x_i\in V}\sum_{x_j\sim x_i}\sqrt{w(x_i,x_j)}f(x_i)\psi[x_j,x_i] - \sum_{x_i\in V}\sum_{x_j\sim x_i}\sqrt{w(x_i,x_j)}f(x_i)\psi[x_i,x_j]\\
&= \sum_{x_i\in V} f(x_i)\left(\sum_{x_j\sim x_i}\sqrt{w(x_i,x_j)}(\psi[x_j,x_i]-\psi[x_i,x_j])\right)\\
&= \sum_{x_i\in V} f(x_i)(-(div\ \psi))(x_i)
\end{aligned}$$

where in last equality we use (3.9). Hence,

$$-(div\ \psi)(x_i) = \sum_{x_j\sim x_i}\sqrt{w(x_i,x_j)}(\psi[x_j,x_i]-\psi[x_i,x_j])\ , \tag{3.11}$$

from which (3.10) follows. □

Hence, we can state the following definition:

Definition 3.9. The graph Laplacian is an operator $\Delta_G : \mathtt{F}(V) \to \mathtt{F}(V)$ defined by:

$$\Delta_G f := -\frac{1}{2} div(\nabla f) \tag{3.12}$$

In fact, by (3.11), we have that:

$$\begin{aligned}
\Delta_G f(x_i) &= \frac{1}{2}\sum_{x_j\sim x_i}\sqrt{w(x_i,x_j)}(\nabla f[x_j,x_i]-\nabla f[x_i,x_j])\\
&= \frac{1}{2}\sum_{x_j\sim x_i}\sqrt{w(x_i,x_j)}(2\sqrt{w(x_i,x_j)}f(x_i) - 2\sqrt{w(x_i,x_j)}f(x_j)\\
&= \sum_{x_j\sim x_i} w(x_i,x_j)(f(x_i)-f(x_j))\ .
\end{aligned} \tag{3.13}$$

The following result holds:

Lemma 3.2.2. *For each function $f \in \mathtt{F}(V)$, we have that*

$$\sum_{x_i\in V}\Delta_G f(x_i) = 0 \tag{3.14}$$

Proof. By using (3.11), (3.12) we have:

$$\sum_{x_i\in V}\Delta_G f(x_i)=\sum_{x_i\in V}\sum_{x_j\sim x_i}w(x_i,x_j)(f(x_i)-f(x_j))=-\frac{1}{2}\sum_{x_i\in V}(div(\nabla f))(x_i)=$$

$$\frac{1}{2}\sum_{x_i\in V}\sum_{x_j\sim x_i}\sqrt{w(x_i,x_j)}(\nabla f[x_j,x_i]-\nabla f[x_i,x_j])$$

$$=\frac{1}{2}\sum_{[x_i,x_j]\in E}\sqrt{w(x_i,x_j)}(\nabla f[x_j,x_i]-\nabla f[x_i,x_j])\,. \tag{3.15}$$

As the graph is undirected we have that the pairs $[x_i,x_j]$ and $[x_j,x_i]$ are edges of G. Hence, equation (3.15) is sum of terms:

$$\sqrt{w(x_i,x_j)}(\nabla f(x_j,x_i)-\nabla f(x_i,x_j))+\sqrt{w(x_j,x_i)}(\nabla f(x_i,x_j)-\nabla f(x_j,x_i))$$

and as w is symmetric the sum is null. □

In other word, the previous result affirms that each function in $\mathtt{F}(E)$ has null divergence over the entire set of vertices.
Other general definitions of graph Laplacian have been proposed in litterature that we will present in the next section and for which lemma 3.2.2 does not hold or holds in some cases.
We will conclude this section stating one of the main tools when working with the Laplace Operator.
Let $\nabla_{x_i,x_j}f=f(x_j)-f(x_i)=\frac{(\nabla f)[x_i,x_j]}{\sqrt{w(x_i,x_j)}}$, the following result holds:

Theorem 3.2.3. *Let (V,E) be a finite weighted graph without isolated points, let Ω be a non-empty finite subset of V. Then, for any two functions $f,g\in\mathtt{F}$ it holds:*

$$\sum_{x_i\in\Omega}-\Delta_G f(x_i)g(x_i)=-\frac{1}{2}\sum_{x_i,x_j\in\Omega}(\nabla_{x_i,x_j}f)(\nabla_{x_i,x_j}g)w(x_i,x_j)$$
$$+\sum_{x_i\in\Omega,x_j\in\Omega^c}(\nabla_{x_i,x_j}f)g(x_i)w(x_i,x_j)\,. \tag{3.16}$$

Remark 6. When $\Omega=V$, equation (3.16) becomes:

$$\sum_{x_i\in V}-\Delta_G f(x_i)g(x_i)=-\frac{1}{2}\sum_{x_i,x_j\in V}(\nabla_{x_i,x_j}f)(\nabla_{x_i,x_j}g)w(x_i,x_j)\,. \tag{3.17}$$

Proof. We have:

$$\begin{aligned}\sum_{x_i\in\Omega} -\Delta_G f(x_i)g(x_i) &= \sum_{x_i\in\Omega}\sum_{x_j\sim x_i} w(x_i,x_j)(f(x_j)-f(x_i))g(x_i)\\ &= \sum_{x_i\in\Omega}\sum_{x_j\sim x_i} w(x_i,x_j)(\nabla_{x_i,x_j}f)g(x_i)\\ &= \sum_{x_i\in\Omega}\sum_{x_j\in V} w(x_i,x_j)(\nabla_{x_i,x_j}f)g(x_i)\\ &= \sum_{x_i\in\Omega}\sum_{x_j\in\Omega} w(x_i,x_j)(\nabla_{x_i,x_j}f)g(x_i) + \sum_{x_i\in\Omega}\sum_{x_j\in\Omega^c} w(x_i,x_j)(\nabla_{x_i,x_j}f)g(x_i)\\ &= \sum_{x_j\in\Omega}\sum_{x_i\in\Omega} w(x_i,x_j)(\nabla_{x_j,x_i}f)g(x_j) + \sum_{x_i\in\Omega}\sum_{x_j\in\Omega^c} w(x_i,x_j)(\nabla_{x_i,x_j}f)g(x_i)\,.\end{aligned} \tag{3.18}$$

where in the third equality we use fact that if the vertex x_j is not adjacent to the vertex x_i, the weight $w(x_i,x_j)=0$ and in the first sum of the last equality we switch notation of the variables x_i and x_j and use the fact that $w(x_i,x_j)=w(x_j,x_i)$. Adding together the last two lines and dividing by 2, we obtain:

$$\begin{aligned}&\sum_{x_i\in\Omega} -\Delta_G f(x_i)g(x_i)\\ &\quad= \frac{1}{2}\sum_{x_i,x_j\in\Omega} w(x_i,x_j)(\nabla_{x_i,x_j}f)(g(x_i)-g(x_j)) + \sum_{x_i\in\Omega,x_j\in\Omega^c} w(x_i,x_j)(\nabla_{x_i,x_j}f)g(x_i)\\ &\quad= -\frac{1}{2}\sum_{x_i,x_j\in\Omega} w(x_i,x_j)(\nabla_{x_i,x_j}f)(\nabla_{x_i,x_j}g) + \sum_{x_i\in\Omega,x_j\in\Omega^c} w(x_i,x_j)(\nabla_{x_i,x_j}f)g(x_i)\end{aligned} \tag{3.19}$$

that is what we want to prove. □

We observe that (3.16) is the discrete analogous to the Green formula for the Laplace operator in $\mathbb{R}^2$: if Ω is a bounded domain in $\mathbb{R}^2$ with smooth boundary then, for all smooth enough functions f,g on $\bar{\Omega}$

$$\int_\Omega (\Delta f)g dx = -\int_\Omega \nabla f\cdot\nabla g dx + \int_{\partial\Omega}\frac{\partial f}{\partial\nu} g d\ell$$

where ν is the unit normal vector field on $\partial\Omega$ and ℓ is the length element on $\partial\Omega$.

3.3 Eigenvalue of the Laplace operator on graphs

As was already mentioned, the Laplace operator Δ_G is a linear operator in a h-dimensional vector space, where $h = |h|$. We will focus now on the spectral proprieties of this operator.

We recall that, given a linear operator A in a vector space V, a vector $v \in V_{\setminus\{0\}}$ is called *eigenvector* of A if $Av = \lambda v$, for some scalar λ; the latter is said *eigenvalue* of A. The set of all (complex) eigenvalues of A is said the *spectrum* of A.

In the case when the underlying vector space is the space $\mathtt{F}(V)$ of functions on the graphs, the eigenvectors are also referred to as *eigenfunctions*. Consider in the vector space $\mathtt{F}(V)$, the inner product:

$$\langle f, g\rangle = \sum_{x_i \in V} f(x_i)g(x_i) \text{ for any two fuctions } f, g \in V \ .$$

Hence, $\mathtt{F}(V)$ is an inner product space and the graph Laplacian is symmetric with respect to this inner product. More precisely, we can state the following result:

Lemma 3.3.1. *The operator Δ_G is symmetric with respect to the inner product $\sum_{x_i \in V}$, that is:*

$$\langle \Delta_G f, g\rangle = \langle f, \Delta_G g\rangle$$

for all $f, g \in \mathtt{F}(V)$.

Proof. By discrete Green formula (3.17), we have that:

$$\langle \Delta_G f, g\rangle = \sum_{x_i \in V} \Delta_G f(x_i)g(x_i) = \sum_{x_i \sim x_j} (f(x_j) - f(x_i))(g(x_j) - g(x_i))w(x_i, x_j) \ , \quad (3.20)$$

and the last expression is symmetric in f and g; thus, it is equal to $\langle f, \Delta_G g\rangle$. □

As Δ_G is symmetric, its eigenvalues are real. In particular, the eigenvalues can be enumerated in increasing order $\lambda_1 \leq \lambda_2 \leq \cdots \leq \lambda_h$, where $\dim \mathtt{F}(V) = |V| = h$ and each eigenvalue is counted with multiplicity.

We can use the variational charatherization of the eigenvalues in terms of the Rayleigh quotient of Δ_G:

$$R(f) = \frac{\langle \Delta_G f, f\rangle}{\langle f, f\rangle} \quad (3.21)$$

for an arbitrary function $f \in F(V)$. The following identities holds for all $k = 1, \ldots, h$:

$$\lambda_k = R(f_k) = \inf_{f \perp f_1, f_2, \ldots, f_{k-1}} R(f) = \sup_{f \perp f_h, f_{h-1}, \ldots, f_{k+1}} R(f) \ .$$

In particular:

$$\lambda_1 = \inf_{f\neq 0} R(f) \text{ and } \lambda_h = \sup_{f\neq 0} R(f) .$$

By Green formula (3.17), the Rayleigh quotient of Δ_G is:

$$R(f) = \frac{\langle \Delta_G f, f\rangle}{\langle f, f\rangle} = \frac{\sum_{x_i\sim x_j}(f(x_j)-f(x_i))^2 w(x_i,x_j)}{\sum_{x_i\in V} f(x_i)^2} . \tag{3.22}$$

We can state now the following result:

Theorem 3.3.2. *Let $G=(V,E)$ a finite, connected, weighted graph with $|V|>1$, then zero is a simple eigenvalue of Δ_G.*

Proof. Let $\mathbf{1}$ denote the function which value is 1 on each vertex, thus, $\Delta_G\mathbf{1}=0$. Hence, the constant function is an eigenfunction with eigenvalue zero. Assuming now that $f\neq 0$ is an eigenfunction of the eigenvalue zero, we will prove that $f\equiv$ const, which will imply that 0 is a simple eigenvalue. If $\Delta_G f = 0$, by (3.17) it follows that:

$$\frac{\langle \Delta_G f, f\rangle}{\langle f, f\rangle} = \frac{\sum_{x_i\sim x_j}(f(x_j)-f(x_i))^2 w(x_i,x_j)}{\langle f, f\rangle} = 0 .$$

Hence, $\sum_{x_i\sim x_j}(f(x_j)-f(x_i))^2 w(x_i,x_j)=0$. In particular, $f(x_i)=f(x_j)$, for any two vertices x_i,x_j such that $x_i\sim x_j$. Since the graph is connected, we have that for any pair of vertices $x,y\in V$ there exists a path $\{x_k\}_{k=1}^m$ such that

$$x = x_1 \sim x_2 \sim \cdots \sim x_m = y .$$

Hence, $f(x_1)=f(x_2)=\cdots=f(x_m)$ and $f(x)=f(y)$. This is true for all pairs $x,y\in V$, we obtain $f\equiv$ const. □

Hence, we can enumerate the eigenvalues of Δ_G in increasing order as follows:

$$0=\lambda_0<\lambda_1\leq\cdots\leq\lambda_{h-1} .$$

We note that the first eigenvalue is called λ_0 rather than λ_1. We observe that the eigenvalues of Δ_G are all positive (with a zero smallest eigenvalue); for this reason Δ_G, as defined in (3.7), is said the *positive* graph laplacian.
In addiction, theorem 3.3.2 allows us to investigate the solvability of the problem:
find $u\in \mathtt{F}(V)$ such that

$$\Delta_G u = f \tag{3.23}$$

for any $f \in \mathtt{F}(V)$. We multiply both sides of the equality by a function $g \in \mathtt{F}(V)$ such that $g(x_i) = 1$ for all $x_i \in V$ and we sum up over all $x_i \in V$. Therefore, by Green formula (3.17) we have that

$$\sum_{x_i \in V} (\Delta u)(x_i) = 0 \ ;$$

this implies, as necessary condition of solvability

$$\sum_{x_i \in V} f(x_i) = 0 \ .$$

Assuming that, we will show that the equation 3.23 has a solution. In fact, the above condition of solvability means that $f \perp 1$, that is f is orthogonal to a function $g \in \mathtt{F}(V)$ such that $g(x_i) = 1$ for all $x_i \in V$. This tell us in which subspace of $\mathtt{F}(V)$ we have to find a solution of (3.23).
Consider the subspace $\mathtt{F}_0(V)$ of $\mathtt{F}(V)$ of all functions orthogonal to 1. Since 1 is the eigenfunction with eigenvalue $\lambda_0 = 0$, the spectrum of Δ_G in $\mathtt{F}_0(V)$ is $\lambda_1, \ldots, \lambda_{h-1}$. As all $\lambda_j > 0$, for $j = 1, \ldots, h-1$, we see that Δ_G is invertible in $\mathtt{F}_0(V)$. This means that equation $\Delta_G u = f$ has for each $f \in \mathtt{F}_0(V)$ a unique solution $u \in \mathtt{F}_0(V)$, such that $u = (\Delta_G)^{-1} f$.

3.4 The normalized Laplacian matrix for graphs

Starting from the standard Laplacian matrix for graphs, we can define the *symmetric normalized Laplacian matrix* and the *random walk normalized Laplacian matrix* for graphs. This two definitions are motivated by the fact that both highlights spectral proprieties of the graph in significant way and, in addiction, the latter is deeply connected with Markov chains.
Let (V, G) be a finite, simple weighted graph with $|V| = h$ and let T be the degree matrix (we recall that it is the diagonal matrix with the (i, i)-th entry having the value $deg(x_i)$), the symmetric normalized Laplacian matrix for a weighted graph is defined to be:

$$\mathbf{L} = T^{\frac{-1}{2}} \Delta_G T^{\frac{-1}{2}}$$

where Δ_G is the standard Laplacian matrix for weighted graphs (3.7). Therefore $\mathbf{L}$ is the following $h \times h$ matrix:

$$\mathbf{L}_{i,j} = \begin{cases} 1 & \text{if } i = j \text{ and } deg(x_i) \neq 0 \\ \frac{-w(x_i,x_j)}{\sqrt{deg(x_i)deg(x_j)}} & \text{if } x_i \text{ and } x_j \text{ are adjacent} \\ 0 & \text{otherwise} \end{cases} \tag{3.24}$$

Obviously, the case of unweighted graphs follows by setting $w(x_i, x_j) = 1$ if $x_i \sim x_j$ and $w(x_i, x_j) = 0$ if x_i is not adjacent to the vertex x_j.
For any function $f \in \mathtt{F}(V)$, we have that:

$$\mathbf{L}f(x_i) = f(x_i) - \sum_{x_j \sim x_i} f(x_j) \frac{w(x_i, x_j)}{\sqrt{deg(x_i)deg(x_j)}} \tag{3.25}$$

For any two functions $f, g \in \mathtt{F}(V)$ we can consider the inner product $\langle f, g \rangle = \sum_{x_i} f(x_i)g(x_i)$, with respect to $\mathbf{L}$ is symmetric.
The Rayleigh quotient of $\mathbf{L}$ is:

$$R(f) = \frac{\sum_{x_i \sim x_j} (f(x_j) - f(x_i))^2 w(x_i, x_j)}{\sum_{x_i \in V} f(x_i)^2 deg(x_i)} \, . \tag{3.26}$$

The random walk normalized Laplacian matrix is defined to be :

$$L = T^{-1}\Delta_G$$

Hence, L is the following $h \times h$ matrix:

$$L_{i,j} = \begin{cases} 1 & \text{if } i = j \text{ and } \mathbf{w}(x_i) \neq 0 \\ \frac{-w(x_i,x_j)}{\mathbf{w}(x_i)} & \text{if } x_i \text{ and } x_j \text{ are adjacent} \\ 0 & \text{otherwise} \end{cases} \tag{3.27}$$

where $\mathbf{w}(x_i) = \sum_{x_j \in V : x_j \sim x_i} w(x_i, x_j)$ is a function defined on the set of vertices V and represents the weight of the vertex x_i. We observe that we refer to $\mathbf{w}(x_i)$ also as the degree of the vertex x_i ($deg(x_i)$), $i = 1, \ldots, h$.
Moreover, $\mathbf{w}(x_i)$ gives rise to a measure of subsets: for any subset $A \subset V$ define its measure as $\mathbf{w}(A) = \sum_{x_i \in A} \mathbf{w}(x_i)$.

For any function $f \in \mathtt{F}(V)$, we have that:

$$Lf(x_i) = \frac{1}{\mathbf{w}(x_i)} \sum_{x_j \in V} (f(x_i) - f(x_j)) w(x_i, x_j) \ . \tag{3.28}$$

We can consider in $\mathtt{F}(V)$ the following inner product:

$$\langle f, g \rangle = \sum_{x_i} f(x_i) g(x_i) \mathbf{w}(x_i) \ \text{ for any two functions } f, g \in \mathtt{F}(V) \ .$$

that can be seen like as integration of f, g against measure $\mathbf{w}$ on V. The operator L is symmetric with respect to this inner product and a discrete analogous of Green formula holds: for any two functions $f, g \in \mathtt{F}$ it holds:

$$\begin{aligned} \sum_{x_i \in \Omega} -Lf(x_i) g(x_i) \mathbf{w}(x_i) = -\frac{1}{2} \sum_{x_i, x_j \in \Omega} (\nabla_{x_i, x_j} f)(\nabla_{x_i, x_j} g) w(x_i, x_j) \\ + \sum_{x_i \in \Omega, x_j \in \Omega^c} (\nabla_{x_i, x_j} f) g(x_i) w(x_i, x_j) \ . \end{aligned} \tag{3.29}$$

The Rayleigh quotient of L is:

$$R(f) = \frac{\langle Lf, f \rangle}{\langle f, f \rangle} = \frac{\sum_{x_i \sim x_j} (f(x_j) - f(x_i))^2 w(x_i, x_j)}{\sum_{x_i \in V} f(x_i)^2} \mathbf{w}(x_i) \ . \tag{3.30}$$

As holds for the operator Δ_G, also $\mathbf{L}$ and L have a zero simple eigenvalue and the eigenvalues $\lambda_1, \ldots, \lambda_{h-1}$ are all positive.
The propriety that each function $f \in \mathtt{F}(V)$ has null graph Laplacian over the entire set of vertices, as expressed in Lemma 3.2.2, does not hold for the symmetric normalized graph Laplacian and holds for the random walk normalized graph Laplacian only in the case $w(x_i) = 1$ for each $x_i \in V$.
The symmetric normalized graph Laplacian $\mathbf{L}$ and the random walk graph Laplacian L have the propriety that its eigenvalues are contained in $[0, 2]$, as shown in Theorem below. The statement and the proof are provided for the operator L, but are analogous for the operator $\mathbf{L}$. This propriety does not hold for Δ_G.

Theorem 3.4.1. *Let $G = (V, E)$ be a finite, connected, weighted graph with $|V| > 1$, then all the eigenvalues of L are contained in $[0, 2]$.*

Proof. Let λ be an eigenvalue of L with an eigenfunction f. By the fact that $Lf = \lambda f$ and the discrete Green formula (3.29), we have:

$$\lambda \sum_{x_i \in V} f(x_i)^2 \mathbf{w}(x_i) = \sum_{x_i \in V} Lf(x_i) f(x_i) \mathbf{w}(x_i) = \sum_{x_i \sim x_j} (f(x_j) - f(x_i))^2 w(x_i, x_j) \tag{3.31}$$

From (3.31), it follows that $\lambda \geq 0$. Using the fact that $(f(x_j) - f(x_i))^2 \leq 2(f(x_j)^2 + f(x_i)^2)$, we get:

$$\begin{aligned}
\lambda \sum_{x_i \in V} f(x_i)^2 \mathbf{w}(x_i) &= \sum_{x_i \sim x_j} (f(x_j) - f(x_i))^2 w(x_i, x_j) \\
&= \frac{1}{2} \sum_{x_i, x_j \in V : x_i \sim x_j} (f(x_j) - f(x_i))^2 w(x_i, x_j) \\
&\leq \sum_{x_i, x_j \in V : x_i \sim x_j} (f(x_j)^2 + f(x_i)^2) w(x_i, x_j) \\
&= \sum_{x_i, x_j \in V} f(x_j)^2 w(x_i, x_j) + \sum_{x_i, x_j \in V} f(x_i)^2 w(x_i, x_j) \\
&= \sum_{x_j \in V} f(x_j)^2 \mathbf{w}(x_j) + \sum_{x_i \in V} f(x_i)^2 \mathbf{w}(x_i) \\
&= 2 \sum_{x_i \in V} f(x_i)^2 \mathbf{w}(x_i) \, .
\end{aligned} \tag{3.32}$$

Hence, it follows that $\lambda \leq 2$. □

We will conclude this chapter achieving few notions on the relation between the graph Laplacian and Markov chains.
Let V be a finite set. A *Markov Kernel* on V is a non negative function P on $V \times V$ with the property that

$$\sum_{y \in V} P(x, y) = 1 \quad \text{for all } x \in V \, . \tag{3.33}$$

Any Markov kernel gives rise to a *Markov chain* $\{X_n\}_{n=1}^{\infty}$ that is a random walk on V. It is determined by a family $\{\mathbb{P}_x\}_{x \in V}$ of probability measures on the set of all paths starting from x (that is $X_0 = x$), that satisfies the following property: for all positive integers n and for all $x, x_1, \ldots, x_n \in V$

$$\mathbb{P}_x(X_1 = x_1, X_2 = x_2, \cdots, X_n = x_n) = P(x, x_1) P(x_1, x_2) \ldots P(x_{n-1}, x_n) \, .$$

A weighted graph $((V, E), w)$ with a weight function:

$$w : V \times V \longrightarrow \mathbb{R}$$

induces a natural Markov kernel

$$P(x_i, x_j) = \frac{w_{i,j}}{\mathbf{w}(x_i)} \ .$$

Since $\mathbf{w}(x_i) = \sum_{x_j \in V : x_j \sim x_i} w(x_i, x_j)$, we see that $\sum_{x_j} P(x_i, x_j) = 1$, so that $P(x_i, x_j)$ is a Markov Kernel.
Thus, in terms of the Markov kernel we have that

$$Lf(x_i) = \sum_{x_j} P(x_i, x_j) f(x_j) - f(x_i) \ . \tag{3.34}$$

Defining the Markov operator P on $\mathtt{F}(V)$ by

$$Pf(x_i) = \sum_{x_j} P(x_i, x_j) f(x_j) \tag{3.35}$$

we see that the random walk normalized Laplacian operator L and the Markov operator P are related by a simple identity $L = P - Id$, where Id is the identity operator on $\mathtt{F}(V)$.

Bibliography

[1] Y. Achdou, B. Franchi, N. Marcello, and M. C. Tesi. A qualitative model for aggregation and diffusion of β-amyloid in Alzheimer's disease. *J. Math. Biol.*, 67(6-7):1369–1392, 2013.

[2] G Alvarez, JR Munoz-Montano, J Satrustegui, J Avila, E Bogonez, and J Diaz-Nido. Lithium protects cultured neurons against beta-amyloid induced neurodegeneration. *FEBS*, 453:260–264, 1999.

[3] A Alzheimer, RA Stelzmann, HN Schnitzlein, and FR Murtagh. An english translation of alzheimer's 1907 paper, "uber eine eigenartige erkankung der hirnrinde". *Clin Anat.*, 8(6):429–31, 1995.

[4] T Arendt, C Schindler, M.K. Bruckner, K. Eschrich, V. Bigl, and Zedlick D. Plastic neuronal remodeling is impaired in patients with alzheimer's disease carrying apolipoprotein epsilon 4 allele. *J Neurosci*, 17:516–529, 1997.

[5] GM et al Ashraf. Protein misfolding and aggregation in alzheimer's disease and type 2 diabetes mellitus. *CNS Neurol Disord Drug Targets.*, 13:1280–93, 2014.

[6] J. Avila, J. J. Lucas, M. Perez, and Fritz Hernandez. Role of tau protein in both physiological and pathological conditions. *Physiol. Rev.*, 84:361–84, 2004.

[7] J. Avila, J.J. Lucas, T. Engel, and F. Hernandez. Full reversal of alzheimer's disease-like phenotype in a mouse model with conditional overexpression of glycogen synthasekinase-3. *The Journal Of Neuroscience*, 26, 2006.

[8] J. Avila, J.J. Lucas, F. Hernandez, P. Gomez-Ramos, MA. Moran, and R. Hen. Decreased nuclear beta-catenin, tau hyperphosphorylation and neurodegeneration in gsk-3beta conditional transgenic mice. *EMBO J*, 20:27–39, 2001.

[9] J. M. Ball and J. Carr. The discrete coagulation-fragmentation equations: Existence, uniqueness, and density conservation. *Journal of Statistical Physics*, 61(1):203–234, 1990.

[10] Michiel Bertsch, Bruno Franchi, Norina Marcello, Maria Carla Tesi, and Andrea Tosin. Alzheimer's disease: a mathematical model for onset and progression. *Math. Med. Biol.*, 34(2):193–214, 2017.

[11] H Braak and E Braak. Neuropathological stageing of Alzheimer-related changes. *Acta neuropathologica*, 82(4):239–259, 1991.

[12] H Braak and E Braak. Evolution of neuronal changes in the course of Alzheimer's disease. *Journal of neural transmission. Supplementum*, 53:127–40, jan 1998.

[13] Heiko Braak and Kelly Del Tredici. Alzheimer's pathogenesis: Is there neuron-to-neuron propagation? *Acta Neuropathologica*, 121(5):589–595, 2011.

[14] F Carbonell, Y Iturria-Medina, and Alan C Evans. Mathematical modeling of protein misfolding mechanisms in neurological diseases: A historical overview. *Frontiers Neurology*, 9(37):863–876, 2018.

[15] Mdel C Cardenas-Aguayo, L Gomez-Virgilio, S DeRosa, and MA Meraz-Rios. The role of tau oligomers in the onset of alzheimer's disease neuropathology. *ACS Chem Neurosci.*, 5(12):1178–91, 2014.

[16] MS Celej, R Sarroukh, E Goormaghtigh, GD Fidelio, J-M Ruysschaert, and V Raussens. Toxic prefibrillar alpha-synuclein amyloid oligomers adopt a distinctive antiparallel beta-sheet structure. *Biochem J.*, 443:712–726, 2012.

[17] Florence Clavaguera, Tristan Bolmont, R Anthony Crowther, Dorothee Abramowski, Stephan Frank, Alphonse Probst, Graham Fraser, Anna K Stalder, Martin Beibel, Matthias Staufenbiel, Mathias Jucker, Michel Goedert, and Markus Tolnay. Transmission and spreading of tauopathy in transgenic mouse brain. *Nature cell biology*, 11(7):909–913, jul 2009.

[18] Florence Clavaguera, Isabelle Lavenir, Ben Falcon, Stephan Frank, Michel Goedert, and Markus Tolnay. ?prion-like? templated misfolding in tauopathies. *Brain Pathology*, 23(3):342–349, 2013.

[19] F. Cornelis, O. Saut, P. Cumsille, D. Lombardi, A. Iollo, J. Palussiere, and T. Colin. In vivo mathematical modeling of tumor growth from imaging data: Soon to come in the future? *Diagnostic and Interventional Imaging*, 94(6):593 – 600, 2013.

[20] L Cruz, B Urbanc, SV Buldyrev, R Christie, T Gomez-Isla, S Havlin, M McNamara, HE Stanley, and BT Hyman. Aggregation and disaggregation of senile plaques in alzheimer?disease. *Proc Natl Acad Sci USA*, 94(14):7612–7616, 1999.

[21] Bibiana DaRocha-Souto, Thomas C Scotton, Mireia Coma, Alberto Serrano-Pozo, Tadafumi Hashimoto, Lidia Serenó, Marta Rodríguez, Belen Sánchez, Bradley T Hyman, and Teresa Gómez-Isla. Brain oligomeric β-amyloid but not total amyloid plaque burden correlates with neuronal loss and astrocyte inflammatory response in amyloid precursor protein/tau transgenic mice. *Journal of neuropathology and experimental neurology*, 70(5):360–376, 2011.

[22] Elena Posse de Chaves and Vasanthy Narayanaswami. Apolipoprotein e and cholesterol in aging and disease in the brain. *Future Lipidol*, 3:505–530, 2008.

[23] Rahul S Desikan, Mert R Sabuncu, Nicholas J Schmansky, Martin Reuter, Howard J Cabral, Christopher P Hess, Michael W Weiner, Alessandro Biffi, Christopher D Anderson, Jonathan Rosand, David H Salat, Thomas L Kemper, Anders M Dale, Reisa A Sperling, and Bruce Fischl. Selective disruption of the cerebral neocortex in Alzheimer's disease. *PloS one*, 5(9):e12853, jan 2010.

[24] Bradford C Dickerson and David A Wolk. Biomarker-based prediction of progression in MCI: Comparison of AD signature and hippocampal volume with spinal fluid amyloid-β and tau. *Frontiers in aging neuroscience*, 5:55, jan 2013.

[25] GBD 2015 Disease, Injury Incidence, and Prevalence Collaborators. Global, regional, and national incidence, prevalence, and years lived with disability for 310 diseases and injuries, 1990-2015: a systematic analysis for the global burden of disease study 2015. *Lancet.*, 388(10053):1545–1602, 2016.

[26] R. L. Drake. A general mathematical survey of the coagulation equation. In *Topics in Current Aerosol Research (Part 2), International Reviews in Aerosol Physics and Chemistry*, pages 203–376. Pergamon Press, Oxford, UK, 1972.

[27] L Edelstein-Keshet and A Spiross. Exploring the formation of alzheimer's disease senile plaques in silico. *J Theor Biol*, 216(3):301–26, 2002.

[28] D. Eisenberg and M. Jucker. The amyloid state of proteins in human diseases. *Cell*, 148(6):1188?1203, 2012.

[29] Arriagada et al. Neurofibrillary tangles but not senile plaques parallel duration and severity of alzheimer's disease. *Neurology*, 42:631–639, 1992.

[30] Gomez-Isla et al. Neuronal loss correlates but exceeds neurofibrillary tangles in alzheimer's disease. *Ann Neurol*, 41:17–24, 1997.

[31] Ittner et al. Site-specific phosphorylation of tau inhibits amyloid-beta toxicity in alzheimer's mice. *Science*, 354:904–908, 2016.

[32] Morsch et al. Neurons may live for decades with neurofibrillary tangles. *Neuropathol Exp Neurol*, 58:188–197, 1999.

[33] Shi Y et al. Apoe4 markedly exacerbates tau-mediated neurodegeneration in a mouse model of tauopathy. *Nature*, 549:523–527, 2017.

[34] Bruce Fischl, David H Salat, Evelina Busa, Marilyn Albert, Megan Dieterich, Christian Haselgrove, Andre van der Kouwe, Ron Killiany, David Kennedy, Shuna Klaveness, Albert Montillo, Nikos Makris, Bruce Rosen, and Anders M Dale. Whole brain segmentation: automated labeling of neuroanatomical structures in the human brain. *Neuron*, 33(3):341–55, jan 2002.

[35] F.Leyvraz. Existence and properties of post gel solutions for the kinetic equations of coagulation. *J.Phys. A*, 16:2861–2873, 1983.

[36] B. Franchi and S. Lorenzani. From a microscopic to a macroscopic model for Alzheimer disease: two-scale homogenization of the Smoluchowski equation in perforated domains. *J. Nonlinear Sci.*, 26(3):717–753, 2016.

[37] Bruno Franchi and Silvia Lorenzani. Smoluchowski equation with variable coefficients in perforated domains: homogenization and applications to mathematical models in medicine. In *Harmonic analysis, partial differential equations and applications*, Appl. Numer. Harmon. Anal., pages 49–67. Birkhäuser/Springer, Cham, 2017.

[38] Bess Frost and Marc I Diamond. Prion-like mechanisms in neurodegenerative diseases. *Nature reviews. Neuroscience*, 11(3):155–9, mar 2010.

[39] Bess Frost, Rachel L Jacks, and Marc I Diamond. Propagation of tau misfolding from the outside to the inside of a cell. *The Journal of biological chemistry*, 284 19:12845–52, 2009.

[40] P Garaud, F Meru, M Galvagni, and C Olczak. From dust to planetesimals: an improved model for collisional growth in protoplanetary disks. *The Astrophysical Journal*, 764(2):156–165, 2013.

[41] Julia Gerson and Rakez Kayed. Formation and propagation of tau oligomeric seeds. *Frontiers in Neurology*, 4:93, 2013.

[42] J.E. Gillam and C.E. MacPhee. Modelling amyloid fibril formation kinetics: mechanisms of nucleation and growth. *Journal of Physics: Condensed Matter*, 25(373101):1–20, 2013.

[43] GG Glenner and CW Wong. Alzheimer's disease and down's syndrome: sharing of a unique cerebrovascular amyloid fibril protein. *Biochem. Biophys. Res. Commun*, 122:1131?1135, 1984.

[44] Alberto Gomez-Ramos, Miguel Diaz-Hernandez, Raquel Cuadros, Felix Hernandez, and Jesus Avila. Extracellular tau is toxic to neuronal cells. *FEBS Letters*, 580(20):4842–4850, 2006.

[45] CX Gong, I Grundke-Iqbal, and K. Iqbal. Dephosphorylation of alzheimer's disease abnormally phosphorylated tau by protein phosphatase-2a. *Neuroscience*, 61:765–772, 1994.

[46] A Grigoryan. Analysis and geometry on graphs part 1. laplace operator on weighted graphs. *Notes at Tsinghua University*, 2012.

[47] Marcos J Guerrero-Munoz, Julia Gerson, and Diana L. Castillo-Carranza. Tau oligomers: The toxic player at synapses in alzheimer's disease. *Front Cell Neurosc*, 9:464, 2015.

[48] C. Haass and D. J. Selkoe. Soluble protein oligomers in neurodegeneration: lessons from the Alzheimer's amyloid beta-peptide. *Nat. Rev. Mol. Cell. Biol.*, 8(2):101–112, 2007.

[49] Cho Hanna, Choi Jae Yong, Hwang Mi Song, Kim You Jin, Lee Hye Mi, Lee Hye Sun, Lee Jae Hoon, Ryu Young Hoon, Lee Myung Sik, and Lyoo Chul Hyoung. In vivo cortical spreading pattern of tau and amyloid in the alzheimer disease spectrum. *Annals of Neurology*, 80(2):247–258, 2016.

[50] P. Hartman. *Ordinary differential equations*. John Wiley & Sons, Inc., New York-London-Sydney, 1964.

[51] M. C. Heine and S. E. Pratsinis. Brownian coagulation at high concentration. *Langmuir*, 23(19):9882–9890, 2007. PMID: 17685639.

[52] F Hernandez, JJ Lucas, R Cuadros, and Avila J. Gsk-3 dependent phospho-epitopes recognized by phf-1 and at-8 antibodies are present in different tau isoforms. *Neurobiol Aging*, 2003.

[53] F Hernandez, JJ Lucas, M Perez, and J Avila. Role of tau protein in both physiological and pathological conditions. *Physiol Rev*, 2004.

[54] C Hooper, R Killick, and S Lovestone. The gsk3 hypothesis of alzheimer's disease. *J. Neurochem.*, 104:1433–1439, 2008.

[55] M Hoshi, M Sato, S Matsumoto, A Noguchi, K Yasutake, N Yoshida, and K Sato. Spherical aggregates of beta amyloid (amylo-spheroid)show high neurotoxicity and activate tau protein kinase i/glycogen synthase kinase 3beta. *Proc Natl Acad Sci USA*, 100:6370–6375, 2003.

[56] Michiyo Iba, Jennifer D McBride, Jing L Guo, Bin Zhang, John Q Trojanowski, and Virginia M-Y Lee. Tau pathology spread in PS19 tau transgenic mice following locus coeruleus (LC) injections of synthetic tau fibrils is determined by the LC's afferent and efferent connections. *Acta neuropathologica*, 130(3):349–62, sep 2015.

[57] NC Inestrosa and E Arenas. Emerging roles of wnts in the adult nervous system. *Nat Rev Neurosci*, 11(2):77–86, 2010.

[58] Khalid Iqbal, Cheng-Xin Gong, and Fei Liu. Tau oligomers: The toxic player at synapses in alzheimer's disease. *Front Neurol*, 4:112, 2013.

[59] Yasser Iturria-Medina, Roberto C. Sotero, Paule J. Toussaint, Alan C. Evans, , and the Alzheimer's Disease Neuroimaging Initiative. Epidemic spreading model to characterize misfolded proteins propagation in aging and associated neurodegenerative disorders. *PLOS Computational Biology*, 10(11):1–16, 11 2014.

[60] Zhou J and Liu B. Alzheimer's disease and prion protein. *Intractable Rare Disease*, 2:35–44, 2013.

[61] Clifford R Jack Jr, David S Knopman, William J Jagust, Leslie M Shaw, Paul S Aisen, Michael W Weiner, Ronald C Petersen, and John Q Trojanowski. Hypothetical model of dynamic biomarkers of the Alzheimer's pathological cascade. *The Lancet Neurology*, 9(1):119–128, jan 2010.

[62] Darlene E. Jenkins, Yoko Oei, Yvette S. Hornig, Shang-Fan Yu, Joan Dusich, Tony Purchio, and Pamela R. Contag. Bioluminescent imaging (bli) to improve and refine traditional murine models of tumor growth and metastasis. *Clinical & Experimental Metastasis*, 20(8):733–744, Dec 2003.

[63] Cho JH and Johnson GV. Glygogen synthase kinase 3beta phosphorylates tau at both primed and unprimed sites: differential impact on microtubule binding. *J Biol Chem*, 2002.

[64] M Jucker and LC Walker. Self-propagation of pathogenic protein aggregates in neurodegenerative diseases. *Nature*, 501:45–51, 2013.

[65] Mathias Jucker and Lary C Walker. Self-propagation of pathogenic protein aggregates in neurodegenerative diseases. *Nature*, 501(7465):45–51, sep 2013.

[66] F. Kappel and R. O. Peer. A mathematical model for fundamental regulation processes in the cardiovascular system. *Journal of Mathematical Biology*, 31(6):611–631, Jul 1993.

[67] BB Kent, JW Drane, BB Blumenstein, and JW Manning. A mathematical model to assess changes in the baroreceptor reflex. *Cardiology*, 57:295–310, 1972.

[68] Jungsu Kim, Jacob M. Basak, and David M. Holtzman. The role of apolipoprotein e in alzheimer's disease. *Neuron*, 63:287–303, 2009.

[69] Adam Kline. Apolipoprotein e, amyloid-beta clearance and therapeutic opportunities in alzheimer's disease. *Alzheimers Res Ther*, 4:32, 2012.

[70] Michala Kolarova, Francisco García-Sierra, Ales Bartos, Jan Ricny, and Daniela Ripova. Structure and pathology of tau protein in Alzheimer disease. *International journal of Alzheimer's disease*, 2012:731526, jan 2012.

[71] K.S. Kosik. Tau protein and neurodegeneration. *Mol. Neurobiol.*, 4:171–179, 1990.

[72] Amy Kuceyeski, Jun Maruta, Norman Relkin, and Ashish Raj. The Network Modification (NeMo) Tool: elucidating the effect of white matter integrity changes on cortical and subcortical structural connectivity. *Brain connectivity*, 3(5):451–63, jan 2013.

[73] M Larson, MA Sherman, F Amar, M Nuvolone, JA Schneider, DA Bennett, A Aguzzi, and SE Lesne. The complex prp(c)-fyn couples human oligomeric a-beta with pathological tau changes in alzheimer's disease. *J. Neurosci.*, 32:16857–16871, 2012.

[74] Cristian A Lasagna-Reeves, Diana L Castillo-Carranza, Urmi Sengupta, Audra L Clos, George R Jackson, , and Rakez Kayed. Tau oligomers impair memory and induce synaptic and mitochondrial dysfunction in wild-type mice. *Mol Neurodegener*, 6, 2011.

[75] J Lauren, DA Gimbel, HB Nygaard, JW Gilbert, and SM Strittmatter. Cellular prion protein mediates impairment of synaptic plasticity by amyloid-beta oligomers. *Nature*, 457:1128–1132, 2009.

[76] Lee, Hyoung-Gon, Perry, George, Moreira, Paula I, Garrett, Matthew R, Liu, Quan, Zhu, Xiongwei, Takeda, Atsushi, Nunomura, Akihiko, Smith, and Mark A. Tau phosphorylation in alzheimer's disease: pathogen or protector? *Trends in Molecular Medicine*, 11:164–169, 2005.

[77] C Y Lee and G E Landreth. The role of microglia in amyloid clearance from the ad brain. *J Neural Transm*, 117:949–60, 2010.

[78] F Leyvraz and H R Tschudi. Singularities in the kinetics of coagulation processes. *Journal of Physics A: Mathematical and General*, 14(12):3389–3405, dec 1981.

[79] S Lovestone and C H Reynolds. The phosphorylation of tau:a critical stage in neurodevelopment and neurodegenerative process. *Neuroscience*, 78:309–324, 1997.

[80] D. Wrzosek M.A.Herrero, J.J.L. Velazquez. Sol-gel transition in a coagulation-diffusion model. *Phisica D*, 141:221–247, 2000.

[81] J Masel, VA Jansen, and MA Nowak. Quantifying the kinetic parameters of prion replication. *Biophysical Chemistry*, 77(37):139–152, 1999.

[82] Franziska Matthäus. Diffusion versus network models as descriptions for the spread of prion diseases in the brain. *Journal of Theoretical Biology*, 240(37):104–113, 2006.

[83] A.M. Morris, M.A. Watzky, and R.G. Finke. Protein aggregation kinetics, mechanism, and curve-fitting: a review of the literature. *Biochimica et Biophysica Acta - Proteins and Proteomics*, 1794(3):375–397, 2009.

[84] R. M. Murphy and M. M. Pallitto. Probing the kinetics of β-amyloid self-association. *Biophysical Journal*, 130(2-3):109–122, 2000.

[85] Richard J O'Brien and Philip C Wong. Amyloid precursor protein processing and Alzheimer's disease. *Annual review of neuroscience*, 34:185–204, jan 2011.

[86] D. Wrzosek P. Benilan. On an infinite system of reaction-diffusion equations. *Adv. Math. Sci. Appl.*, 7:351–366, 1997.

[87] RJ Payne and DC Krakauer. The spatial dynamics of prion disease. *Proceedings of Biological Sciences*, 265(37):2341–6, 1998.

[88] Michela Pievani, Willem de Haan, Tao Wu, William W Seeley, and Giovanni B Frisoni. Functional network disruption in the degenerative dementias. *The Lancet. Neurology*, 10(9):829–43, sep 2011.

[89] Stanley B Prusiner, Michael Scott, Dallas Foster, Keh-Ming Pan, Darlene Groth, Carol Mirenda, Marilyn Torchia, Shu-Lian Yang, Dan Serban, George A Carlson, Peter C Hoppe, David Westaway, and Stephen J DeArmond. Transgenetic studies implicate interactions between homologous prp isoforms in scrapie prion replication. *Cell*, 63(3):673–86, 1990.

[90] Qiang, Liang, Sun, Xiaohuan, Austin, O Timothy, Muralidharan, Hemalatha, Jean, C Daphney, Liu, Mei, Yu, Wenqian, Baas, and Peter W. Tau does not stabilize axonal microtubules but rather enables them to have long labile domains. *Current Biology*, 2018.

[91] Ashish Raj, Amy Kuceyeski, and Michael Weiner. A Network Diffusion Model of Disease Progression in Dementia. *Neuron*, 73(6):1204–1215, mar 2012.

[92] Ashish Raj, Eve LoCastro, Amy Kuceyeski, Duygu Tosun, Norman Relkin, and Michael Weiner. Network Diffusion Model of Progression Predicts Longitudinal Patterns of Atrophy and Metabolism in Alzheimer's Disease. *Cell Reports*, in print(3):359–369, jan 2015.

[93] Fan R.K.Chung. Spectral graph theory. *American Mathematical Society*, 1997.

[94] L.C. Serpell, M. Sunde, and C.C. Blake. The molecular basis of amyloidosis. *Cellular and molecular life sciences*, 53(11-12):871–887, 1997.

[95] Louise C Serpell. Alzheimer's amyloid fibrils: structure and assembly. *Biochimica et Biophysica Acta (BBA) - Molecular Basis of Disease*, 1502(1):16 – 30, 2000.

[96] Alberto Serrano-Pozo, Matthew P Frosch, Eliezer Masliah, and Bradley T Hyman. Neuropathological alterations in Alzheimer disease. *Cold Spring Harbor perspectives in medicine*, 1(1):a006189, sep 2011.

[97] M.A. et al Smith. Amyloid-beta and tau serve antioxidant function in the aging and alzheimer's brain. *Free Radic. Biol. Med.*, 33:1194–1199, 2002.

[98] M. Smoluchowski. Versuch einer mathematischen theorie der koagulationskinetik kolloider lösungen. *IZ. Phys. Chem.*, 92:129–168, 1917.

[99] W Stockmayer. Theory of molecular size distribution and gel formation in branched-chain polymers. *J.Chem Phys.*, 11(2):45–55, 1943.

[100] Ilaria Stura, Ezio Venturino, and Caterina Guiot. A two-clones tumor model: Spontaneous growth and response to treatment. *Mathematical Biosciences*, 271:19 – 28, 2016.

[101] John R King Susan C Davies and Jonathan AD Wattis. The smoluchowski coagulation equations with continuous injection. *J.Phys.A.*, 32:7745–7763, 1999.

[102] O. G. Tatarnikova, M. A. Orlov, and Bobkova N.V. Beta-amyloid and tau protein: Structure, interaction and prion-like properties. *Biochemistry (Moscow)*, 80(13):1800–1819, 2015.

[103] David R Taylor and Nigel M Hooper. The prion protein and lipid rafts. *Molecular membrane biology*, 23(1):89–99, jan 2006.

[104] Dietmar R Thal, Udo Rüb, Mario Orantes, and Heiko Braak. Phases of A beta-deposition in the human brain and its relevance for the development of AD. *Neurology*, 58(12):1791–800, jun 2002.

[105] Justin Torok, Pedro D Maia, Fon Powell, Sneha Pandya, and Ashish Raj. A method for inferring regional origins of neurodegeneration. *Brain*, 141(3):863–876, 2018.

[106] John Q Trojanowski, Hugo Vandeerstichele, Magdalena Korecka, Christopher M Clark, Paul S Aisen, Ronald C Petersen, Kaj Blennow, Holly Soares, Adam Simon, Piotr Lewczuk, Robert Dean, Eric Siemers, William Z Potter, Michael W Weiner, Clifford R Jack, William Jagust, Arthur W Toga, Virginia M-Y Lee, and Leslie M Shaw. Update on the biomarker core of the Alzheimer's Disease Neuroimaging Initiative subjects. *Alzheimer's & dementia : the journal of the Alzheimer's Association*, 6(3):230–8, may 2010.

[107] H Tsuruta, T Sato, and N Ikeda. Mathematical model of cardiovascular mechanics for diagnostic analysis and treatment of heart failure.part 2.analysis of vasodilator therapy and planning of optimal drug therapy. *Med Biol Eng Comput*, 32(1):11–28, 1994.

[108] H Tsuruta, T Sato, M Shirataka, and N Ikeda. Mathematical model of cardiovascular mechanics for diagnostic analysis and treatment of heart failure.part 1. model description and theoretical analysis. *Med Biol Eng Comput*, 32(1):3–11, 1994.

[109] B Urbanc, L Cruz, SV Buldyrev, S Havlin, MC Irizarry, HE Stanley, and BT Hyman. Dynamics of plaque formation in alzheimer's disease. *Biophys J*, 76(3):1330–4, 1999.

[110] Vinay G. Vaidya and Frank J. Alexandro. Evaluation of some mathematical models for tumor growth. *International Journal of Bio-Medical Computing*, 13(1):19 – 35, 1982.

[111] Prashanthi Vemuri, Jennifer L Whitwell, Kejal Kantarci, Keith A Josephs, Joseph E Parisi, Maria S Shiung, David S Knopman, Bradley F Boeve, Ronald C Petersen, Dennis W Dickson, and Clifford R Jack. Antemortem MRI based STructural Abnormality iNDex (STAND)-scores correlate with postmortem Braak neurofibrillary tangle stage. *NeuroImage*, 42(2):559–67, aug 2008.

[112] D. M. Walsh and D. J. Selkoe. Oligomers on the brain: the emerging role of soluble protein aggregates in neurodegeneration. *Protein Pept Lett*, 11:213–28, 2004.

[113] D. M. Walsh and D. J. Selkoe. Aβ oligomers: a decade of discovery. *J. Neurochem.*, 101(5):1172–1184, 2007.

[114] Dominic M Walsh, Igor Klyubin, Julia V Fadeeva, William K Cullen, Roger Anwyl, Michael S Wolfe, Michael J Rowan, and Dennis J Selkoe. Naturally secreted oligomers of amyloid beta protein potently inhibit hippocampal long-term potentiation in vivo. *Nature*, 416(6880):535–9, apr 2002.

[115] R. Wetzel. For protein misassembly, it's the "i" decade. *Cell*, 86(5):699–702, 1996.

[116] J L Whitwell, K A Josephs, M E Murray, K Kantarci, S A Przybelski, S D Weigand, P Vemuri, M L Senjem, J E Parisi, D S Knopman, B F Boeve, R C Petersen, D W Dickson, and C R Jack. MRI correlates of neurofibrillary tangle pathology at autopsy: a voxel-based morphometry study. *Neurology*, 71(10):743–9, sep 2008.

[117] Kristin R Wildsmith, Monica Holley, Julie C Savage, Rebecca Skerrett, and Gary E Landreth. Evidence for impaired amyloid beta clearance in alzheimer's disease. *Alzheimers Res Ther*, 5:33, 2013.

[118] D. Wrzosek. Existence of solutions for the discrete coagulation-fragmentation model with diffusion. *Topol. Methods Nonlinear Anal.*, 9(2):279–296, 1997.

[119] D. Wrzosek. Mass conserving solutions to the discrete coagulation-fragmentation model with diffusion. *Nonlinear Anal.*, 49:297–314, 2002.

[120] Chun-Fang Xia, Janna Arteaga, Gang Chen, Umesh Gangadharmath, Luis F Gomez, Dhanalakshmi Kasi, Chung Lam, Qianwa Liang, Changhui Liu, Vani P Mocharla, Fanrong Mu, Anjana Sinha, Helen Su, A Katrin Szardenings, Joseph C Walsh, Eric Wang, Chul Yu, Wei Zhang, Tieming Zhao, and Hartmuth C Kolb. [(18)F]T807, a novel tau positron emission tomography imaging agent for Alzheimer's disease. *Alzheimer's & dementia : the journal of the Alzheimer's Association*, 9(6):666–76, nov 2013.

[121] L Xie, E Helmerhorst, K Taddei, B Plewright, W Van Bronswijk, and R Martins. Alzheimer's beta-amyloid peptides compete for insulin binding to the insulin receptor. *J Neurosci.*, 22(10):RC221, 2002.

[122] ZX Yao and V Papadopoulos. Function of beta-amyloid in cholesterol transport: a lead to neurotoxicity. *FASEB J*, 16:33, 2002.

[123] M Yu, M Steipenbusch, J Yang, and H Jin. A new analytical solution for the smoluchowski equation due to nanoparticle brownian coagulation for non-self preserving system. *Aerosol and Air Quality Research*, 14:1726–1733, 2014.

[124] D. Zhou and B. Scholkopf. Discrete regularization. *Semi-supervised learning*, pages 221–232, 2006.

[125] Juan Zhou, Efstathios D. Gennatas, Joel H. Kramer, Bruce L. Miller, and William W. Seeley. Predicting regional neurodegeneration from the healthy brain functional connectome. *Neuron*, 73(6):1216–27, mar 2012.